frontiers in Earth Science

ORIGINAL RESEARCH
published: 23 March 2022
doi: 10.3389/feart.2022.830984

Calcium Carbonate Dissolution Triggered by High Productivity During the Last Glacial–Interglacial Interval in the Deep Western South Atlantic

Jaime Y. Suárez-Ibarra[1,2], Cristiane F. Frozza[1], Pâmela L. Palhano[1], Sandro M. Petró[3], Manuel F. G. Weinkauf[2] and Maria A. G. Pivel[4]*

[1]Programa de Pós-Graduação Em Geociências, Instituto de Geociências, Universidade Federal Do Rio Grande do Sul, Porto Alegre, Brazil, [2]Ústav Geologie a Paleontologie, Přírodovědecká Fakulta, Univerzita Karlova, Prague, Czech Republic, [3]itt OCEANEON, Instituto Tecnológico de Paleoceanografia e Mudanças Climáticas, Universidade Do Vale Do Rio Dos Sinos, São Leopoldo, Brazil, [4]Instituto de Geociências, Universidade Federal do Rio Grande do Sul, Porto Alegre, Brazil

OPEN ACCESS

Edited by:
Jacek Raddatz,
Goethe University Frankfurt, Germany

Reviewed by:
Selvaraj Kandasamy,
Xiamen University, China
Patrick Grunert,
University of Cologne, Germany

***Correspondence:**
Jaime Y. Suárez-Ibarra
jysuarezibarra@gmail.com
suarezij@natur.cuni.cz

Specialty section:
This article was submitted to Quaternary Science, Geomorphology and Paleoenvironment, a section of the journal Frontiers in Earth Science

Received: *07 December 2021*
Accepted: *17 February 2022*
Published: *23 March 2022*

Citation:
Suárez-Ibarra JY, Frozza CF, Palhano PL, Petró SM, Weinkauf MFG and Pivel MAG (2022) Calcium Carbonate Dissolution Triggered by High Productivity During the Last Glacial–Interglacial Interval in the Deep Western South Atlantic. Front. Earth Sci. 10:830984. doi: 10.3389/feart.2022.830984

Studies reconstructing surface paleoproductivity and benthic environmental conditions allow us to measure the effectiveness of the biological pump, an important mechanism in the global climate system. In order to assess surface productivity changes and their effect on the seafloor, we studied the sediment core SAT-048A, spanning 43–5 ka, recovered from the continental slope (1,542 m water depth) of the southernmost Brazilian continental margin, deep western South Atlantic. We assessed the sea surface productivity, the organic matter flux to the seafloor, and calcite dissolution effects, based on micropaleontological (benthic and planktonic foraminifers, ostracods), geochemical (benthic $\delta^{13}C$ isotopes), and sedimentological data (carbonate and bulk sand content). Superimposed on the induced changes related to the last glacial–interglacial transition, the reconstruction indicates a significant and positive correlation between the paleoproductivity proxies and the summer insolation. From the reconstructed data, it was possible to identify high (low) surface productivity, high (low) organic matter flux to the seafloor, and high (low) dissolution rates of planktonic Foraminifera tests during the glacial (postglacial). Furthermore, within the glacial, enhanced productivity was associated with higher insolation values, explained by increased northeasterly summer winds that promoted meandering and upwelling of the nutrient-rich South Atlantic Central Water. Statistical analyses support the idea that productivity is the main cause for seafloor calcium carbonate dissolution, as opposed to changes in the Atlantic Meridional Overturning Circulation (at least for the 25–4 ka period). Further efforts must be invested in the comprehension and quantification of the total organic matter and biogenic carbonate burial during time intervals with an enhanced biological pump, aiming to better understand their individual roles.

Keywords: planktonic Foraminifera, stable isotopes, Atlantic meridional overturning circulation, upper circumpolar deep water, North Atlantic deep water

INTRODUCTION

The oceanic biological pump is a primary mechanism to exchange CO_2 between the atmosphere and the oceans, and is therefore critically important for the acidity of the sea water and associated carbonate dissolution (Riebesell, 2004). An intensified biological pump in the oceans leads to an increase of exported biogenic carbon and carbonate burial in the sediments (Brummer and van Eijden, 1992). Since planktonic Foraminifera are important contributors to the pelagic calcium carbonate flux (Milliman et al., 1999; Schiebel, 2002; Kučera, 2007) they represent an important component of the global climate system through their role in the oceanic carbon and carbonate pump. The connection between strong changes in the oceanic biological pump and calcite dissolution is difficult to study in modern oceans, as sample areas with sufficient differences in bioproductivity also differ in several other environmental factors, thus confounding the results. In contrast, Pleistocene climate scenarios offer the possibility to investigate a relatively stable ecosystem under intensely changing bioproductivity scenarios.

The Late Quaternary climate is characterized by orbit-related glacial–interglacial fluctuations (EPICA Community Members, 2004; Jouzel et al., 2007) associated with CO_2 variations (Petit et al., 1999; Shakun et al., 2012). Nevertheless, the orbital forcing alone is not strong enough to induce the observed temperature changes and, thus, feedback mechanisms in the Earth's climate system are expected to have amplified (or reduced) the primary signal (Lorius et al., 1990; Shackleton, 2000). The oceanic carbonate pump system is critically influenced by changes in bioproductivity. High biological surface productivity can boost population densities and biomass of benthic communities, increasing the respiration processes and leading to the remineralization of higher percentages of organic matter (OM), resulting in the release of CO_2 and a reduction of the biologic carbon burial (Cronin et al., 1999; Hales, 2003). Besides, higher CO_2 release at the seafloor can lead to increased dissolution of biogenic carbonate, (e.g., planktonic Foraminifera tests; Schiebel, 2002). Therefore, an enhanced biological pump can have an unexpected effect, both decreasing the OM burial and dissolving biogenic carbonates, inhibiting higher quantities of C to be stored in the seafloor sediments (e.g., Zamelczyk et al., 2012; Naik et al., 2014).

Supra-lysoclinal pelagic carbonate dissolution has been described from the western South Atlantic in the past, being related to changes in bottom water masses (Petró et al., 2018a; Petró and Burone, 2018; Petró et al., 2021). Nevertheless, the relation between calcium carbonate dissolution and sea surface productivity has not yet been approached in the studied area. In this paper, we 1) reconstruct past changes in primary and export productivity during the last glacial–interglacial interval, 2) determine mechanisms that triggered calcium carbonate dissolution, and 3) investigate the role of productivity changes on carbonate corrosion from a core retrieved above the lysocline.

Oceanographic Setting

The studied sediment core was recovered off Santa Marta Cape in the western South Atlantic (**Figure 1A,B**). The proximal portion of the continental shelf of the Pelotas Basin represents a submerged coastal plain (Martins, 1984) that was exposed during the last Pleistocene regression (Marine Isotope Stage 2) and dissected by drainage networks from fluvial systems (Weschenfelder et al., 2014), which contributed to larger nutrient inputs from continental outflows compared to the Holocene.

Surface circulation in the shelf portion of the study area is dominated by the northward flowing Brazil Coastal Current, which carries the Coastal Water (CW), a mixture of oceanic and continental drainage waters. Offshore, the Brazil Current (BC) transports the warm (temperature, $T > 20^{\circ}C$) and salty (salinity, $S > 36$) Tropical Water (TW) southwards within the surface layer. The BC flows along the South American margin slope until it converges with the Malvinas Current (MC), a northward flowing surface current carrying the cold ($T < 15^{\circ}C$) and fresher ($S < 34.2$) Subantarctic Water, forming the Brazil/Malvinas Confluence (BMC) close to 38°S (Gordon and Greengrove, 1986). The BMC forms a large meander, which separates southward of the continental margin (Peterson and Stramma, 1991; Piola and Matano, 2017), and varies seasonally and interannually, moving to the north in austral autumn and winter, and to the south in spring and summer. This variation influences the nutrient distribution along the continental shelf of the Argentinian, Uruguayan, and south Brazilian coasts (Gonzalez-Silvera et al., 2006). Presently, two main continental sources of nutrients and freshwater for the area are the Río de la Plata Estuary (RdlPE) and the Patos-Mirim Lagoon System (PMLS). Although the configuration of continental drainage certainly changed under the varying sea-level conditions of the late Quaternary, they both represent sources of continental drainage and, thus, nutrients to the study area.

The water masses that circulate in the subsurface (**Figure 1C**) immediately below the TW are: the South Atlantic Central Water (SACW), the Antarctic Intermediate Water (AAIW), the Upper Circumpolar Deep Water (UCDW), the North Atlantic Deep Water (NADW), and the Antarctic Bottom Water (AABW) (Reid et al., 1976; Campos et al., 1995; Hogg et al., 1996; Stramma and England, 1999). The NADW promotes the preservation of carbonate, due to its oversaturation with carbonate ion (CO_3^{2-}) when compared to the overlying UCDW and the underlying AABW. Both, the UCDW and AABW, are undersaturated in CO_3^{2-} and, therefore, may lead to the dissolution of carbonate (Frenz et al., 2003). Indeed, Frenz and Henrich (2007) have shown that the depth of the interface between the NADW and the AABW defines the lysocline, below which carbonate dissolution occurs.

MATERIALS AND METHODS

The piston core SAT-048A was collected by *FUGRO Brasil–Serviços Submarinos e Levantamentos Ltda* for the *Agência Nacional do Petróleo* (ANP, Brazilian National Agency of Petroleum, Natural Gas and Biofuels) at 29°11′ S and 47°15′ W at 1,542 m water depth (**Figure 1**). The core, with a total recovery of 315 cm, was sampled at intervals of about 6 cm, for a total of 54

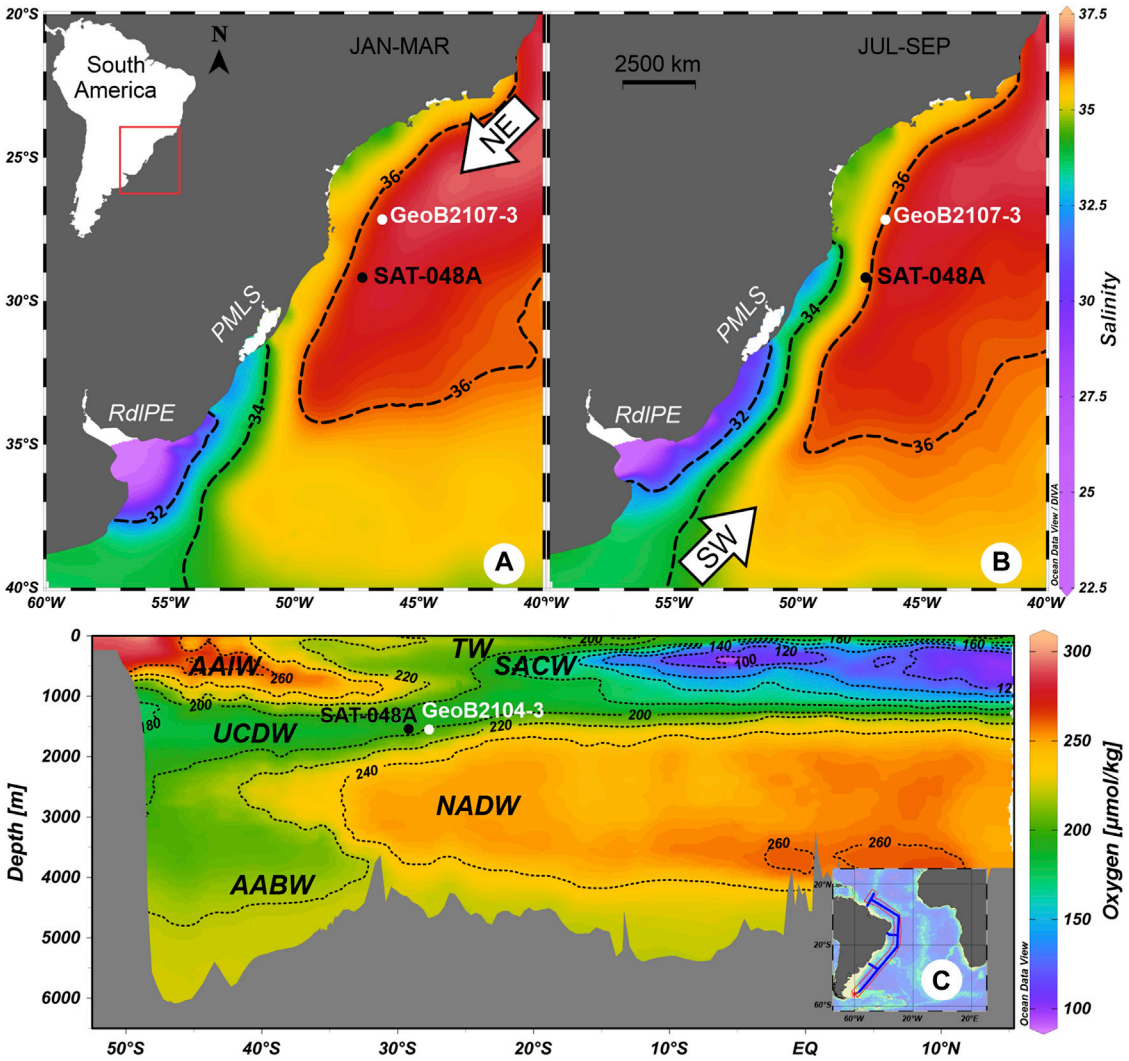

FIGURE 1 | Location of sediment core SAT-048A and other mentioned cores (GeoB2107-3, Gu et al., 2017, Pereira et al., 2018; GeoB2104-3, Howe J. N. W. et al., 2016) in the studied area, in map view **(A,B)** and as latitudinal cross section (C). Seasonal variation of average sea surface salinity (measured on the psu scale) for the months of (a) January–March (austral summer) and (b) July–September (winter) are based on data from the World Ocean Atlas 2013 (WOA13, Zweng et al., 2013). The isohalines 32, 34, and 36 (dashed lines) highlight the northward intrusion of less saline water from the south during winter (b) when compared to summer (a) conditions. This is related to seasonally predominating wind regimes, indicated as white arrows. The present Río de la Plata Estuary (RdlPE) and Patos-Mirim Lagoon System (PMLS) represent important continental nutrient sources in the study area. Dissolved oxygen concentrations (c; µmol/kg) in a transect along the South American continental margin show the South Atlantic water masses that circulate in the region: Tropical Water (TW), South Atlantic Central Water (SACW), Antarctic Intermediate Water (AAIW), Upper Circumpolar Deep Water (UCDW), North Atlantic Deep Water (NADW), and Antarctic Bottom Water (AABW).

samples. The core was missing the top 20 cm and the 196–217 cm interval. Each sample was washed over a 63 µm sieve and oven dried at temperatures below 60°C. The taxonomical identification of the planktonic Foraminifera species, from subsamples of at least 300 specimens larger than 150 µm split with a microsplitter, followed Bé (1967), Bé et al. (1977), Bolli and Saunders (1989), Hemleben et al. (1989), Kemle-von Mücke and Hemleben (1999), Schiebel and Hemleben (2017), and Morard et al. (2019).

We used a revised version of the Frozza et al. (2020) age model, based on the *rbacon* package (Blaauw and Christen, 2011; version 2.4.2) for the R software (R Core Team, 2019). The age model (**Supplementary Material**) used the ten AMS radiocarbon dates presented by Frozza et al. (2020), carried out on monospecific samples of planktonic Foraminifera, and the Laschamp geomagnetic excursion (J. Savian, personal communication, June 5, 2020) as an additional control point.

Past sea surface temperatures (SST) at 100 m water depth (SST_{100m}) were estimated using the modern analogue technique (MAT; Hutson, 1980) in the software PAST (version 4.05; Hammer et al., 2001). The paleo-SST_{100m} were calibrated with a dataset composed of: 1) relative abundances of planktonic Foraminifera of surface sediments from the South Atlantic Ocean extracted from the ForCenS database (Siccha and Kučera, 2017) as training data and 2) modern mean annual

temperature estimates for 100 m below sea level, obtained from the World Ocean Atlas 2013 (Locarnini et al., 2013) and extracted with the software Ocean Data View (Schlitzer, 2020). For the weighting parameter, we used the inverse dissimilarity based on the squared Chord dissimilarity index with a threshold of 0.28 and five analogues.

Sea surface paleo-productivity was assessed from the relative abundances of the species *Globigerinita glutinata* (Conan and Brummer, 2000; Souto et al., 2011) and the ratio between *Globigerina bulloides* and *Globigerinoides ruber* (*albus* and *ruber*) (*G.bull*:*G.rub*; Conan et al., 2002; Toledo et al., 2008). The OM flux to the seafloor, as a response to sea surface productivity, was estimated based on the benthic:planktonic Foraminifera ratio (B:P; Berger and Diester-Haass, 1988; Loubere, 1991; Gooday, 2002). While this parameter was applied on different size fractions in the past, with no clearly defined standard, it was shown that small size fraction differences do not impact analyses considerably (Schönfeld 2012; Weinkauf. 2018). As long as data for benthic and planktonic communities, as in our case, were extracted from the same sieve size fraction. The resulting B:P ratios will be comparable, indeed, being used in the literature (e.g., de Almeida et al., 2022). The ostracod valves abundances (number of valves in the >150 μm fraction per gram of sediment), and the $\delta^{13}C$ record of *Uvigerina* spp. ($\delta^{13}C_{Uvi}$; Mackensen, 2008) were also used to infer the OM flux to the seafloor. Part of these data (relative abundances of *G. bulloides* and *G. ruber*, $\delta^{13}C_{Uvi}$) were previously published by Frozza et al. (2020). For the $\delta^{13}C_{Uvi}$ measurements, approximately seven specimens of the benthic foraminiferal genus *Uvigerina* were selected from the 250 μm sediment fraction from each sample. The geochemical analyses were performed with a Thermo Scientific MAT-253 mass spectrometer, coupled to a Kiel IV carbonate device, by the Laboratory of Stable Isotopes of the University of California–Santa Cruz (SIL-UCSC). All results are expressed in *δ*-notation relative to the Vienna Pee-Dee Belemnite (VPDB) standard.

Dissolution effect proxies for this core were published by Suárez-Ibarra et al. (2021) and were based on the 1) the planktonic Foraminifera fragmentation intensity, which follows Berger (1970)'s fragments and broken shells counting, 2) the bulk sand fraction (%; Berger et al., 1982; Gonzales et al., 2017), 3) the number of whole planktonic Foraminifera tests per Gram of sediment (PF/g, Le and Shackleton, 1992), and 4) the relative $CaCO_3$ content of the sediment. Bulk sand contents were determined using a laser diffraction particle size analyzer Horiba Partica-LA-950 at the Climate Studies Center Centro de Estudo de Geologia Costeira e Oceânica (CECO) of the Universidade Federal do Rio Grande do Sul (UFRGS). The calcium carbonate content for the samples was determined by weight loss after reaction with 10% hydrochloric acid (HCl) at the Calcareous Microfossils Laboratory of the UFRGS.

All statistical analyses were conducted in the software PAST (version 4.05; Hammer et al., 2001). An overall relation between productivity and dissolution proxies was quantified using Spearman rank-order correlation. To objectively define phases of changing conditions through the analyzed time interval, a principal component analysis (PCA) on the correlation matrix including all the correlatable paleo-productivity proxies (PCA_P) and all dissolution proxies (PCA_D), respectively, was carried out. Using the first principal component of PCA_P ($PC1_P$), we objectively defined the borders between the three phases using a piecewise ordinary least-squares regression (OLS; Weinkauf et al., 2013): 1) We subdivided the $PC1_P$ vs age date into three subsets. The age-borders for each subset varied over a range of reasonable values (25.11–31.46 ka for the phase 1–Phase 2 border, 18.274–15.515 ka for the phase 2–Phase 3 border); 2) for each possible combination of phase borders, we calculated three independent OLS regression lines and their associated R^2-value; 3) we calculated the overall fit of the solution as the product of the three individual R^2-values; 4) the best phase border solution was the one that showed the highest overall R^2-value. The relationship between summer insolation and paleo-productivity, represented by the score of $PC1_P$, was analyzed using a reduced major axis regression. To study the interaction between productivity ($PC1_P$), bottom water intensity (reconstructed by the $^{231}Pa/^{230}Th$ ratio; McManus et al., 2004; Böhm et al., 2015), and dissolution ($PC1_D$), a multiple linear regression was carried out.

RESULTS

Sediments from core SAT-048A represent hemipelagic muds rich in carbonate. The average grain size of the samples is slightly sandy mud, and in general, ranges from slightly clayey mud to muddy sand in some cases. The recovered sediments correspond to the latest Pleistocene and early/middle Holocene muds of the Imbé formation. The age model (**Supplementary Material**) indicates sample ages ranging from 43 to 5 ka.

Planktonic Foraminifera species indicate two contrasting temporal distribution patterns: 1) species with higher abundances during the Late Pleistocene that decreased in abundance towards the Holocene, *Globigerinita glutinata* (**Figure 2C**), *Globigerina bulloides*, *Globoconella inflata*, and *Neogloboquadrina incompta* (**Supplementary Material**); 2) species with lower abundance values during the Late Pleistocene and higher abundances in the Holocene, *Globigerinoides ruber albus* and *G. ruber ruber*, *Trilobatus sacculifer*, *Globorotalia menardii*, *Globigerinella calida*, *Orbulina universa*, *Globorotalia tumida*, and *Globigerinoides conglobatus* (**Supplementary Material**).

The performance of the MAT (shown in the **Supplementary Material**) was generally very good, with an R^2 of 0.993. The annual mean paleo-SST_{100m} estimates for core SAT-048A are shown in **Figure 2E** (residuals shown in **Supplementary Material**). The annual mean reconstructions show lower values from the bottom of the core until 37 ka (on average 16°C), although the lowest value occurred at 25 ka (15.2°C). For the 37–15 ka period, the observed temperature variation was larger and fluctuated faster than during the rest of the record, spanning from 15 to 19°C. A warming trend is indicated to have occurred before the Last Glacial Maximum (LGM) at 25 ka, with values between 19 and 23°C and the warmest SST_{100m} value (22.5°C) observed at 7 ka.

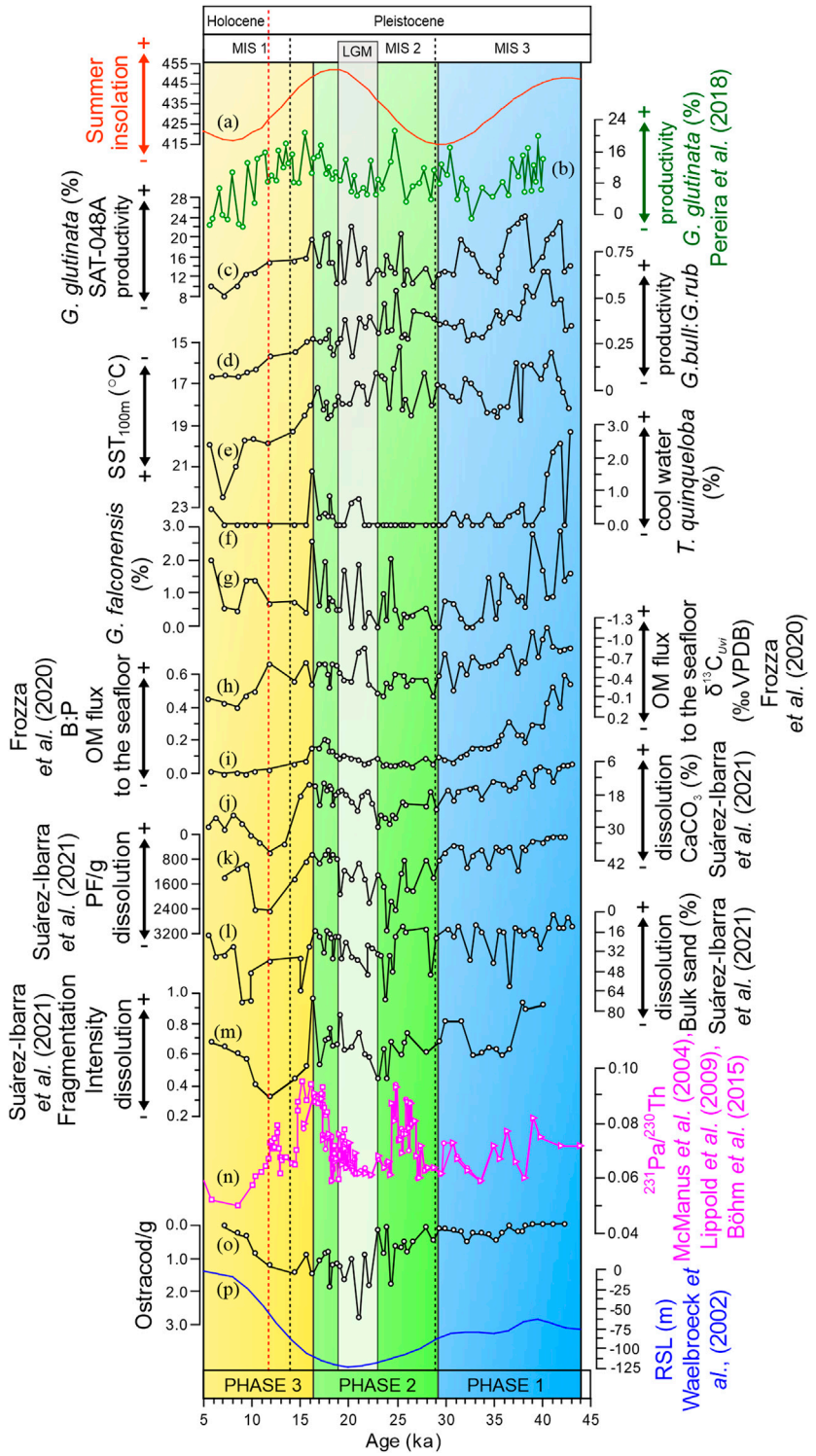

FIGURE 2 | Fluctuations in summer insolation, paleoenvironmental proxies for surface productivity, organic matter (OM) flux to the seafloor, $CaCO_3$ dissolution, Atlantic Meridional Overturning Circulation (AMOC) speed, and relative sea level. **(A)** Austral summer (February) insolation at 31° S (Laskar et al., 2004) **(B–C)** relative abundance of *G. glutinata* in cores GeoB2107-3 (b; Pereira et al., 2018) and SAT-048A (c; this study); **(D)** *G. bulloides*/*G. ruber* ratio (*G.bull*:*G.rub*); **(E)** SST_{100m} (°C) **(F–G)** relative abundance of *T. quinqueloba* (f) and *G. falconensis* (g); **(H)** $\delta^{13}C_{Uvi}$ (‰); **(I)** Benthic/Planktonic Foraminifera ratio (B:P) **(J)** $CaCO_3$ content of the sediment **(K)** number of planktonic Foraminifera tests per gram of sediment (PF/g) **(L)** sand bulk content (%) **(M)** fragmentation intensity **(N)** $^{231}Pa/^{230}Th$ values from McManus et al. (2004; squares), Lippold et al. (2009; circles), and Böhm et al. (2015; triangles) **(O)** Ostracods per gram of sediment (valves/g) **(P)** relative sea level (RSL; Waelbroeck et al., 2002). Note the inverted *y*-axes in (f), (g), and (i–k) to aid visualization. Proxies printed in black belong to sediment core SAT-048A. The three phases indicated in the plot are based on a principal component analysis of all productivity values, as shown in **Figure 3**.

All reconstructed paleoenvironmental proxies are shown in **Figure 2**. Paleo-productivity shows highest values in the 43–32/34 ka interval (superimposed on a decreasing trend), when reconstructed from *G. glutinata* abundances (**Figure 2C**) and the *G. bull*:*G.rub* ratios (**Figure 2D**), respectively. A relative plateau is witnessed for both proxies from 32/34 to 25 ka. The following time interval (25–17 ka) is characterized by an increasing trend. From 17 to 5 ka, *G. glutinata* and the *G. bull*:*G.rub* ratio show a decreasing trend with some of the lowest values of the entire record. The abundance of ostracods valves (**Figure 2**) is low during the 43–27 ka interval, then increases until 10 ka, and decreases afterward.

We ran a Spearman rank-order correlation to test the relationship between different productivity and dissolution proxies (**Table 1**). When the correlation was significant at the α = 0.05-level, the correlation coefficients ρ were categorized as either weak ($|\rho|$ = 0–0.33), medium ($|\rho|$ = 0.34–0.66), or strong ($|\rho|$ = 0.67–1). The paleo-productivity proxies *G. bull*/*G.rub* and *G. glutinata* (%) are not significantly correlated (p = 0.556), nevertheless, the correlations between productivity and OM flux proxies are all significant, ranging from medium to strong correlations. All the dissolution proxies are significantly correlated, also ranging from medium to strong. The correlation between productivity, OM flux and dissolution proxies are all significant, ranging from weak to strong relations, except for the FI vs *G. glutinata* (%) and the bulk sand (%) vs *G. glutinata* (%) proxies. The OM flux proxy Ostracod valves only showed a medium correlation with the *G. bull*/*G.rub* proxy and was also weakly–moderately correlated to three dissolution proxies.

These results indicate that all these proxies are also influenced by other environmental parameters, not just productivity and dissolution, respectively. Therefore, not any single proxy is suitable to provide an unbiased picture of the past environment. We, thus, aimed to develop synthetic productivity and dissolution proxies by combining all information in a PCA, which on its first axis amplifies the direction of largest variation in both parameters. PCAs were run both for productivity/OM flux (*G.bull*/*G.rub*, *G. glutinata* (%), $\delta^{13}C_{Uvi}$, and B:P; PCA_P) and dissolution proxies ($CaCO_3$, FI, PF/g, and bulk sand (%), PCA_D) on the data centered at zero and scaled to unit variance (**Supplementary Material**). The first principal component of the productivity/OM flux analysis ($PC1_P$) explains 62.14% of the variance in the data, while the first principal component for the dissolution proxies ($PC1_D$) captures 74.88% of data variance. The trends of $PC1_P$ and $PC1_D$ are shown in **Figure 3**, where the borders between three phases are based on the best solution of a set of piecewise OLS regressions with combinations of 70 feasible phase border scenarios. The loadings of the components on the principal component axes and the individual R^2-values from the piecewise regressions on which the phase borders are based are shown in the **Supplementary Material**. The optimal phase borders were determined by the R^2-product of 0.251 as follows: phase 1 (42.32–29.12 ka), where $PC1_p$ values decreased, indicating a reduction in productivity; phase 2 (28.56–16.15 ka), with stable to slightly increasing paleo-productivities; and phase 3 (15.51–5.77 ka), where productivity decreased again during the Holocene.

A reduced major axis regression between summer insolation and $PC1_P$ (**Supplementary Material**) yielded a significant (p < 0.001) correlation value of 0.476. A multiple linear regression between the independent variable $PC1_P$ and bottom water velocity ($^{231}Pa/^{230}Th$) and $PC1_D$ as dependent variable was carried out and results are shown in **Table 2**. Only $PC1_P$ is

TABLE 1 | Correlation coefficient (ρ) and statistical significance (p) for productivity and dissolution indices in sediment core SAT-048A from the western South Atlantic. *G. glutinata* (%): Relative abundance of *Globigerinita glutinata*; $\delta^{13}C_{Uvi}$: VPDB $\delta^{13}C$-values of shells of the benthic foraminifer genus *Uvigerina*; B:P: Ratio between benthic and planktonic Foraminifera; $CaCO_3$ (%): Relative $CaCO_3$ content of the sediment; FI: Planktonic foraminifera fragmentation intensity; PF/g: Number of Planktonic foraminiferal tests per gram of sediment; bulk sand (%): Relative sand content of the sediment; Ostracod valves: Number of Ostracod valves per Gram of sediment. Significant p-values (at α = 0.05) are highlighted in bold; for these, the correlation coefficient was marked as weak (italics), medium (bold), or strong (bold-italics).

	—	*G.bull/ G.rub*	*G. glutinata* (%)	$\delta^{13}C_{Uvi}$	B:P	$CaCO_3$ (%)	FI	PF/g	Sand bulk (%)
G. glutinata (%)	ρ	0.086	—	—	—	—	—	—	—
	p	0.556	—	—	—	—	—	—	—
$\delta^{13}C_{Uvi}$	ρ	**–0.441**	**–0.508**	—	—	—	—	—	—
	p	**0.002**	**<0.001**	—	—	—	—	—	—
B:P	ρ	**0.458**	**0.511**	***–0.795***	—	—	—	—	—
	p	**0.001**	**<0.001**	**<0.001**	—	—	—	—	—
$CaCO_3$ (%)	ρ	**–0.518**	**–0.430**	0.777	***–0.914***	—	—	—	—
	p	**<0.001**	**0.002**	**<0.001**	**<0.001**	—	—	—	—
FI	ρ	*0.329*	0.287	*–0.304*	**0.452**	**–0.567**	—	—	—
	p	**0.024**	**0.05**	**0.038**	**0.001**	**<0.001**	—	—	—
PF/g	ρ	**–0.371**	*–0.302*	***0.703***	***–0.811***	***0.831***	**–0.53**	—	—
	p	**0.009**	**0.035**	**<0.001**	**<0.001**	**<0.001**	**<0.001**	—	—
Sand bulk (%)	ρ	**–0.389**	–0.204	**0.473**	**–0.579**	**0.629**	**–0.606**	**0.576**	—
	p	**0.006**	0.16	**0.001**	**<0.001**	**<0.001**	**<0.001**	**<0.001**	—
Ostracod valves	ρ	**–0.354**	0.129	0.187	–0.229	0.24	**–0.334**	**0.479**	**0.304**
	p	**0.015**	0.387	0.207	0.121	0.104	**0.022**	**0.001**	**0.038**

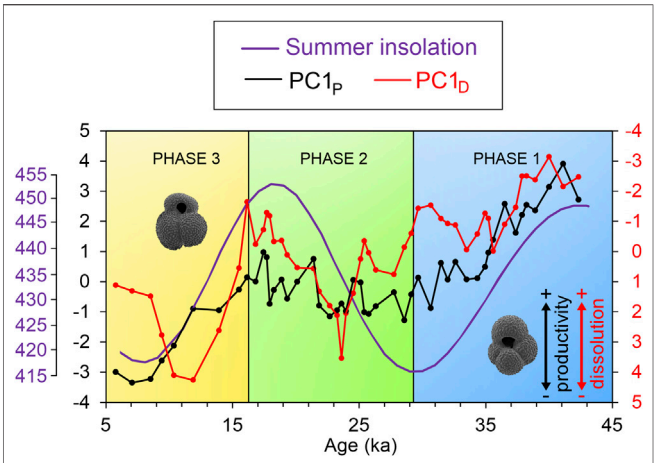

FIGURE 3 | Mean average for the first principal components of principal component analyses on all productivity proxies ($PC1_P$, black line) and all dissolution proxies ($PC1_D$, red line) in samples from sediment core SAT-048A in the South Atlantic. The purple line represents the Austral summer (February) insolation at 31° S (Laskar et al., 2004). The three phases defined by productivity trends (decreasing in phases 1 and 3, increasing in phase 2) are indicated. Dominant species of planktonic Foraminifera (*Globigerina bulloides* in phase 1, *Globigerinoides ruber* in phase 3) are indicated.

significantly influencing dissolution, and explains around 51% of the observed dissolution signal.

DISCUSSION

Radiocarbon Reversals

The occurrence of reversals in planktonic Foraminifera radiocarbon dates are not rare in the studies of the south Brazilian continental margin (SBCM, e.g., Sortor and Lund, 2011; Hoffman and Lund, 2012; Portilho-Ramos et al., 2019), being related either to: 1) morphological features of the sea bottom that remobilize sediments (such as turbidity or contour currents), or to 2) post-depositional chemical processes that affect the ^{14}C concentrations. The age model of core SAT-048A here presented (**Supplementary Figure S3**) indicates three intervals where samples yielded mean older ages (**Supplementary Table S3**). Nevertheless, the only significant difference is shown in the sample at 183.5 cm depth (31.1 ka before calibration), between 217 and 149 cm (27.8–22.7 ka), an interval constituted by hemipelagic mud rich in carbonate. According to Kowsmann et al. (2014), features of geological instability for the SBCM usually occurred between 28 and 15 ka, during relative low sea levels. Nevertheless, reversals of AMS ^{14}C planktonic Foraminifera dates from core SAT-048A are not associated to abrupt changes on the grain size record (**Supplementary Figure S4**). Moreover, the action of contour currents in the proximities of the study area (Viana, 2001; Duarte and Viana, 2007; Hernández-Molina et al., 2016) could, have gradually remobilized older particles (such as planktonic Foraminifera shells), masking the ^{14}C ages and increasing the temporal mixing.

Regarding the chemical processes, Rodrigues et al. (2020) reported older radiocarbon dates likely due to the upward migration of ^{14}C-depleted methane fluids from gas chimneys, as already reported for the south portion of the SBCM (Portilho-Ramos et al., 2018; Ketzer et al., 2020), which can precipitate in shell interstitial pores (Wycech et al., 2016), producing an alteration in the radiocarbon dates. Given the above, we tried to diminish the impact of radiocarbon reversals by using 1) a high number of correlation points (10 radiocarbon dates and one geomagnetic correlation point) and, 2) the *rbacon* package for software R, which implements Bayesian statistics that calculate mean ages for age model constructions, and has the capacity to deal with ^{14}C reversals.

Sea Surface Productivity

Three phases were defined from the $PC1_P$ trends (**Figure 3**). Phases 3 and 1 fall into time intervals with decreasing summer insolation values, while phase 2 is characterized by increasing summer insolation. The correlation between $PC1_P$ and summer insolation values is supported by the significant ($p < 0.001$) values of a reduced major axis regression ($r = 0.476$). This is supported by mechanisms, reported in the literature, that drove the paleo-productivity changes in the western South Atlantic. Portilho-Ramos et al. (2019) explained the high glacial productivity by a combination of short – but highly productive – austral summer upwelling periods and prolonged winter conditions favorable to the intrusion of RdlPE.

The short summer upwelling periods resulted from the enhanced northeasterly (NE) winds blowing along the shore during intervals with high summer insolation, both directly, by pushing surface waters offshore due to the Ekman transport (Chen et al., 2019), and indirectly by strengthening the BC meandering and, therefore, enhancing shelf break upwelling (Portilho-Ramos et al., 2015; Pereira et al., 2018). This interpretation is supported by the observed changes in the relative abundances of: 1) *Globigerinita glutinata* (Conan and Brummer, 2000; Souto et al., 2011), a species that feeds on

TABLE 2 | Results from a multiple linear regression between summarized paleo-productivity ($PC1_P$; first axis of a principal component analysis including all correlatable productivity proxies) and bottom water velocity $^{231}Pa/^{230}Th$ and summarized dissolution (first axis of a principal component analysis including all dissolution proxies) as dependent variable for sediment core SAT-048A from the South Atlantic. *p*-values significant at $\alpha = 0.05$ are indicated in bold.

	Coefficient	Standard error	*t*	*p*	R^2	*r*
Constant	0.286	1.425	0.201	0.842	—	—
$PC1_P$	−0.781	0.122	−6.402	**<0.001**	0.519	0.720
$^{231}Pa/^{230}Th$	−4.141	20.458	−0.202	0.840	0.091	0.302

diatoms (Schiebel and Hemleben, 2017) and therefore benefits from the glacial silicic acid-rich SACW intrusions in the area (Portilho-Ramos et al., 2019) (**Figure 2B,C**); 2) *Turborotalita quinqueloba*, which is associated with stronger intrusions of cooler SACW into the photic zone (Souto, et al., 2011; Lessa et al., 2014, 2016) (**Figure 2F**); and 3) *Globigerina falconensis*, which is associated with eutrophic conditions (Sousa et al., 2014) (**Figure 2G**). Additionally, a reconstructed SST_{100m} cooler than 20°C (Campos et al., 2000; Silveira et al., 2000; Castelão et al., 2004) along with a *G. bull*:*G.rub* ratio higher than 0.25 (Lessa et al., 2014) for the Pleistocene portion of the record indicates a constant presence of the SACW in the subsurface during the short austral upwelling of the late glacial.

Prolonged winter conditions involved prevalent southwesterly (SW) winds year-round which carried outflows from the Río de La Plata (RdlPE) (Pimenta et al., 2005; Piola et al., 2005) and other continental sources (Camaquã, Jaguarão, and Jacuí rivers)—presently converging in the PMLS–closer to the study area (Piola et al., 2000; Nagai et al., 2014). Strengthened SW winds would also displace the BMC to a location closer to the area (Gonzalez-Silvera et al., 2006), which is supported by the higher relative abundances of *Globoconella inflata* and *Neogloboquadrina incompta* (**Supplementary Material**). The abundances of these two species can be interpreted as an indicator for a BMC closer to the study area (Boltovskoy et al., 1996), induced by the enhanced SW winds during the late last glacial.

Several authors suggest that during low relative sea levels (glacial times), periods of higher nutrient availability and increased terrigenous sediment input were favored due to the more offshore position of the BC and the exposure of the continental shelf (Mahiques et al., 2007; Gu et al., 2017; Pereira et al., 2018, Portilho-Ramos et al., 2019). Moreover, the Río de la Plata (Lantzsch et al., 2014) and Jacuí and Camaquã river paleo-drainages (Weschenfelder et al., 2014) were closer to the study area during this interval (higher influence of the PMLS). Higher Fe/Ca values (Heil, 2006), higher relative abundances of eutrophile dinoflagellate cysts species (Gu et al., 2017), and high terrestrial palynomorph proportions (Bottezini et al., 2022), are all evidence of the greater influence of continental outflow in the study area under lower relative sea levels during the late last glacial (which approximately corresponds to our phases 1 and 2). Medium paleo-productivity estimates during the LGM (relative sea level approximately 120 m lower; **Figure 3**) stand in contrast to the higher sea levels during phase 1 (relative sea level approximately 75 m below, Waelbroeck et al., 2002), where higher (terrigenous-related) fertilization was expected due the lower eustatic sea level. This suggests a different influence for the continental terrigenous fertilization for mid-depth cores retrieved from the continental slope. In contrast, for the Holocene, the higher relative sea level and onshore displacement of the BC, as well as the absence of the SACW, inhibited the photic zone fertilization, leading to oligotrophic conditions (Mahiques et al., 2007), witnessed in the phase 3.

Organic Matter Flux to the Seafloor and Carbonate Dissolution

Orbital to suborbital climate cycles can influence the abundance of deep-sea benthic communities (Cronin et al., 1999). Since abundance fluctuations of benthic Foraminifera and ostracods are related to variations in particulate organic carbon fluxes to the seafloor (Smith et al., 1997; Rex et al., 2006; Rex and Etter, 2010), their use as surface paleo-productivity indicators is widespread (Nees et al., 1999; Herguera, 2000; Rasmussen et al., 2002; Gooday, 2003; Yasuhara et al., 2012). The surface productivity fluctuations, indicated by the *G. glutinata* abundance and *G. bull*:*G.rub*, are significantly correlated to those of the OM flux recorded by the B:P ratio and the $\delta^{13}C_{Uvi}$ (**Table 1**). This effective OM export from the surface to the seafloor revealed a high benthic–pelagic coupling (Toledo et al., 2007). The B:P changes are accompanied by a similar trend in inverse $\delta^{13}C_{Uvi}$ (**Figure 2H,I**), which are expected to decrease when higher OM fluxes, rich in ^{12}C due to the preferential incorporation of the light isotope during photosynthesis (Wefer et al., 1999), reach the seabed (Ravello and Hillaire-Marcel, 2007). Nevertheless, the abundance of ostracod valves (**Figure 2**) was only significantly correlated with *G. bull*:*G. rub* ratio values. Intriguingly, ostracod valves showed a hump-shaped relation with productivity (Yasuhara et al., 2012), where values increased under moderate OM supply and declined under very low and very high productive conditions. This is because under high-productivity scenarios, oxygen levels at the sea floor tend to decrease and deep-sea ostracods, which are mostly epifaunal (Jöst et al., 2017), would not respond well to such an environment. On the other hand, ostracods valves had a significant ($p > 0.001$) strong correlation ($\rho = -0.701$) with paleo-bathymetric variations, where abundances decreased exponentially with water depth increase (Rex et al., 2006; Rex and Etter, 2010).

Dissolution indicators suggest higher calcium carbonate dissolution during the beginning of Phases 1 and the transition of phases 2 and 3 (**Figure 2**, **3**), related to the OM flux. Enhanced dissolution could theoretically be triggered by two different processes: 1) increase in CO_2 concentrations (decreasing the water pH) due to the remineralization of OM at the seafloor (Jahnke et al., 1997; Schiebel, 2002) or 2) changes in the bottom water mass configuration related to AMOC dynamics (speed or geometry). Although the B:P ratios are also used as a dissolution indicator (Berger and Diester-Haass, 1988; Conan et al., 2002), Kučera (2007) states that this is only applicable for abyssal depths. We also have evidence from regional studies (Petró et al., 2018b) that benthic foraminifera are more prone to dissolution in this setting than planktonic foraminifers. This means that our observed B:P ratios are, in the worst case, an underestimate of the real situation because dissolution would attenuate it.

In the SBCM basins, the $\delta^{13}C_{Uvi}$ values have been used to infer oscillations of OM input (Toledo et al., 2007; Dias et al., 2018; Rodrigues et al., 2018; Frozza et al., 2020). Nevertheless, $\delta^{13}C_{Uvi}$ values are influenced by several factors, such as

accumulation rates of organic carbon, regional changes of water masses, the global carbon cycle, photosynthesis respiration processes, temperature, and pH (Ravelo and Hillaire-Marcel, 2007; Hesse et al., 2014). Calcite dissolution has, in contrast, no influence on the foraminiferal $\delta^{13}C$ (Petró et al., 2018b). Lund et al. (2015) suggested that lower values of benthic $\delta^{13}C$ during glacial times are associated with a weak AMOC. Nevertheless, the fluctuations of $\delta^{13}C_{Uvi}$ and the carbonate preservation could be the result of the interplay between the OM flux and water masses changes.

Based on εNd in planktonic Foraminifera at mid-depths in the western South Atlantic, Howe et al. (2016, 2018) showed variations of water masses at intermediate depths of 1,000–1,200 m (cores GeoB2107-3 and KNR159-3-36GGC) during the Holocene, and at 2,200 m (core GL-1090) since Heinrich Stadial 1. After the Heinrich Stadial 1, core GL-1090s εNd values decreased, becoming less radiogenic and more related to modern upper NADW values, while cores GeoB2107-3's and KNR159-3-36GGC's εNd values increased after about 10 ka, becoming more radiogenic and showing more affinity with modern AAIW. Sediment core GeoB2104-3 (1,500 m) is located between these aforementioned cores, at the same depth as sediment core SAT-048A on which the present study is based, at its εNd values remained stable during the 25–4 ka interval (Howe J. N. W. et al., 2016). This indicates that SAT048A's $\delta^{13}C_{Uvi}$ fluctuations were produced by the OM bottom flux rather than water masses reconfigurations–at least throughout the studied time interval.

In addition, the $^{231}Pa/^{230}Th$ ratio (**Figure 2N**) has been used to track the intensity of the AMOC (McManus et al., 2004; Lippold et al., 2009; Böhm et al., 2015), where lower values indicate a strengthened AMOC. During periods of high $^{231}Pa/^{230}Th$ values and indicating AMOC slowdown (like Heinrich Stadials), a higher concentration of respired CO_2 is accumulated in seafloor water masses. As proposed by Howe JN. et al. (2016), this is a possible explanation for the intervals of increased calcium carbonate dissolution. Nevertheless, the results from the multiple linear regression (**Table 2**) point to paleo-productivity as the main factor to influence dissolution. The multiple linear regression designates the sea surface productivity and OM flux to the seafloor as the principal agents of the calcium carbonate dissolution (**Figure 4**), at least for the 25–4 ka interval, which is related to changes in the summer insolation. This is true, even including the decoupling between productivity and dissolution visible in our data during the last ca. 5 kyrs (**Figure 3**). We hypothesize that the increasing dissolution at constantly low productivity, high AMOC rates (**Figure 2N**) and stable water mass configuration during this last segment of the record is related to the rising temperatures in this period, which increased the Mg/Ca values of the biogenic carbonate. Since higher Mg content facilitates dissolution of calcite, shells produced during this time would be more prone to dissolution, so that other environmental parameters were no longer the major factors that affected calcite dissolution. Future studies should investigate possible changes in bottom water mass configuration through εNd isotopes for the entire

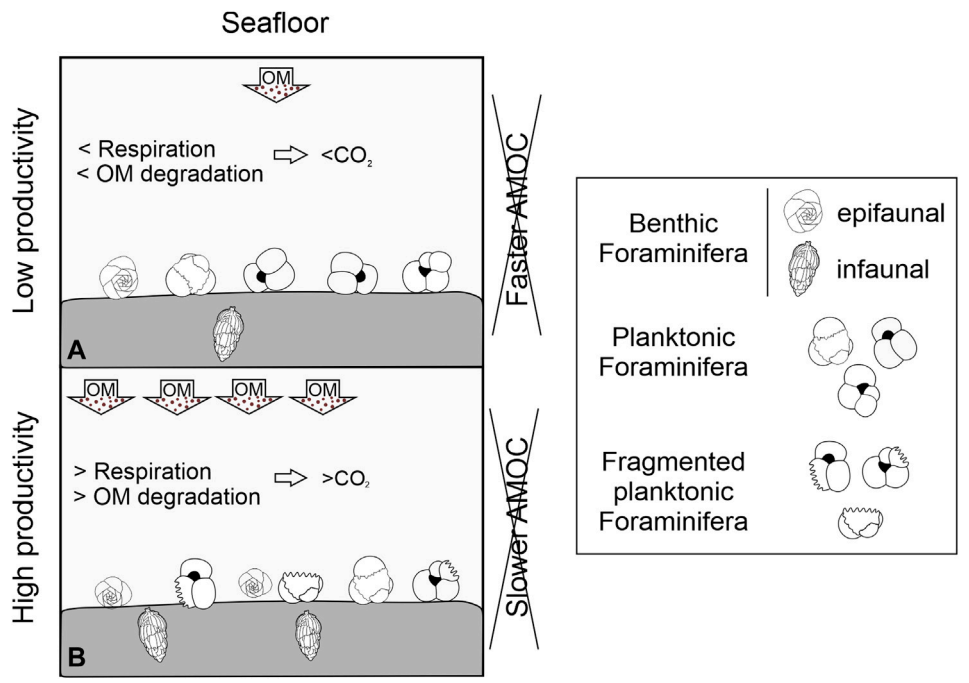

FIGURE 4 | Schematic representation of two possible end-member scenarios affecting carbonate dissolution on deep-water assemblages of sediment core SAT-048A (South Atlantic). The paleoceanographic changes could be triggered by: **(A)** Low organic matter (OM) inputs to the seafloor, which results in lower benthic abundances and better preservation of $CaCO_3$, or **(B)** high OM input that increases benthic abundances and CO_2 concentrations, decreases the seawater pH, and dissolves the planktonic Foraminifera tests (fragmentation on benthic Foraminifera was not assessed).

studied section to 1) increase our understanding of productivity-related carbon dissolution at the sea floor and 2) quantify the impact of changes of the biological pump on the total organic carbon and biogenic carbonates burial. This will considerably aid the understanding of the glacial inorganic carbon sequestration.

CONCLUSION

Planktonic Foraminifera assemblages from sediment core SAT-048A, along with geochemical analyses and sedimentological data, enabled us to reconstruct the surface and bottom water conditions that occurred during the last 43 kyrs in the western South Atlantic, and to contextualize the related production-dissolution processes in the area. The Pleistocene–Holocene transition was characterized by a shift from a glacial eutrophic environment to more oligotrophic post-glacial conditions, as suggested by the *G. bull*:*G.rub* ratio and the SST_{100m}, where intrusions of the nutrient-rich SACW were inhibited and the RdlPE and local river discharges (nowadays PMLS) were placed further away from the core site. The orbital-scale fluctuations of the upwelling dynamics (indicated by the relative abundances of *G. glutinata* and *T. quinqueloba*), modulated by insolation and NE wind changes, directly influenced the surface productivity and the OM fluxes to the seafloor (as shown by the B:P ratio and $\delta^{13}C_{Uvi}$). Imposed on the mechanisms behind the glacial–interglacial changes, stronger NE winds, generated by higher summer insolation, fertilized the photic zone, strengthened the BC, increased meandering, and enhanced intrusion of cooler and nutrient-richer waters into the subsurface layers. The enhanced upwelling conditions were also registered at the sea floor, where the bacterial decomposition of OM and the respiration of higher abundances of benthic communities increased the CO_2 concentration, which created more acidic conditions that caused different levels of carbonate dissolution, evidenced in the fragmentation of the planktonic Foraminifera tests. While changes in the bottom water masses could hypothetically cause the calcium carbonate dissolution, εNd analyses in a nearby sediment core at the same depth suggest no changes in the bottom water mass influence for the 25–4 ka interval, pointing to sea surface productivity and the intensity of the AMOC as possible causes of the carbonate dissolution. A multiple linear regression between summarized productivity and $^{231}Pa/^{230}Th$ (proxy for AMOC intensity), indicates that productivity is the main controlling factor of calcium carbonate dissolution. The continental influence (i.e., terrigenous input) must be better assessed in future studies, since, in contrast to expectations, no increased productivity was registered during the lowest relative sea level (LGM), when terrestrial input should have been highest. The dissolution of planktonic Foraminifera tests, induced by an enhanced biological pump (evidenced in the high glacial surface productivity and the high OM fluxes to the sea floor), must call the attention to future research, since a strong biological pump influences biogenic carbonate burial and CO_2 sequestration and burial at the seafloor.

DATA AVAILABILITY STATEMENT

The original contributions presented in the study are included in the article/**Supplementary Material**, further inquiries can be directed to the corresponding author.

AUTHOR CONTRIBUTIONS

JYSI and MAGP conceptualized the study; JYSI curated the data; JYSI conducted the formal analyses; MAGP and MFGW acquired funding; JYSI, CFF and PLP investigated the samples; JYSI, CFF, MFGW, MAGP developed the methods; MAGP provided the resources; MFGW and MAGP supervised the project; MFGW and MAGP validated the results; JYSI visualized the results; JYSI wrote the original draft; JYSI, CFF, PLP, SMP, MFGW, and MAGP reviewed and edited the manuscript.

FUNDING

This work was supported by the Brazilian Coordination of Higher Education Staff Improvement (CAPES) (grant number 88887.091729/2014-01), the Brazilian National Council for Scientific and Technological Development (CNPq) (grant number 407922/2016-4) and the PRIMUS program (grant number PRIMUS/20/SCI/019) and PROGRES Q45 grants, Charles University. JS-I was supported by the CNPq (MSc) and the STARS programs (PhD) from the Charles University, respectively. CF was supported by the CAPES (PhD).

ACKNOWLEDGMENTS

The authors are grateful to Gilberto Griep (*in memoriam*) for his commitment to making sediment cores retrieved for the industry available to the scientific community. We thank Dr. Igor Venâncio (Instituto Nacional de Pesquisas Espaciais, Brazil), Dr. João Coimbra (Universidade Federal do Rio Grande do Sul, Brazil), Dr. Geise dos Anjos Zerfass (Petróleo Brasileiro S.A., Brazil), Editor Dr. Jacek Raddatz and two reviewers, Dr. Selvaraj and Dr. Patrick Grunert for comments and suggestions that helped to improve this manuscript.

SUPPLEMENTARY MATERIAL

The Supplementary Material for this article can be found online at: https://www.frontiersin.org/articles/10.3389/feart.2022.830984/full#supplementary-material

REFERENCES

Bé, A. W. H. (1967). Foraminifera Families: Globigerinidae and Globorotaliidae, Conseil Permanent International Pour L'exploration De La Mer, Zooplankton. *Charlottenlund, Denmark: Conseil Int. pour l'Exploration*

Bé, A. W. H., Hemleben, C., Anderson, O. R., Spindler, M., Hacunda, J., Tuntivate-Choy, S., et al. (1977). Laboratory and Field Observations of Living Planktonic Foraminifera. *Micropaleontology* 23 (2), 155–179. doi:10.2307/1485330

Berger, W. H., Bonneau, M. C., and Parker, F. L. (1982). Foraminifera on the Deep-Sea Floor: Lysocline and Dissolution Rate. *Oceanologica acta* 5 (2), 249.

Berger, W. H., and Diester-Haass, L. (1988). Paleoproductivity: the Benthic/planktonic Ratio in Foraminifera as a Productivity index. *Mar. Geology.* 81, 15–25. doi:10.1016/00254813227(88)90014-X

Berger, W. H. (1970). Planktonic Foraminifera: Selective Solution and the Lysocline. *Mar. Geology.* 8, 111–138. doi:10.1016/0025-3227(70)90001-0

Blaauw, M., and Christen, J. A. (2011). Flexible Paleoclimate Age-Depth Models Using an Autoregressive Gamma Process. *Bayesian Anal.* 6 (3), 457–474. doi:10.1214/1148410.1214/ba/1339616472

Böhm, E., Lippold, J., Gutjahr, M., Frank, M., Blaser, P., Antz, B., et al. (2015). Strong and Deep Atlantic Meridional Overturning Circulation during the Last Glacial Cycle. *Nature* 517, 73–76. doi:10.1038/nature14059

Bolli, H. M., and Saunders, J. B. (1989). "Oligocene to Holocene Low Latitude Planktic Foraminifera," in *Plankton Stratigraphy* (K. Cambridge Earth Sciences SeriesCambridge University Press), 1, 155

Boltovskoy, E., Boltovskoy, D., Correa, N., and Brandini, F. (1996). Planktic Foraminifera from the Southwestern Atlantic (30 °-60 °S): Species-specific Patterns in the Upper 50 M. *Mar. Micropaleontology* 28, 53–72. doi:10.1016/0377-8398(95)00076-3

Bottezini, S. R., Leonhardt, A., Diniz, D., and Gonçalves, J. F. (2022). Climatic and Vegetational Dynamics in Southern Brazil between 47.8 and 7.4 Cal Ka BP: a Palynological Analysis. *Revista Brasileira de Paleontologia* 24 (4), 345–356. doi:10.4072/rbp.2021.4.05

Brummer, G. J. A., and van Eijden, A. J. M. (1992). "Blue-ocean" Paleoproductivity Estimates from Pelagic Carbonate Mass Accumulation Rates. *Mar. Micropaleontology* 19, 99–117. doi:10.1016/0377-8398(92)90023-D

Campos, E. J. D., Gonçalves, J. E., and Ikeda, Y. (1995). Water Mass Characteristics and Geostrophic Circulation in the South Brazil Bight: Summer of 1991. *J. Geophys. Res.* 100 (9), 18537–18550. doi:10.1029/95jc01724

Campos, E. J. D., Velhote, D., and da Silveira, I. C. A. (2000). Shelf Break Upwelling Driven by Brazil Current Cyclonic Meanders. *Geophys. Res. Lett.* 27, 751–754. doi:10.1029/1999GL010502

Castelão, R. M., Campos, E. J. D., and Miller, J. L. (2004). A Modelling Study of Coastal Upwelling Driven by Wind and Meanders of the Brazil Current. *J. Coastal Res.* 203, 662–671. doi:10.2112/1551-5036(2004)20662AMSOCU2.0.CO;2

Chen, H.-H., Qi, Y., Wang, Y., and Chai, F. (2019). Seasonal Variability of SST Fronts and Winds on the southeastern continental Shelf of Brazil. *Ocean Dyn.* 69, 1387–1399. doi:10.1007/s10236-019-01310-1

Conan, S. M.-H., and Brummer, G. J. A. (2000). Fluxes of Planktic Foraminifera in Response to Monsoonal Upwelling on the Somalia Basin Margin. *Deep Sea Res. Part Topical Stud. Oceanography* 47 (9-11), 2207–2227. doi:10.1016/s09670645(00)00022-99

Conan, S. M.-H., Ivanova, E., and Brummer, G. J. (2002). Quantifying Carbonate Dissolution and Calibration of Foraminiferal Dissolution Indices in the Somali Basin. *Mar. Geology.* 182 (3-4), 325–349. doi:10.1016/s0025-3227(01)00238-9

Cronin, T. M., De Martino, D. M., Dwyer, G. S., and Rodriguez-Lazaro, J. (1999). Deepsea Ostracode Species Diversity: Response to Late Quaternary Climate Change. *Mar. Micropaleontology* 37 (3-4), 231–249. doi:10.1016/S0377-8398(99)00026-2

de Almeida, F. K., de Mello, R. M., Rodrigues, A. R., and Bastos, A. C. (2022). Bathymetric and Regional Benthic Foraminiferal Distribution on the Espírito Santo Basin Slope, Brazil (SW Atlantic). *Deep Sea Res. Oceanographic Res. Pap.* 181, 103688. doi:10.1016/j.dsr.2022.103688

de Oliveira Lessa, D. V., Ramos, R. P., Barbosa, C. F., Da Silva, A. R., Belem, A., Turcq, B., et al. (2014). Planktonic Foraminifera in the Sediment of a Western Boundary Upwelling System off Cabo Frio, Brazil. *Mar. Micropaleontology* 106, 55–68. doi:10.1016/j.marmicro.2013.12.003

Dias, B. B., Barbosa, C. F., Faria, G. R., Seoane, J. C. S., and Albuquerque, A. L. S. (2018). The Effects of Multidecadal-Scale Phytodetritus Disturbances on the Benthic Foraminiferal Community of a Western Boundary Upwelling System, Brazil. *Mar. Micropaleontology* 139, 102–112. doi:10.1016/j.marmicro.2017.12.003

Duarte, C. S. L., and Viana, A. R. (2007). Santos Drift System: Stratigraphic Organization and Implications for Late Cenozoic Palaeocirculation in the Santos Basin, SW Atlantic Ocean. *Geol. Soc.* 276, 171–198. doi:10.1144/GSL.SP.2007.276.01.09

EPICA Community Members. (2004). Eight Glacial Cycles from an Antarctic Icecore. *Nature* 429, 623–628. doi:10.1038/nature02599

Frenz, M., Höppner, R., Stuut, J.-B. W., Wagner, T., and Henrich, R. (2003). Surface Sediment Bulk Geochemistry and Grain-Size Composition Related to the Oceanic Circulation along the South American Continental Margin in the Southwest Atlantic. In: *The South Atlantic in the Late Quaternary*, *Wefer, G., Mulitza, S., Ratmeyer. V.*, Springer-Verlag, Berlin, Heidelberg, New York, Tokyo, v. (eds), pp. 347–373.doi:10.1007/978-3-642-18917-3_17

Frenz, M., and Henrich, R. (2007). Carbonate Dissolution Revealed by silt Grain-Size Distribution: Comparison of Holocene and Last Glacial Maximum Sediments from the Pelagic South Atlantic. *Sedimentology* 54, 391–404. doi:10.1111/j.1365-3091.2006.00841.x

Frozza, C. F., Pivel, M. A. G., Suaáez-Ibarra, J. Y., Ritter, M. N., and Coimbra, J. C. (2020). Bioerosion on Late Quaternary Planktonic Foraminifera Related to Paleoproductivity in the Western South Atlantic. *Paleoceanography and Paleoclimatology*, e2020PA003865. doi:10.1029/2020pa003865

Gonzales, M. V., de Almeida, F. K., Costa, K. B., Santarosa, A. C. A., Camillo, E., de Quadros, J. P., et al. (2017). Help Index: Hoeglundina Elegans Preservation Index for Marine Sediments in the Western South Atlantic. *J. Foraminiferal Res.* 47, 56–69. doi:10.2113/gsjfr.47.1.56

Gonzalez-Silvera, A., Santamaría-del-Angel, E., and Millán-Núñez, R. (2006). Spatial and Temporal Variability of the Brazil-Malvinas Confluence and the La Plata Plume as Seen by SeaWIFS and AVHRR Imagery. *J. Geophys. Res.* 111, C06010. doi:10.1029/2004JC002745

Gooday, A. J. (2003). Benthic Foraminifera (Protista) as Tools in Deep-Water Palaeoceanography: Environmental Influences on Faunal Characteristics. *Adv. Mar. Biol.* 46, 1–90. doi:10.1016/S0065-28810(03)46002-110.1016/s0065-2881(03)46002-1

Gooday, A. J. (2002). Biological Responses to Seasonally Varying Fluxes of Organic Matter to the Ocean Floor: A Review. *J. oceanography* 58, 305–332. doi:10.1023/A:1015865826379

Gordon, A. L., and Greengrove, C. L. (1986). Geostrophic Circulation of the Brazil-Falkland confluence. *Deep Sea Res. A. Oceanographic Res. Pap.* 33 (5), 573–585. doi:10.1016/0198-0149(86)90054-3

Gu, F., Zonneveld, K. A. F., Chiessi, C. M., Arz, H. W., Pätzold, J., and Behling, H. (2017). Long-term Vegetation, Climate and Ocean Dynamics Inferred from a 73,500 Years Old marine Sediment Core (GeoB2107-3) off Southern Brazil. *Quat. Sci. Rev.* 172, 55–71. doi:10.1016/j.quascirev.2017.06.028

Hales, B. (2003). Respiration, Dissolution and the Lysocline. *Paleoceanography* 18 (4), 1–14. doi:10.1029/2003PA000915

Hammer, O., David, A. T., and Paul, D. (2001). Past: Paleontological Statistics Software Package for Education and Data Analysis. *Palaeontol. Electronica* 4 (1), 1–9

Heil, G. M. N. (2006). Abrupt Climate Shifts in the Western Tropical to Subtropical Atlantic Region during the Last Glacial. PhD Thesis. *Universtity of Bremen* 121.

Hemleben, C., Spindler, M., and Anderson, O. R. (1989). New York: Estados Unidos de América: Springer. doi:10.1007/978-1-4612-3544-6Modern Planktonic Foraminifera

Herguera, J. C. (2000). Last Glacial Paleoproductivity Patterns in the Eastern Equatorial Pacific: Benthic Foraminifera Records. *Mar. Micropaleontology* 40 (3), 259–275. doi:10.1016/S0377-8398(00)00041-4

Hernández-Molina, F. J., Soto, M., Piola, A. R., Tomasini, J., Preu, B., Thompson, P., et al. (2016). A Contourite Depositional System along the Uruguayan continental Margin: Sedimentary, Oceanographic and Paleoceanographic Implications. *Mar. Geology.* 378, 333–349. doi:10.1016/j.margeo.2015.10.008

Hesse, T., Wolf-Gladrow, D., Lohmann, G., Bijma, J., Mackensen, A., and Zeebe, R. E. (2014). Modelling $\delta^{13}C$ in Benthic Foraminifera: Insights from Model Sensitivity Experiments. *Mar. Micropaleontology* 112, 50–61. doi:10.1016/j.marmicro.2014.08.001

Hoffman, J. L., and Lund, D. C. (2012). Refining the Stable Isotope Budget for Antarctic Bottom Water: New Foraminiferal Data from the Abyssal Southwest Atlantic. *Paleoceanography* 27, PA1213. doi:10.1029/2011PA002216

Hogg, N. G., Owens, W. B., Siedler, G., and Zenk, W. (1996). Circulation in the Deep Brazil BasinThe South Atlantic: Present and Past Circulation. in *Berlin Heidelberg*. Editors G. Wefer, W. H. Berger, G. Siedler, and D. J. Webb (Springer-Verlag), 13–44.

Howe, J. N., Piotrowski, A. M., Noble, T. L., Mulitza, S., Chiessi, C. M., and Bayon, G. (2016a). North Atlantic Deep Water Production during the Last Glacial Maximum. *Nat. Commun.* 7, 11765. doi:10.1038/ncomms11765

Howe, J. N. W., Huang, K.-F., Oppo, D. W., Chiessi, C. M., Mulitza, S., Blusztajn, J., et al. (2018). Similar Mid-depth Atlantic Water Mass Provenance during the Last Glacial Maximum and Heinrich Stadial 1. *Earth Planet. Sci. Lett.* 490, 51–61. doi:10.1016/j.epsl.2018.03.006

Howe, J. N. W., Piotrowski, A. M., Oppo, D. W., Huang, K. F., Mulitza, S., Chiessi, C. M., et al. (2016b). Antarctic Intermediate Water Circulation in the South Atlantic over the Past 25,000 Years. *Paleoceanography* 31, 1302–1314. doi:10.1002/2016PA002975

Hutson, W. H. (1980). The Agulhas Current during the Late Pleistocene: Analysis of Modern Faunal Analogs. *Science* 207, 64–66. doi:10.1126/science.207.4426.64

Jahnke, R. A., Craven, D. B., McCorkle, D. C., and Reimers, C. E. (1997). $CaCO_3$ Dissolution in California continental Margin Sediments: The Influence of Organic Matter Remineralization. *Geochimica et Cosmochimica Acta* 61 (17), 3587–3604. doi:10.1016/S00167037(97)00184-110.1016/s0016-7037(97)00184-1

Jöst, A. B., Yasuhara, M., Okahashi, H., Ostmann, A., Arbizu, P. M., and Brix, S. (2017). Vertical Distribution of Living Ostracods in Deep-Sea Sediments, North Atlantic Ocean. *Deep Sea Res. Part Oceanographic Res. Pap.* 122, 113–121. doi:10.1016/j.dsr.2017.01.012

Jouzel, J., Masson-Delmotte, V., Cattani, O., Dreyfus, G., Falourd, S., Hoffmann, G., et al. (2007). Orbital and Millennial Antarctic Climate Variability over the Past 800,000 Years. *Science* 317, 793–796. doi:10.1126/science.1141038

Kemle-von Mücke, S., and Hemleben, C. (1999). *Foraminifera*. Editors D. Boltovskoy (Leiden: Backhuys Publishers), 43–73

Ketzer, M., Praeg, D., Rodrigues, L. F., Augustin, A., Pivel, M. A. G., Rahmati-Abkenar, M., et al. (2020). Gas Hydrate Dissociation Linked to Contemporary Ocean Warming in the Southern Hemisphere. *Nat. Commun.* 11, 3788. doi:10.1038/s41467-020-17289-z

Kowsmann, R. O., Lima, A. C., and Vicalvi, M. A. (2014). Feições indicadoras de instabilidade geológica no talude continental e no Platô de São Paulo. in *Geologia e Geomorfologia*. Editor R. O. Kowsmann (Rio de Janeiro: Elsevier), 71–98. doi:10.1016/B978-85-352-6937-6.50012-4

Kucera, M. (2007). "Chapter Six Planktonic Foraminifera as Tracers of Past Oceanic Environments," in *Proxies in Late Cenozoic Paleoceanography of Developments in Marine Geology*. Editors C. Hillaire-Marcel, A. de Vernal, and H. Chamley (Amsterdam: Elsevier), 1, 213–262. doi:10.1016/s1572-5480(07)01011-1

Lantzsch, H., Hanebuth, T. J. J., Chiessi, C. M., Schwenk, T., and Violante, R. A. (2014). The High-Supply, Current-Dominated continental Margin of southeastern South America during the Late Quaternary. *Quat. Res.* 81 (2), 339–354. doi:10.1016/j.yqres.2014.01.003

Laskar, J., Robutel, P., Joutel, F., Gastineau, M., Correia, A. C. M., and Levrard, B. (2004). A Long-Term Numerical Solution for the Insolation Quantities of the Earth. *A&A* 428 (1), 261–285. doi:10.1051/0004-6361:20041335

Le, J., and Shackleton, N. J. (1992). Carbonate Dissolution Fluctuations in the Western Equatorial Pacific during the Late Quaternary. *Paleoceanography* 7, 21–42. doi:10.1029/91PA02854

Lessa, D. V., Venancio, I. M., dos Santos, T. P., Belem, A. L., Turcq, B. J., Sifeddine, A., et al. (2016). Holocene Oscillations of Southwest Atlantic Shelf Circulation Based on Planktonic Foraminifera from an Upwelling System (Off Cabo Frio, Southeastern Brazil). *The Holocene* 26 (8), 1175–1187. doi:10.1177/0959683616638433

Lippold, J., Gruetzner, J., Winter, D., Lahaye, Y., Mangini, A., and Christl, M. (2009). Does Sedimentary $^{231}Pa/^{230}Th$ from the Bermuda Rise Monitor Past Atlantic Meridional Overturning Circulation. *Geophysical Research Letters*. 36. L12601. doi:10.1029/2009GL038068

Locarnini, R. A., Mishonov, A. V., Antonov, J. I., Boyer, T. P., Garcia, H. E., Baranova, O. K., et al. (2013). *World Ocean Atlas*. Editor A. Mishonov 2013.

Lorius, C., Jouzel, J., Raynaud, D., Hansen, J., and Treut, H. L. (1990). The Ice-Core Record: Climate Sensitivity and Future Greenhouse Warming. *Nature* 347, 139–145. doi:10.1038/347139a0

Loubere, P. (1991). Deep-sea Benthic Foraminiferal Assemblage Response to a Surface Ocean Productivity Gradient: a Test. *Paleoceanography* 6, 193–204. doi:10.1029/90PA02612

Lund, D. C., Tessin, A. C., Hoffman, J. L., and Schmittner, A. (2015). Southwest Atlantic Water Mass Evolution during the Last Deglaciation. *Paleoceanography* 30 (5), 477–494. doi:10.1002/2014pa002657

Mackensen, A. (2008). On the Use of Benthic Foraminiferal $\delta^{13}C$ in Palaeoceanography: Constraints from Primary Proxy Relationships. *Geol. Soc. Lond. Spec. Publications* 303, 121–133. doi:10.1144/SP303.9

Mahiques, M. M., Fukumoto, M. M., Silveira, I. C. A., Figueira, R. C. L., Bícego, M. C., Lourenço, R. A., et al. (2007). Sedimentary Changes on the Southeastern Brazilian Upper Slope during the Last 35,000 Years. *Acad. Bras. Ciênc.* 79 (1), 171–181. doi:10.1590/S0001-37652007000100018

McManus, J. F., Francois, R., Gherardi, J.-M., Keigwin, L. D., and Brown-Leger, S. (2004). Collapse and Rapid Resumption of Atlantic Meridional Circulation Linked to Deglacial Climate Changes. *Nature* 428 (6985), 834–837. doi:10.1038/nature02494

Milliman, J. D., Troy, P. J., Balch, W. M., Adams, A. K., Li, Y.-H., and Mackenzie, F. T. (1999). Biologically Mediated Dissolution of Calcium Carbonate above the Chemical Lysocline? *Deep Sea Res. Part Oceanographic Res. Pap.* 46 (10), 1653–1669. doi:10.1016/s0967-0637(99)00034-5

Morard, R., Füllberg, A., Brummer, G. A., Greco, M., Jonkers, L., Wizemann, A., et al. (2019). Genetic and Morphological Divergence in the Warm-Water Planktonic Foraminifera Genus *Globigerinoides*. *PLoS One* 14 (12), e0225246–30. doi:10.1371/journal.pone.0225246

Nagai, R. H., Ferreira, P. A. L., Mulkherjee, S., Martins, M. V., Figueira, R. C. L., Sousa, S. H. M., et al. (2014). Hydrodynamic Controls on the Distribution of Surface Sediments from the Southeast South American continental Shelf between 23°S and 38°S. *Continental Shelf Res.* 89, 51–60. doi:10.1016/j.csr.2013.09.016

Naik, S. S., Godad, S. P., Naidu, P. D., Tiwari, M., and Paropkari, A. L. (2014). Early- to Late-Holocene Contrast in Productivity, OMZ Intensity and Calcite Dissolution in the Eastern Arabian Sea. *The Holocene* 24 (6), 749–755. doi:10.1177/0959683614526936

Nees, S., Armand, L., De Deckker, P., Labracherie, M., and Passlow, V. (1999). A Diatom and Benthic Foraminiferal Record from the South Tasman Rise (southeastern Indian Ocean): Implications for Palaeoceanographic Changes for the Last 200,000 Years. *Mar. Micropaleontology* 38 (1), 69–89. doi:10.1016/S0377-8398(99)00039-0

Pereira, L. S., Arz, H. W., Pätzold, J., and Portilho-Ramos, R. C. (2018). Productivity Evolution in the South Brazilian Bight during the Last 40,000 Years. *Paleoceanography and Paleoclimatology* 33, 1339–1356. doi:10.1029/2018pa003406

Peterson, R. G., and Stramma, L. (1991). Upper-level Circulation in the South Atlantic Ocean. *Prog. Oceanography* 26 (1), 1–73. doi:10.1016/0079-6611(91)90006810.1016/0079-6611(91)90006-8

Petit, J. R., Jouzel, J., Raynaud, D., Barkov, N. I., Barnola, J.-M., Basile, I., et al. (1999). Climate and Atmospheric History of the Past 420,000 Years from the Vostok Ice Core, Antarctica. *Nature* 399, 429–436. doi:10.1038/20859

Petró, S. M., and Burone, L. (2018). Changes in Water Masses in the Late Quaternary Recorded at Uruguayan Continental Slope (South Atlantic Ocean)/Mudanças Nas Massas De Água Durante O Quaternário Tardio Registadas No Talude Continental Uruguaio (Oceano Atlântico Sul). *J. Sed. Env.* 3 (4), 280–289. doi:10.12957/jse.201810.12957/jse.2018.39156

Petró, S. M., Costa, E. O., Pivel, M. A. G., and Coimbra, J. C. (2018a). Lysocline and CCD Fluctuations Record in Pelotas Basin during the Late Quaternary. *Anuário IGEO UFRJ* 41 (2), 710–719. doi:10.11137/201810.11137/2018_2_710_719

Petró, S. M., Pivel, M. A. G., and Coimbra, J. C. (2021). Evidence of Supra-lysoclinal Dissolution of Pelagic Calcium Carbonate in the Late Quaternary in the Western South Atlantic. *Mar. Micropaleontology* 166. doi:10.1016/j.marmicro.2021.102013

Petró, S. M., Pivel, M. A. G., and Coimbra, J. C. (2018b). Foraminiferal Solubility Rankings: a Contribution to the Search for Consensus. *J. Foraminiferal Res.* 48 (4), 301–313. doi:10.2113/gsjfr.48.4.301

Pimenta, F. M., Campos, E. J. D., Miller, J. L., and Piola, A. R. (2005). A Numerical Study of the Plata River Plume along the Southeastern South American Continental Shelf. *Braz. J. oceanography* 53 (3/4), 129–146. doi:10.1590/S1679-87592005000200004

Piola, A. R., Campos, E. J. D., Moller, O. O., Charo, M., and Martinez, C. (2000). Subtropical Shelf Front off Eastern South America. *J. Geophys. Res.* 105(C3) (726), 6565–6578. doi:10.1029/1999jc000300

Piola, A. R., and Matano, R. P. Ocean Currents: Atlantic Western Boundary|Brazil Current/Falkland (Malvinas) Current, in Encyclopedia of Ocean Sciences, (2017), pp. 422–430. doi:10.1016/B978-0-12-409548-9.10541-X

Piola, A. R., Matano, R. P., Palma, E. D., Möller, O. O., and Campos, E. J. D. (2005). The Influence of the Plata River Discharge on the Western South Atlantic Shelf. *Geophys. Res. Lett.* 32, L01603. doi:10.1029/2004GL021638

Portilho-Ramos, R. C., Cruz, A. P. S., Barbosa, C. F., Rathburn, A. E., Mulitza, S., Venancio, I. M., et al. (2018). Methane Release from the Southern Brazilian Margin during the Last Glacial. *Sci. Rep.* 8, 5948. doi:10.1038/s41598-018-24420-0

Portilho-Ramos, R. d. C., Ferreira, F., Calado, L., Frontalini, F., and de Toledo, M. B. (2015). Variability of the Upwelling System in the southeastern Brazilian Margin for the Last 110,000years. *Glob. Planet. Change* 135, 179–189. doi:10.1016/j.gloplacha.2015.11.003

Portilho-Ramos, R. d. C., Pinho, T. M. L., Chiessi, C. M., and Barbosa, C. F. (2019). Understanding the Mechanisms behind High Glacial Productivity in the Southern Brazilian Margin. *Clim. Past* 15 (3), 943–955. doi:10.5194/cp-15-943-2019

R Core Team. (2019). *R: A Language and Environment for Statistical Computing*. Vienna: Austria. http://www.R-project.org/.

Rasmussen, T. L., Thomsen, E., Troelstra, S. R., Kuijpers, A., and Prins, M. A. (2002). Millennial-scale Glacial Variability versus Holocene Stability: Changes in Planktic and Benthic Foraminifera Faunas and Ocean Circulation in the North Atlantic during the Last 60,000 Years. *Mar. Micropaleontology* 47 (1-2), 143–176. doi:10.1016/S0377-8398(02)001159

Ravello, A. C., and Hillaire-Marcel, C. (2007). "The Use of Oxygen and Carbon Isotopes of Foraminifera in Paleoceanography," in *Proxies in Late Cenozoic Paleoceanography*. Editors C. Hillaire-Marcel and A. De Vernal (Amsterdam: Developments in Marine Geology, Elsevier).

Reid, J. L., Nowlin, W. D., Jr., and Patzert, W. C. (1976). On the Characteristics and Circulation of the Southwestern Atlanitc Ocean. *J. Phys. oceanography* 7, 62–91. doi:10.1175/1520-0485(1977)007<0062OTCACO>2.0.CO;2

Rex, M. A., and Etter, R. J. (2010). *Deep-sea Biodiversity: Pattern and Scale*. Cambridge: Harvard University Press, 354

Rex, M., Etter, R., Morris, J., Crouse, J., McClain, C., Johnson, N., et al. (2006). Global Bathymetric Patterns of Standing Stock and Body Size in the Deep-Sea Benthos. *Mar. Ecol. Prog. Ser.* 317, 1–8. doi:10.3354/meps317001

Riebesell, U. (2004). Effects of CO2 Enrichment on Marine Phytoplankton. *J. Oceanography* 60, 719–729. doi:10.1007/s10872-004-5764-z

Rodrigues, A. R., Pivel, M. A. G., Schmitt, P., de Almeida, F. K., and Bonetti, C. (2018). Infaunal and Epifaunal Benthic Foraminifera Species as Proxies of Organic Matter Paleofluxes in the Pelotas Basin, South-Western Atlantic Ocean. *Mar. Micropaleontology* 144, 38–49. doi:10.1016/j.marmicro.2018.05.007

Rodrigues, L. F., Macario, K. D., Anjos, R. M., Ketzer, J. M. M., Maraschin, A. J., Augustin, A. H., et al. (2020). Origin and Alteration of Organic Matter in Hydrate-Bearing Sediments of the Rio Grande Cone, Brazil: Evidence from Biological, Physical, and Chemical Factors. *Radiocarbon*, 62, 197–206. doi:10.1017/RDC.2019.109

Schiebel, R. (2002). Planktic Foraminiferal Sedimentation and the marine Calcite Budget. *Glob. Biogeochem. Cycles* 16 (4), 1–21. doi:10.1029/2001GB001459

Schiebel, R., and Hemleben, C. (2017). *Planktic Foraminifers in the Modern Ocean, Pp. 358*. Berlin, Germany: Springer. doi:10.1007/978-3-662-50297-6

Schlitzer, R. (2020). Ocean Data View. Available at: https://odv.awi.de.

Schönfeld, J. (2012). History and Development of Methods in Recent Benthic Foraminiferal Studies. *J. Micropalaeontol.* 31, 53–72. doi:10.1144/0262-821X11-008

Shackleton, N. J. (2000). The 100,000-year Ice-Age Cycle Identified and Found to Lag Temperature, Carbon Dioxide, and Orbital Eccentricity. *Science* 289, 1897–1902. doi:10.1126/science.289.5486.1897

Shakun, J. D., Clark, P. U., He, F., Marcott, S. A., Mix, A. C., Liu, Z., et al. (2012). Global Warming Preceded by Increasing Carbon Dioxide Concentrations during the Last Deglaciation. *Nature* 484, 49–54. doi:10.1038/nature10915

Siccha, M., and Kucera, M. (2017). ForCenS, a Curated Database of Planktonic Foraminifera Census Counts in marine Surface Sediment Samples. *Sci. Data* 4, 170109. doi:10.1038/sdata.2017.109

Silveira, I. C. A. d., Schmidt, A. C. K., Campos, E. J. D., Godoi, S. S. d., and Ikeda, Y. (2000). A corrente Do Brasil ao Largo da Costa Leste Brasileira. *Rev. Bras. Oceanogr.* 48 (2), 171–183. doi:10.1590/S1413-77392000000200008

Smith, C. R., Berelson, W., Demaster, D. J., Dobbs, F. C., Hammond, D., Hoover, D. J., et al. (1997). Latitudinal Variations in Benthic Processes in the Abyssal Equatorial Pacific: Control by Biogenic Particle Flux. *Deep Sea Res. Part Topical Stud. Oceanography* 44 (9-10), 2295–2317. doi:10.1016/S09670645(97)00022-210.1016/s0967-0645(97)00022-2

Sortor, R. N., and Lund, D. C. (2011). No Evidence for a Deglacial Intermediate Water $\Delta^{14}C$ Anomaly in the SW Atlantic. *Earth Planet. Sci. Lett.* 310 (1–2), 65–72. doi:10.1016/j.epsl.2011.07.017

Sousa, S. H. M., de Godoi, S. S., Amaral, P. G. C., Vicente, T. M., Martins, M. V. A., Sorano, M. R. G. S., et al. (2014). Distribution of Living Planktonic Foraminifera in Relation to Oceanic Processes on the southeastern continental Brazilian Margin (23°S-25°S and 40°W-44°W). *Continental Shelf Res.* 89, 76–87. doi:10.1016/j.csr.2013.11.027

Souto, D. D., de Oliveira Lessa, D. V., Albuquerque, A. L. S., Sifeddine, A., Turcq, B. J., and Barbosa, C. F. (2011). Marine Sediments from southeastern Brazilian continental Shelf: A 1200year Record of Upwelling Productivity. *Palaeogeogr. Palaeoclimatol. Palaeoecol.* 299, 49–55. doi:10.1016/j.palaeo.2010.10.032

Stramma, L., and England, M. (1999). On the Water Masses and Mean Circulation of the South Atlantic Ocean. *J. Geophys. Res.* 104 (C9), 20863–20883. doi:10.1029/1999JC900139

Suárez-Ibarra, J. Y., Frozza, C. F., Petró, S. M., and Pivel, M. A. G. (2021). Fragment or Broken? Improving the Planktonic Foraminifera Fragmentation Assessment. *PALAIOS* 36, 165–172. doi:10.2110/palo.2020.062

Toledo, F. A. L., Cachao, M., Costa, K. B., and Pivel, M. A. G. (2007). Planktonic Foraminifera, Calcareous Nannoplankton and Ascidian Variations during the Last 25 Kyr in the Southwestern Atlantic: A Paleoproductivity Signature? *Mar. Micropaleontology* 64 (1-2), 67–79. doi:10.1016/j.marmicro.2007.03.001

Toledo, F., Costa, K. B., Pivel, M. A. G., and Campos, E. J. D. (2008). Tracing Past Circulation Changes in the Western South Atlantic Based on Planktonic Foraminifera. *Rbp* 11 (3), 169–178. doi:10.4072/rbp.2008.3.03

Viana, A. R. (2001). Seismic Expression of Shallow-To Deep-Water Contourites along the South-Eastern Brazilian Margin. *Mar. Geophys. Researches* 22, 509–521. doi:10.1023/A:1016307918182

Waelbroeck, C., Labeyrie, L., Michel, E., Duplessy, J. C., McManus, J. F., Lambeck, K., et al. (2002). Sea-level and Deep Water Temperature Changes Derived from Benthic Foraminifera Isotopic Records. *Quat. Sci. Rev.* 21, 295–305. doi:10.1016/S0277-3791(01)00101-9

Wefer, G., Berger, W. H., Bijma, J., and Fischer, G. (1999). "Clues to Ocean History: A Brief Overview of Proxies," in *Use of Proxies in Paleoceanography: Examples from the South Atlantic*. Editors G. Fischer and G. Wefer (Berlin Heidelberg: Springer-Verlag), 68. doi:10.1007/978-3-642-58646-0_1

Weinkauf, M. F. G., and Milker, Y. (2018). The Effect of Size Fraction in Analyses of Benthic Foraminiferal Assemblages: A Case Study Comparing Assemblages from the >125 and >150 μm Size Fractions. *Front. Earth Sci.* 6, 37. doi:10.3389/feart.2018.00037

Weinkauf, M. F. G., Moller, T., Koch, M. C., and Kučera, M. (2013). Calcification Intensity in Planktonic Foraminifera Reflects Ambient Conditions Irrespective of Environmental Stress. *Biogeosciences*, 10, 6639–6655. doi:10.5194/bg-10-6639-2013

Weschenfelder, J., Baitelli, R., Corrêa, I. C. S., Bortolin, E. C., and dos Santos, C. B. (2014). Quaternary Incised Valleys in Southern Brazil Coastal Zone. *J. South Am. Earth Sci.* 55, 83–93. doi:10.1016/j.jsames.2014.07.004

Wycech, J., Kelly, D. C., and Marcott, S. (2016). Effects of Seafloor Diagenesis on Planktic Foraminiferal Radiocarbon Ages. *Geology* 44 (7), 551–554. doi:10.1130/G37864.1

Yasuhara, M., Hunt, G., Cronin, T. M., Hokanishi, N., Kawahata, H., Tsujimoto, A., et al. (2012). Climatic Forcing of Quaternary Deep-Sea Benthic Communities in the North Pacific Ocean. *Paleobiology* 38 (1), 162–179. doi:10.1666/10068.1

Zamelczyk, K., Rasmussen, T. L., Husum, K., Haflidason, H., de Vernal, A., Ravna, E. K., et al. (2012). Paleoceanographic Changes and Calcium Carbonate Dissolution in the central Fram Strait during the Last 20 Ka. *Quat. Res.* 78, 405–416. doi:10.1016/j.yqres.2012.07.006

Zweng, M. M., Reagan, J. R., Antonov, J. I., Locarnini, R. A., Mishonov, A. V., Boyer, T. P., et al. (2013). *World Ocean Atlas.* Editor A. Mishonov Technical, 2013.

Conflict of Interest: The authors declare that the research was conducted in the absence of any commercial or financial relationships that could be construed as a potential conflict of interest.

Publisher's Note: All claims expressed in this article are solely those of the authors and do not necessarily represent those of their affiliated organizations, or those of the publisher, the editors and the reviewers. Any product that may be evaluated in this article, or claim that may be made by its manufacturer, is not guaranteed or endorsed by the publisher.

frontiers | Frontiers in Ecology and Evolution

TYPE Original Research
PUBLISHED 03 November 2023
DOI 10.3389/fevo.2023.1238334

OPEN ACCESS

EDITED BY
Alessio Fabbrini,
University College London,
United Kingdom

REVIEWED BY
Thomas Mark Cronin,
United States Geological Survey (USGS), United States
Selvaraj Kandasamy,
Central University of Kerala, India
Janne Repschlaeger,
Max Planck Institute for Chemistry, Germany

*CORRESPONDENCE
Jaime Y. Suárez-Ibarra
jysuarezibarra@gmail.com;
suarezij@natur.cuni.cz

†PRESENT ADDRESS
Tiago M. Freire,
Institut für Geologie & Mineralogie,
Universität zu Köln, Köln, Germany

RECEIVED 11 June 2023
ACCEPTED 12 October 2023
PUBLISHED 03 November 2023

CITATION
Suárez-Ibarra JY, Freire TM, Frozza CF, Pinho TML, Petró SM, Dias BB, Chalk TB, Chaabane S, Srivastava M, Costa KB, Toledo FAL, de Garidel-Thoron T, Coimbra JC and Pivel MAG (2023) Surface fertilisation and organic matter delivery enhanced carbonate dissolution in the western South Atlantic.
Front. Ecol. Evol. 11:1238334.
doi: 10.3389/fevo.2023.1238334

Surface fertilisation and organic matter delivery enhanced carbonate dissolution in the western South Atlantic

Jaime Y. Suárez-Ibarra[1*], Tiago M. Freire[2†], Cristiane F. Frozza[2], Tainã M. L. Pinho[3], Sandro M. Petró[4], Bruna B. Dias[5,6], Thomas B. Chalk[7], Sonia Chaabane[7,8,9], Medhavi Srivastava[1], Karen B. Costa[10], Felipe A. L. Toledo[10], Thibault de Garidel-Thoron[7], João C. Coimbra[11] and María A. G. Pivel[11]

[1]Ústav Geologie a Paleontologie, Přírodovědecká fakulta, Univerzita Karlova, Praha, Czechia, [2]Programa de Pós-Graduação em Geociências, Instituto de Geociências, Universidade Federal do Rio Grande do Sul, Porto Alegre, Brazil, [3]Alfred Wegener Institute, Helmholtz Center for Polar and Marine Research, Bremerhaven, Germany, [4]itt OCEANEON – Instituto Tecnológico de Paleoceanografia e Mudanças Climáticas, Universidade do Vale do Rio dos Sinos, São Leopoldo, RS, Brazil, [5]School of Arts, Science and Humanities, University of São Paulo, Cidade Universitária, São Paulo, Brazil, [6]Murray Edwards College, University of Cambridge, Cambridge, United Kingdom, [7]Aix-Marseille Université, CNRS, IRD, INRAE, CEREGE, Europôle Méditerranéen de l'Arbois, Aix-en-Provence Cedex, France, [8]Department of Climate Geochemistry, Max Planck Institute for Chemistry, Mainz, Germany, [9]Fondation pour la recherche sur la biodiversité (FRB-CESAB), Montpellier, France, [10]Laboratório de Paleoceanografia do Atlântico Sul, Instituto Oceanográfico, Universidade de São Paulo, Praça do Oceanográfico, São Paulo, Brazil, [11]Centro de Estudos de Geologia Costeira e Oceânica (CECO), Instituto de Geociências, Universidade Federal do Rio Grande do Sul, Porto Alegre, Brazil

The last glacial inception was characterised by rapid changes in temperature, atmospheric pCO_2, and changes in the water mass geometry of the major ocean basins. Although several climatic feedback mechanisms have been proposed to explain the glacial/interglacial cycles witnessed in the Quaternary, the exact mechanistic responses of these processes are still under constrained. In this study we use proxies including planktonic foraminifera compositional assemblages and oxygen stable isotopes to reconstruct past changes in sea surface productivity, stratification, and carbonate dissolution. We use core SIS-249 (2,091 mbsl, western South Atlantic 30°S 47°W), spanning 30–110 thousand years ago (ka), and currently bathed by modern Northern Component Water. We test existing hypotheses suggesting that the orbital obliquity cycle modulates the biological pump in the study area. Spectral analysis run on our synthesised productivity proxies recognises a ~43 kyr-cycle, related to the obliquity cycle. We propose that the enhanced productivity is produced by two mechanisms: i) the glacial upwelling of subsurface nutrient-rich waters and, ii) the continental (wind-driven dust and riverine outflows) fertilisation of the photic zone, with the latter process being obliquity-paced. We also suggest that not only the increased organic matter export but also a change in its bioavailability (from refractory to labile) led to calcium carbonate dissolution, as the degradation of the more soluble organic matter decreased the pH of the glacial bottom water, partially dissolving the calcium carbonate. Although our correlation analyses show a strong benthic-pelagic coupling through the relation between the

enhanced biological pump and carbonate dissolution (p<0.05, r=0.80), we cannot reject the potential of corrosive Southern Component Water bathing the site during the glacial. Finally, we highlight that these processes are not mutually exclusive and that both can be modulated by the obliquity cycle.

KEYWORDS

planktonic foraminifera, primary productivity, stratification, southern Brazilian continental margin, late Quaternary

1 Introduction

Glacial-interglacial cycles are characterised by cold stages, witnessing decreased temperatures and carbon dioxide (CO_2) concentrations, the growth of ice sheets and the rearrangement of water mass geometry (Lisiecki and Raymo, 2005; Ahn and Brook, 2008; Doughty et al., 2021; Shackleton et al., 2021; Menking et al., 2022). During these cycles, multiple mechanisms contribute to CO_2 drawdown, resulting in a reduction of atmospheric CO_2 levels. These mechanisms include changes in ocean carbonate chemistry (Rickaby et al., 2010), boosted biological pump (Martin, 1990; Sigman and Boyle, 2000), enhanced calcium carbonate preservation (Archer and Maier-Reimer, 1994; Brovkin et al., 2012; Doss and Marchitto, 2013) and expanded Antarctic sea ice (Stephens and Keeling, 2000; Sigman et al., 2010), among others.

The growth of southern ice sheets during glacial stages resulted in a reorganised Atlantic Ocean, marked by the expansion of corrosive carbon-rich deep-water masses to shallower depths (e.g., Duplessy et al., 1988; Curry and Oppo, 2005; Govin et al., 2009; Howe et al., 2016a; Howe et al., 2018) and, the redistribution of nutrients, boosting the biological pump and enhancing the oceans' capacity to sequestrate atmospheric CO_2 during glacial periods (Broecker, 1982; Sigman and Boyle, 2000; Skinner, 2009; Rickaby et al., 2010; Ziegler et al., 2013). Yet, the precise way in which these two mechanisms act and interact is still under debate.

For the western South Atlantic, several studies have documented the impact of glacial-interglacial stages on the carbon cycle (Gu et al., 2017; Pereira et al., 2018; Portilho-Ramos et al., 2019; Frozza et al., 2020; Suárez-Ibarra et al., 2022) and past bottom water mass geometry (Howe et al., 2016a; Howe et al., 2016b; Howe et al., 2018). One important characteristic of these climatic variations is the effect on calcium carbonate preservation, as it plays an important role in the global carbon cycle. The reorganised "glacial" Atlantic Ocean affects the calcium carbonate preservation both hemispheres negatively (i.e., Chalk et al., 2019; Petró et al., 2021). In addition, another well-known mechanism affected by the glacial-interglacial cycles intemperate zones is the expansion of the southwesterly winds (Toggweiler et al., 2006), displacing the north limit of the wind belt (from 40°S to 30°S latitude, Gili et al., 2017). The change in the wind belt position, associated with an increasing wind strength paced by the obliquity cycle, has been pointed to enhance the terrestrial nutrient supply (Lopes et al., 2021). This enhancement is thought to increase the productivity of the marine ecosystems.

Another critical factor that can influence calcium carbonate preservation is the biological pump, transporting organic carbon from the surface to the deep ocean. In the western South Atlantic, Suárez-Ibarra et al. (2022) documented that high primary productivity during the last glacial exported a higher amount of organic matter to the seafloor, where it is remineralised. This process releases $CO_{2(aq)}$, which increases acidity, affecting the preservation of calcium carbonate, and raising questions about the potential of an enhanced glacial biological pump to efficiently sequester carbon in the sediments.

Yet, the extent of the mechanisms driving calcium carbonate preservation and carbon cycling in the western South Atlantic remains to be fully elucidated. It is required an integrated approach encompassing both benthic and pelagic systems to provide insights into the underlying dynamics during the last interglacial-glacial interval. Thus, we use planktonic and benthic foraminifera counts, geochemical analysis (oxygen stable isotopes, $\delta^{18}O$), sedimentological quantifications (size fraction) and various statistical tools such as correlation, spectral and clustering analyses from the western South Atlantic. By comparing our data with other records from the southern and southeastern Brazilian continental margin, our objectives are: i) to infer the mechanisms that modulate the oceanic fertilisation, ii) to quantify the potential effect of sea surface productivity on carbonate dissolution, and iii) to test the influence of the orbital obliquity cycle on surface and bottom conditions.

2 Oceanographic setting

The modern upper ocean circulation of the subtropical South Atlantic is governed by the subtropical gyre (Peterson and Stramma, 1991). The western boundary of the subtropical gyre is impacted mainly by the Brazil Current, which transports warm, salty, oligotrophic waters at the surface (tropical surface water, temperature > 20°C; salinity > 36 psu; Peterson and Stramma, 1991; Stramma and England, 1999). Below this tropical surface water (~100 m) flow the cooler and more nutrient-rich South Atlantic Central Water (Stramma and England, 1999), and the Antarctic Intermediate Water with lower salinity and temperature and higher

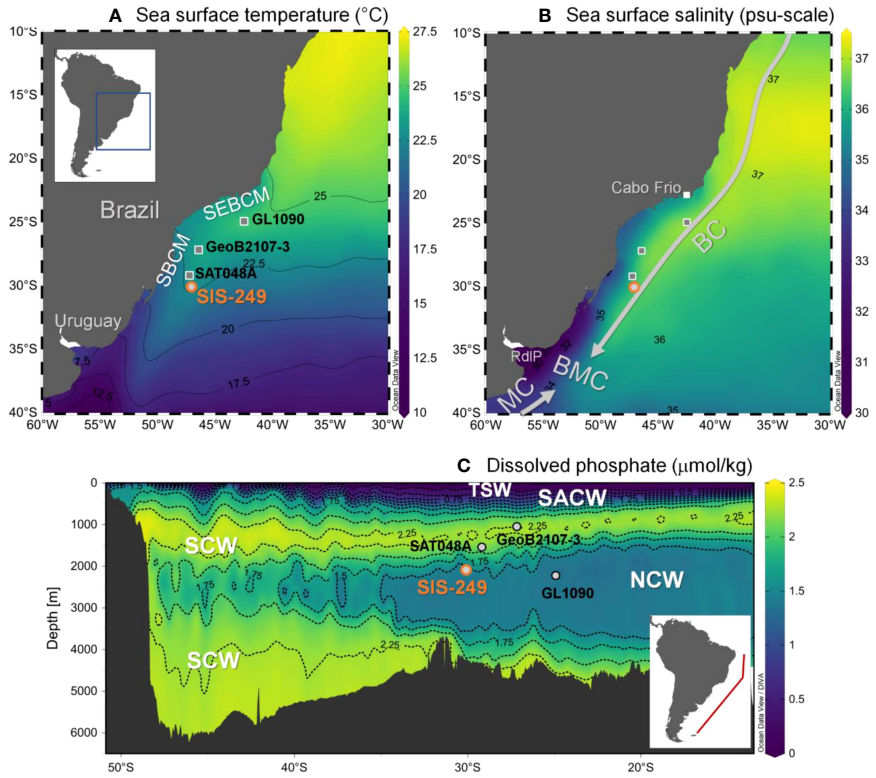

FIGURE 1
(A) Annual mean sea surface temperature and **(B)** annual mean sea surface salinity from the World Ocean Atlas 2013 (WOA13, Locarnini et al., 2013) relative to core SIS-249 location (in orange). Other cores analysed in this study are indicated in grey (GeoB2107-3, Gu et al., 2017; GL1090, Santos et al., 2017a; SAT048A, Suárez-Ibarra et al., 2022). **(C)** Vertical dissolved phosphate section profile through the western South Atlantic according to the World Ocean Circulation Experiment (WOCE, Section A17; Schlitzer, 2000) and recovery depth of cores. SBCM, Southern Brazilian Continental Margin; SEBCM, Southeastern Brazilian Continental Margin; RdlP, Río de la Plata; MC, Malvinas Current; BC, Brazil Current; BMC , Brazil-Malvinas Confluence; TSW, Tropical Surface Water; SACW, South Atlantic Central Water; SCW, Southern Component Water; NCW, Northern Component Water. Plotted using Ocean Data View (Schlitzer, 2020).

oxygen values (Stramma and England, 1999). To the South of our study site (Figure 1), at about 38°S, the Brazil Current encounters the cool, fresher, and nutrient-rich waters of the Malvinas Current (temperature < 15°C; salinity < 34.2 psu), forming the Brazil-Malvinas Confluence (Gordon and Greengrove, 1986; Gordon, 1989; Piola et al., 2000). Currently, the seafloor core location is bathed by the southward movement of North Atlantic Deep Water, (hereafter termed generally as Northern Component water, NCW) a water mass that promotes calcium carbonate preservation due to its oversaturation in carbonate ion (CO_3^{2-}). Conversely, Southern Component water (SCW, comprising the Antarctic Intermediate Water, Circumpolar Deep Water and Antarctic Bottom Water), which is undersaturated in CO_3^{2-}, flows northward above and below the NCW at this location, and its increased corrosiveness leads to calcium carbonate dissolution (Broecker and Peng, 1982; Frenz et al., 2003; Frenz and Henrich, 2007).

Close to the coring site (35° S), the Río de la Plata (RdlP), the second largest continental water outflow in South America, reaches the South Atlantic (Matano et al., 2014). The RdlP drains cool and low salinity waters into the coastal region and increases the nutrient availability, enhancing biological productivity along the continental shelves of Uruguay and southern Brazil during austral winter. Northward displacement of the RdlP outflow occurs in response to the variability of the alongshore wind stress (e.g., Braga et al., 2008; Möller et al., 2008). The RdlP outflows can reach 28° S along the modern inner and mid-shelves (Piola et al., 2000; Piola et al., 2005; Möller et al., 2008). In contrast, during austral summer, NE winds restrict the RdlP outflows to the south (~32° S), inhibiting fertilisation by reducing nutrient supply from continental outflows.

3 Materials and methods

3.1 Marine sediment core

The sediment samples used in this study come from the piston core SIS-249, which measures 1.94 metres in length. This core was retrieved from the lower continental slope of the southern Brazilian continental margin at 2,091 metres below sea level (30°05′ S; 47°05′ W, Figure 1). Core SIS-249 was obtained during an oceanographic campaign in the austral spring-summer of 2007 by *Fugro Brasil Ltda* for the Brazilian National Agency of Petroleum, Natural Gas and Biofuels. Due to the presence of shallower allochthonous sands in the uppermost 48 cm of the core, this study focuses on the carbonate-rich pelagic mud and sandy mud, which lie between 48 and 194 cm. Within this interval, we collected 45 samples with a

sampling spacing of 2 to 4 cm to analyse the planktonic foraminifera fossil assemblages and stable isotopes.

3.2 Planktonic foraminifera compositional assemblage

To assess planktonic foraminifera assemblages, each sample (~9 cc) was sequentially weighed, washed over a 63 μm sieve, dried at 55°C, and weighed again. To avoid juvenile specimens, which would induce taxonomic biases, planktonic foraminifera were only picked from the >150 μm size fraction (CLIMAP Project Members, 1976; Peeters et al., 1999). The processed samples were then divided with a micro splitter to recover at least 300 non-fragmented planktonic foraminifera tests per sample, as to support significant statistical variations of around 10% for assemblage analyses (Patterson and Fishbein, 1989). The taxonomic classification on the species level followed Schiebel and Hemleben (2017).

3.3 Age model improvement

The chronology of core SIS-249 was first published by Rodrigues et al. (2018) based on one single Accelerator Mass Spectrometry (AMS) radiocarbon age combined with benthic oxygen stable isotope ($\delta^{18}O$) stratigraphy. The AMS radiocarbon date from Rodrigues et al. (2018) was measured on tests of *Globigerinoides ruber* at 58 cm core-depth and the age model developed in the software AnalySeries 1.1 (Paillard et al., 1996).

In the present study, we improved the age model by using six $\delta^{18}O$ tie-points (two points from the new $\delta^{18}O_{G.rub}$ record and four from $\delta^{18}O_{Uvig}$), which are now correlated with the records from core GL-1090 (Santos et al., 2017a), a nearby core with high-resolution and well-calibrated age model (based on 14 AMS ^{14}C and 13 stable oxygen isotope correlation points to two reference curves: Lisiecki and Raymo, 2005 and Govin et al., 2014). The new refined age model was created in the R-package "Bacon" v. 2.5.3, which implements Bayesian statistics (Blaauw and Christeny, 2011). We considered a propagated error of 2.5 kyr, conservatively estimated based on the mean accumulation rates of cores SIS-249 and GL-1090 (ca. 1.87 and 0.29 cm/kyr, respectively) and the <2 kyr age error from the GL-1090 reference curve (Santos et al., 2017a). The raw AMS radiocarbon age date from Rodrigues et al. (2018) was calibrated within the R-package "bacon", using the Marine20 curve (Heaton et al., 2020) and applying a regional reservoir effect (ΔR) of −85 ± 40 years (Tables S1 and S2). This estimate follows the Marine Reservoir Correction Database (http://calib.org/marine/), considering the ages of Nadal De Masi (1999), Angulo et al. (2005), and Alves et al. (2015).

3.4 Productivity proxies

We reconstruct past sea surface productivity using the ratio between the species *Globigerina bulloides* and *Globigerinoides ruber* (*G.bull/G.rub*), the relative abundance (%) of *Globigerinita glutinata*, and the benthic foraminifera accumulation rate (BFAR).

The *G.bull/G.rub* ratio is used to reconstruct upwelling events (Conan et al., 2002; Toledo et al., 2008) based on the contrasting ecological preferences of both species. The opportunistic species *G. bulloides* is associated with eutrophic waters in upwelling zones (Sautter and Thunell, 1991; Peeters et al., 2002; Zaric et al., 2005; Mohtadi et al., 2007; Lessa et al., 2014), while *G. ruber*, a symbiont-bearing shallow water-dwelling species, is abundant in tropical/subtropical planktonic foraminiferal provinces (Bé and Hutson, 1977; Kučera, 2007; Schiebel and Hemleben, 2017). Moreover, the *G. glutinata* abundance is typically higher in phytoplankton-rich waters and is used as a proxy for paleoproductivity (Conan and Brummer, 2000; Souto et al., 2011; Pereira et al., 2018).

We also applied the BFAR index, calculated here as the total number of benthic foraminifera multiplied by the sediment accumulation rate as it has been shown to be a reliable proxy for the organic carbon flux to the seafloor in the Brazilian margin (Dias et al., 2021). The BFAR index represents the increments of primary productivity export to the seafloor, in which the increases on benthic biomass are associated to the increasing food availability to the benthic community (Herguera and Berger, 1991; Guichard et al., 1997; Jorissen et al., 2007). Thus, these planktonic and benthic foraminiferal proxies together can indicate changes in the fertilisation mechanisms affecting the photic zone (i.e., biological pump, terrestrial nutrient input) and posterior organic matter export.

3.5 Upper water column stratification proxies

To assess changes in sea surface stratification, we studied both the stable isotopic composition of selected planktonic foraminifera species and assemblage counts. As planktonic foraminifera calcitic tests record a mean value corresponding to that of the local water mass properties (i.e., temperature, salinity) at the different depths where they live, their $\delta^{18}O$ signal allows the reconstruction of the seawater conditions at different depth layers (Emiliani, 1954; Ravelo and Hillaire-Marcel, 2007). The species *G. ruber* dwells at surface-shallow depths, while the species *Globorotalia inflata* is a subsurface-thermocline dweller (Chiessi et al., 2007; Groeneveld and Chiessi, 2011; Schiebel and Hemleben, 2017; Lessa et al., 2020). Therefore, the gradient between the $\delta^{18}O$ values of these two species ($\Delta\delta^{18}O_{G.inf\text{-}G.rub}$) indicates a decreased (increased) upper water column stratification according to the lower (higher) $\Delta\delta^{18}O_{G.inf\text{-}G.rub}$ values (Santos et al., 2017b and references therein).

Around 10 specimens of *G. ruber* and *G. inflata* were collected per sample for the $\delta^{18}O$ analyses from the size fraction >250 μm to limit ontogenetic effects (Elderfield et al., 2002). The tests were cleaned with distilled water using an ultrasonic bath to remove any contamination by external particles. The isotopic measurements were performed on a ThermoFisher Scientific MAT253 gas Isotope Ratio Mass Spectrometer coupled to a Kiel IV automated carbonate device at the Research Center for Geochronology and Isotopic

Geochemistry (CPGeo) from the University of São Paulo. Isotopic data used the Vienna Pee-Dee-Belemnite (VPDB) reference standard. Here we report the standard deviation of the laboratory reference material used for normalisation (SHP2L; Crivellari et al., 2021), being 0.07‰ (n=20 standards) over the measurement period. The standard deviation of the VPDB $\delta^{18}O$ values of the measured samples did not exceed 0.1‰. As no replicated measurements were carried out, we confirmed the consistency of our $\delta^{18}O$ values and value offset between *G. ruber* and *G. inflata* with the expected values for our study site. We verify this by comparing our records with published Holocene (Chiessi et al., 2007) and last glacial and interglacial stage (Santos et al., 2017b) datasets.

In addition, we use the abundances of the *Globorotalia truncatulinoides* right coiling form, as it has been documented to represent a well-mixed upper water column (reduced stratification), since this morphotype migrates to relatively shallower depths to complete its reproductive cycle (e.g., Lohmann and Schweitzer, 1990; Renaud and Schmidt, 2003; Feldmeijer et al., 2015; Billups et al., 2016).

3.6 Dissolution proxies

We quantify the effect of dissolution on foraminiferal assemblages by using: i) the ratio between the benthic and planktonic foraminifera (B/P ratio, Arrhenius, 1952; Parker and Berger, 1971; Kučera, 2007), ii) the number of whole planktonic foraminifera tests per gram of dry sediment (PF/g, Le and Shackleton, 1992; Suárez-Ibarra et al., 2021), iii) the abundance (%) of the coarse fraction i.e. larger than 63 μm (Berger et al., 1982; Gonzales et al., 2017; Suárez-Ibarra et al., 2021) and, iv) the $CaCO_3$ content (%) (Berger et al., 1982; Gonzales et al., 2017; Suárez-Ibarra et al., 2021). The $CaCO_3$ (%) was previously calculated by Rodrigues et al. (2018). The fraction >63 μm was estimated using a laser diffraction particle size analyzer Horiba Partica-LA-950X, which determined the grain size of the bulk sediment samples at the *Centro de Estudo de Geologia Costeira e Oceânica* (CECO) of the *Universidade Federal do Rio Grande do Sul* (UFRGS).

3.7 Multivariate statistical analyses

To divide the time series record into distinct cluster intervals (periods characterised by similar conditions) we carry out a clustering analysis. Posteriorly, to distinguish the dependencies of the grouping process we utilize an ordinate analysis. Both clustering and ordinate analyses are applied on the planktonic foraminifera species with relative abundances >1% (See Supplementary material).

Additionally, since all proxies are inevitably affected by different environmental processes other than the targeted parameters, we decrease the bias by also synthesising the variation through time of i) sea surface productivity, ii) upper water column stratification, and iii) carbonate dissolution. To do so, we run principal component analyses (PCA) on the above proxies, based on the correlation matrix. The data were centralised and standardised by dividing the difference between the dataset mean and the sample value by the dataset standard deviation. The synthesised productivity, stratification and dissolution proxies were extracted from the first axes of the PCAs as $PC1_P$ (productivity), $PC1_S$ (stratification) and $PC1_D$ (dissolution). Correlations between (and within) the first axes of the PCAs and other proxies were calculated using reduced major axis regressions. All PCA and correlation analyses were conducted using the software PAST (version 4.08; Hammer et al., 2001).

3.8 Spectral analysis

To test whether variations through time correspond to cyclic events, paced by orbital forcings, first we run a Multi-Taper-Method (MTM) test using the software "Acycle" (Li et al., 2019). The $PC1_P$ curve was detrended using a locally weighted scatterplot smoothing (LOWESS) and then analysed with the MTM. We set the smoother with a Time-bandwidth product of "2", and calculated the red noise following the Classical autoregressive (AR) model AR(1) (Husson, 2014). Second, we conducted a REDFIT spectral analysis utilising the software PAST (version 4.08; Hammer et al., 2001; Schulz and Mudelsee, 2002). The spectral analysis used the "Welch" window, a configuration of "4" for the oversampling and "2" as number of segments.

4 Results

The *G.bull*/*G.rub* ratio (Figure 2A) varies from 0.18 to 0.52 (mean 0.37 ± 0.09), increasing through MIS 5 up to the boundary with MIS 4 (90.1 to 75 ka) and again during MIS 3 (38.7 to 29.5 ka). Relative abundances of *G. glutinata* (Figure 2B) range between 4.9 and 24.8% (average 15 ± 4.05%) and show an increasing trend towards the MIS 5/4 boundary (from 91.9 to 72.7 ka). The BFAR (Figure 2C) varies between 11 (at 90 ka) and 230 $ind.cm^{-2}.kyr^{-1}$ (at 59 ka), with three intervals: first, a low decreasing trend from 105 to 87 ka (mean 27 $ind.cm^{-2}.kyr^{-1}$), followed by an abrupt jump and another decreasing trend from 84 to 39 ka (mean 92 $ind.cm^{-2}.kyr^{-1}$), and a final increasing trend until 30 ka (mean 67 $ind.cm^{-2}.kyr^{-1}$).

The abundance of *G. truncatulinoides* right coiling (Figure 2D) is low throughout the core (0 to 6.5%, mean 1.73). However, the 73–51 ka interval (approximately MIS 4) is marked by increased abundances and two abrupt peaks. The $\delta^{18}O_{G.rub}$ values range between -0.96 and 0.29‰ (mean -0.25 ± 0.33‰), with lower values during MIS 5, increasing towards MIS 4 and decreasing at the MIS 3 onset (Figure S1). The $\delta^{18}O_{G.inf}$ values vary between 0.56 and 1.56‰ (mean 1.16 ± 0.18‰) and display a progressively increasing trend from MIS 5 to MIS 3 (Figure S1). The $\delta^{18}O_{G.inf}$ record from core SIS-249 shows a good fit with the values from core GL-1090, except at 80 ka. The $\Delta\delta^{18}O$ between *G. inflata* and *G. ruber* (Figure 2E) presents values from 0.90 to 1.90‰ (mean 1.38 ± 0.24‰). $\Delta\delta^{18}O_{G.inf\text{-}G.rub}$ values are higher during MIS 5 (around 1.6‰), intermediate during MIS 3 (above 1.30‰), and generally lower during MIS 4 (mean 1.16 ± 0.18‰).

The B/P ratio (Figure 2F) ranges between 0.02 and 0.19, with low values during MIS 5d-c, an increase through MIS 5b, a reduction during MIS 5a (with a steep peak at 65 ka), followed by an increase at

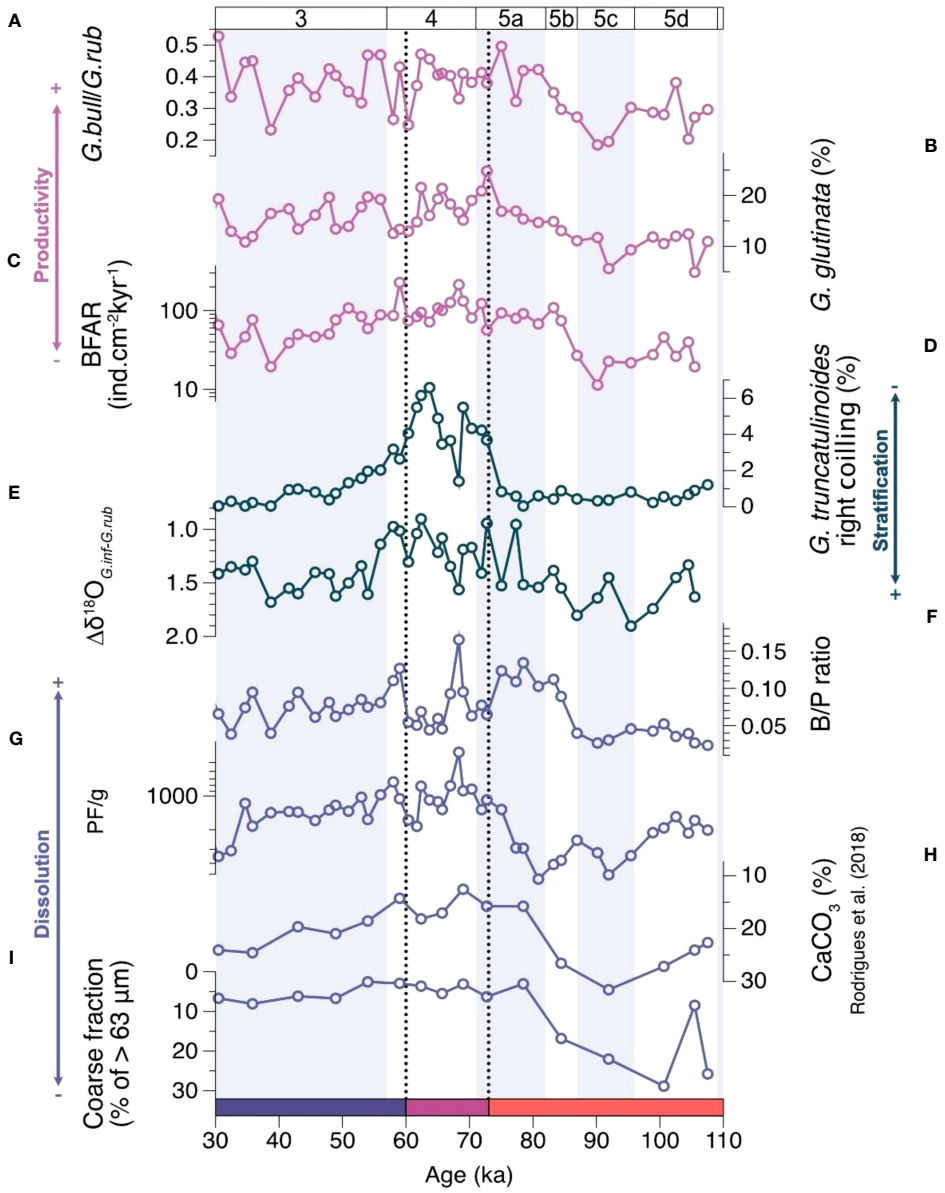

FIGURE 2
Time series records used to estimate productivity (in lilac: **(A)** *G. bulloides*/*G. ruber*, **(B)** *G. glutinata* abundance and **(C)** BFAR), stratification (in teal: **(D)** abundance of *G. truncatulinoides* right coiling and I $\Delta\delta^{18}O_{G.inf\text{-}G.rub}$), and dissolution (in steel blue: **(F)** B/P ratio, **(G)** PF/g, **(H)** $CaCO_3$ content (Rodrigues et al., 2018) and **(I)** >63 µm fraction). The black vertical dotted lines divide the record into biotic clusters where: Cluster I (red) is dominated by species characteristic of warm and oligotrophic water; cluster II (purple) by species related to eutrophic water, characterised by high productivity and low stratification; and cluster III (blue) by species from cooler waters. Y axes in **(E–I)** are reversed.

the end of MIS 4 and a further decrease with relatively stable values during MIS 3. The PF/g (Figure 2G) varies between 400 and 5540 (mean 1922 ± 1141 ind./g) and presents a decreasing trend from 91.9 to 70.3 ka, remaining low throughout MIS 4 and 3. The fraction coarser than 63 µm (Figure 2I) presents relatively high values (around 22%) during the 107–84 ka time interval, except at 105 ka when values drop to 8.5%. At 78 ka, values reach 3% and remain under 8% until the top of the record (30.4 ka). All the productivity, stratification, and dissolution proxies are shown in Figure 2.

Concerning the multivariate analyses, the first principal components of the PCA's analyses run on the productivity, stratification, and dissolution proxies ($PC1_P$, $PC1_S$ and $PC1_D$) synthesise 61.9, 78.6 and 66.4% of the variance, respectively. The results for the reduced major axis regressions within the $PC1_P$, $PC1_S$, $PC1_D$, $\delta^{13}C_{Uvig}$, accumulation rate (Acc. rates) and accumulation rates of total organic carbon (ARTOC) are shown in Table 1. All regression analyses show a significant (p <0.05) correlation except between $\delta^{13}C_{Uvig}$ and $PC1_D$.

Finally, the MTM spectral analyses yield significant results for the $PC1_P$ (supplementary material). The Classic AR(1) indicates the strongest power at the frequency 0.023 (>99%), associated with a 43 kyr-cycle (period = 1/frequency). The REDFIT points the strongest power also at the frequency 0.023 (>99%), associated with the same 43 kyr-cycle.

TABLE 1 Reduced major axis regression results.

RMA Regression	$PC1_P$-$PC1_S$	$PC1_P$- $\delta^{13}C_{Uvig}$	$PC1_P$-$PC1_D$	$\delta^{13}C_{Uvig}$-$PC1_D$	$PC1_P$-Acc. rates	$PC1_S$-Acc. rates	$PC1_S$-ARTOC
r:	**0.51**	**-0.32**	**0.80**	-0.28	**0.58**	**0.77**	**0.66**
r^2:	0.26	0.01	0.64	0.08	0.34	0.59	0.44
t:	3.90	-2.13	4.99	-1.07	4.62	7.79	3.20
p:	**<0.05**	**0.04**	**<0.05**	0.30	**<0.05**	**<0.05**	**0.01**
Permutation *p*:	**<0.05**	**0.04**	**<0.05**	0.31	**<0.05**	**<0.05**	**0.01**

In bold are significant (p <0.05) values. PC1 stands for first component axes of productivity ($PC1_P$) stratification ($PC1_S$), and dissolution ($PC1_D$) proxies. Accumulation rates (Acc. rates) were calculated according to the age model presented in this study. the accumulation rates of total organic carbon (TOC*AR) used data from Rodrigues et al. (2018).

5 Discussion

5.1 Upper water column conditions

The relatively high *G.bull*/*G.rub* ratios, *G. glutinata* (%) and BFAR values (Figures 2A–C) imply a period of enhanced sea surface productivity during MIS 4 and, to a lesser extent, MIS 3. The high glacial productivity recorded by core SIS-249 agrees with previous studies for the southern Brazilian continental margin (SBCM), that also document enhanced productivity during the last glacial stage (e.g., Gu et al., 2017; Pereira et al., 2018; Portilho-Ramos et al., 2019; Frozza et al., 2020; Suárez-Ibarra et al., 2022). The increase of around 40% in *G.bull*/*G.rub* mean ratios from ~0.27 (110–83 ka) to ~0.39 (83–30 ka) suggests an increase in the upwelling of subsurface more nutrient-rich South Atlantic Central Water (Venancio et al., 2016; Lessa et al., 2017; Lessa et al., 2019; Portilho-Ramos et al., 2019).

As the upwelling of subsurface waters necessarily implies a break in the upper water column stratification, we should also expect a similar behaviour in the stratification proxies. This can be primarily confirmed by the high relative abundances of *G. truncatulinoides* right coiling form, which also point to a less stratified, well-mixed upper water column during MIS 4 (Figure 2D, Lohmann and Schweitzer, 1990; Renaud and Schmidt, 2003; Feldmeijer et al., 2015; Billups et al., 2016; Pinho et al., 2021). Furthermore, *G. truncatulinoides* types II and V (right coiling forms) have also been associated with a shallow thermocline and eutrophic conditions (de Vargas et al., 2001; Ujiié and Lipps, 2009; Ujiié et al., 2010; Quillévéré et al., 2013). Finally, the less stratified upper water column during MIS 4 (and to a lesser extent MIS 3) is also supported by the lower $\Delta\delta^{18}O_{G.inf\text{-}G.rub}$values (Figure 2E), which implies a reduced stratification between the mixed layer and the thermocline (Santos et al., 2017b).

Considering that the utilised foraminiferal proxies also depend on other environmental parameters (for instance, changes in the relative abundances of one species can be due to variations in the abundances of other species), the use of the principal component analysis helps to synthesise the variation of the proxies through time. The $PC1_P$ (the synthesised first principal component of the *G.bull*/*G.rub* ratios, *G. glutinata* (%), and BFAR proxies) from our core SIS-249 (in the SBCM) suggests a transition, from MIS 5 to MIS 4, to more eutrophic conditions in the upper water column (Figure 3B). This shift in nutrient availability is also evident in the clustering and PCoA analyses (Figures S3 and S4), where the dominant/significant species shift from warm and oligotrophic conditions during MIS 5 (*G. ruber albus*, *O. universa* and *G. menardii*) to species associated with high productivity during MIS 4 (*G. glutinata, G. bulloides* and *G. truncatulinoides* dextral coiling). However, studies for the southeastern Brazilian continental margin (SEBCM) document a shift to less eutrophic conditions during the same time interval (e.g., Portilho-Ramos et al., 2015; Lessa et al., 2017; Lessa et al., 2019), associated with the eccentricity cycle. Our study suggests two different mechanisms fertilising the SBCM and SEBCM regions i) enhanced Fe-fertilisation through dust delivery and riverine input due to the strengthening of southwesterly winds during glacial stadials and ii) boosted upwelling delivering subsurface nutrient rich waters to the surface during interstadials, respectively.

Notably, our $PC1_P$ (along with the $PC1_S$ and $PC1_D$) varies alongside the obliquity cycle, as shown by the spectral analyses (Figure 3). The Classic AR(1) (Figure S5) and REDFIT (Figure S6) give a >99% confidence for our $PC1_P$ to be orbitally paced by the obliquity cycle (43 kyr). Our results support the hypothesis that the obliquity cycle modulates a dust delivered Fe-fertilising mechanism at the studied site (Lopes et al., 2021). Briefly, under low-obliquity values, annual average insolation decreases at the poles (Paillard, 2021), which would favour the expansion of Antarctica's ice sheets (Doughty et al., 2021), intensifying the southwesterly winds (SWW, Toggweiler et al., 2006) and the wind-driven dust delivery. Then, during low-obliquity intervals, the north limit of the SWW belt migrates north (from 40°S to 30°S latitude, Lamy et al., 2015; Gili et al., 2017) close to our coring site. This would allow the northward/offshore transport of more nutrient-rich, fresher, and cooler waters of the RdlP closer to our study area, also fertilising the photic zone (e.g., Gu et al., 2017; Pereira et al., 2018; Portilho-Ramos et al., 2019; Bottezini et al., 2021; Bottezini et al., 2022).

In fact, a northern/offshore influence of RdlP outflows during periods of low obliquity values would be supported by the population collapses of the dinoflagellate species *Operculodinium centrocarpum*, associated with the Brazil Current, documented by Gu et al. (2017) (core GeoB2107-3) for the SBCM during MIS 4 and the MIS 3/2 boundary (Figure 3D). Also, the decreased influence of the core of the Brazil Current (which transports warm oligotrophic water) in the study area would lead to a decrease in upper water column stratification, evidenced by our $PC1_S$ (Figure 3B). In addition, a northern/offshore intrusion of the nutrient-rich RdlP

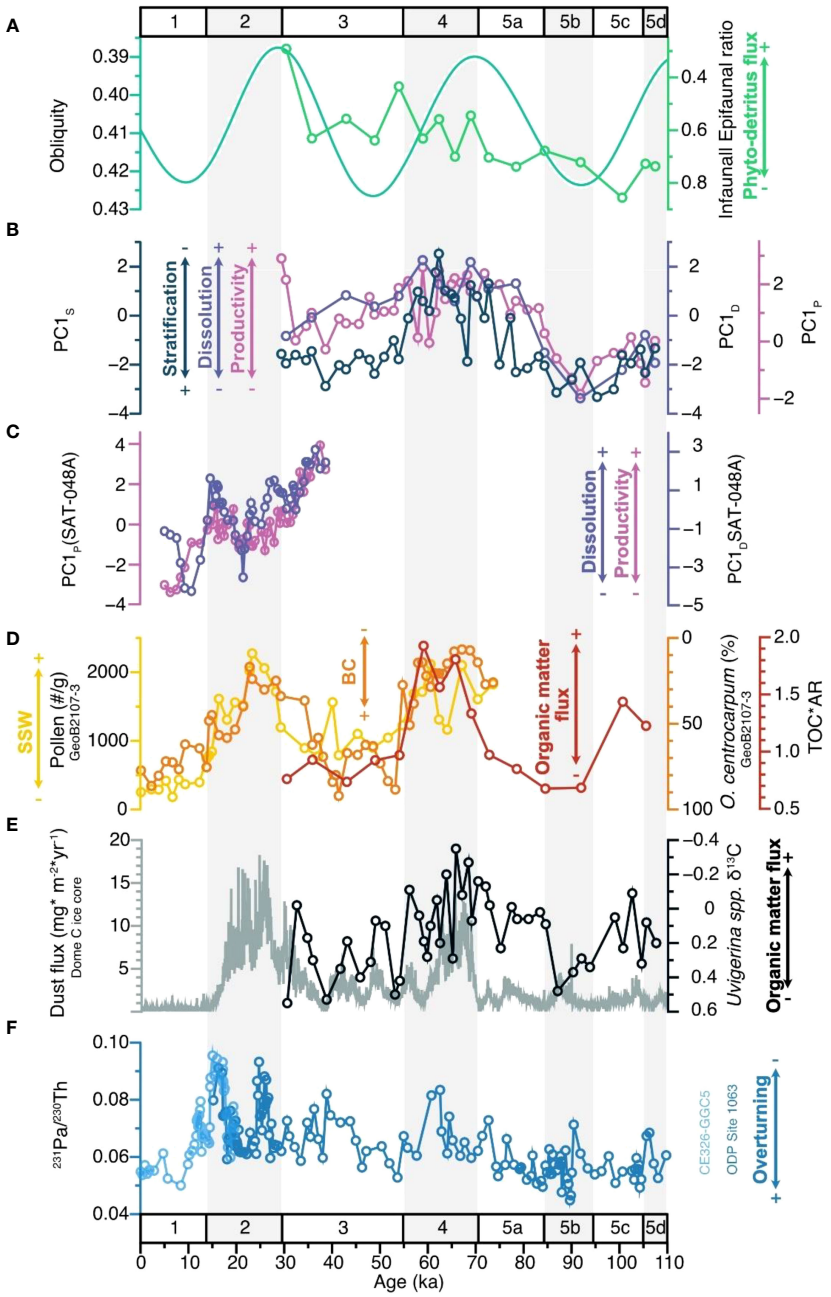

FIGURE 3
Time series graph showing the close relation between **(A)** obliquity values (Laskar et al., 2004), Infaunal/Epifaunal benthic foraminifera ratio by Rodrigues et al. (2018), and **(B)** the proxies for productivity ($PC1_P$), stratification ($PC1_S$) and dissolution ($PC1_D$) from core SIS-249. On **(C)**, synthesised record of productivity ($PC1_P$) and dissolution ($PC1_D$) from core SAT-048A (Suárez-Ibarra et al., 2022) and **(D)** SWW strength, as inferred by terrestrial pollen and the dinoflagellate species *O. centrocarpum* recorded by Gu et al. (2017, core GeoB2107-3, southern Brazilian continental margin), and the Total Organic Carbon (values from Rodrigues et al., 2018, also in core SIS-249) times the Accumulation Rates are shown. On **(E)**, the dust flux in Antarctica (Dome C ice core, Lambert et al., 2008) and core SIS-249 $\delta^{13}C_{Uvig}$ values (Rodrigues et al., 2018). Finally, on **(F)** the $^{231}Pa/^{230}Th$ proxy by McManus et al. (2004, light blue line, sediment core CE326-GGC5, 33°42'N, 57°35'W, 4550 mbsl) and Böhm et al. (2015, dark blue line, sediment core ODP Site 1063, Leg 172, 33°41'N, 57°37'W, 4,584 mbsl). Y axes in **(A)**, *O. centrocarpum* (%) and *Uvigerina* spp. $\delta^{13}C$ are reversed.

outflows (or freshwater bodies formed along the continental shelf) can also be inferred from the presence of freshwater diatoms during MIS 3–2 from core SIS-188 (Bottezini et al., 2021; Bottezini et al., 2022).

Moreover, strengthened SWW would also transport wind-driven particles from southern South America to the study area, increasing the Fe-fertilisation from terrestrial sources (Lopes et al., 2021). During MIS 5/4 and 3/2 boundaries, the elevated pollen concentrations (e.g., Gu et al., 2017, SBCM, core GeoB2107-3) can be interpreted as enhanced aeolian transport (Figure 3), and thus, terrestrial dust fertilisation. Additionally, the presence of the Andean pollen *Nothofagus*, recorded by Gu et al. (2017) during the late MIS 3 and MIS 2, corroborates the idea of enhanced windiness, strengthened SWW and aeolian Fe-fertilisation from

South American sources. On top of it, Lopes et al. (2021) compiled chemical studies analysing the provenance of glacial terrigenous dust in the southwest Atlantic, pointing southern South America (central-western Argentina and Patagonia) as the main source (e.g., Delmonte et al., 2010; Weber et al., 2012; Gili et al., 2017).

In summary, our record suggests two mechanisms to have fertilised the study area: i) upwelling, enhanced by the interplay of lower glacial sea level and the local bathymetry allowing the shoaling of nutrient-rich South Atlantic Central Water (also richer in silicic acid, Portilho-Ramos et al., 2019) to the sub-surface (e.g., Mahiques et al., 2007; Lessa et al., 2016) and; ii) obliquity-paced fertilisation from southern South America (wind-driven dust and the RdlP outflows) through enhanced aeolian transport, associated with expanded SWW. Both processes lead to a decrease in the upper water column stratification, first, by the ascension of cooler and less salty subsurface South Atlantic Central Water and, second, by the offshore displacement of the core of the Brazil Current. Ultimately, the correlation value between $PC1_P$ and $PC1_S$ (ρ<0.05, r=0.51) corroborates the synergy between the boosted biological pump and less stratified conditions.

5.2 Organic matter export and seafloor dynamics

Enhanced primary productivity (i.e., *G.bull*/*G.rub* and *G. glutinata* %) and decreased upper water column stratification ($PC1_S$) are mirrored by high accumulation rates of total organic carbon during MIS 4 (TOC*AR, Figure 3, TOC data from Rodrigues et al., 2018, and accumulation rates from this study). In addition, the BFAR proxy, commonly employed to reconstruct past surface productivity by examining organic matter export to the seafloor (Herguera and Berger, 1991), demonstrates significant co-variation (ρ<0.05) with both *G.bull*/*G.rub* (r=0.5) and *G. glutinata* relative abundances (r=0.55). Although the BFAR proxy has been widely used to quantitatively estimate past productivity changes, this relationship is not always straightforward (e.g., Naidu and Malmgren, 1995; Den Dulk et al., 2000; Jorissen et al., 2007). This limitation arises from the lack of calibration across various productivity settings, among other factors (for an in-depth discussion, please refer to Jorissen et al., 2007). However, Dias et al. (2021) demonstrated that the BFAR can indicate variations in the Cabo Frio Upwelling System, located in the SEBCM, where higher BFAR values correspond to increased export of fresh marine organic carbon.

The above-mentioned coupling suggests efficient glacial carbon sequestration via biological pump in the study area. A schematic representation of coupled benthic-pelagic changes observed in mid-latitude southwest Atlantic during the 107–30 ka time interval is presented in Figure 4.

The here evidenced increase in the export of organic matter (OM) to the seafloor from MIS 5 to MIS 4 (and to a lesser extent in MIS 3) aligns with the findings of Rodrigues et al. (2018). They observe a decrease in the infaunal/epifaunal benthic foraminifera ratio in core SIS-249, indicating a shift in the bioavailability of OM from refractory to labile forms (Gooday, 1993; Smart et al., 1994; Gooday, 2003; Garcia-Chapori et al., 2014; de Almeida et al., 2022). This change has significant implications for calcium carbonate preservation. As highlighted in our study, during phytoplankton blooms in glacial periods, higher amounts of OM (more labile, more soluble, and more easily remineralised) are exported to the seafloor, resulting in increased CO_2 release, lower pH, and the dissolution of $CaCO_3$ (Figure 4). In addition, despite the relatively brief sinking time of planktonic foraminifera tests (Takahashi and Bé, 1984; Schiebel and Hemleben, 2017), they could experience minor dissolution during transit through the CO_3^{2-} under-saturated intermediate SCWs (Frenz et al., 2003). These findings shed light on the important role of sea surface productivity and water mass properties in influencing the dynamics of carbonate preservation during different climatic periods.

Despite the sparser sampling in $PC1_D$ compared to $PC1_P$ and $PC1_S$, our study found a strong correlation between $PC1_P$ and $PC1_D$ in core SIS-249 (ρ<0.05, r=0.80, Table 1). This correlation supports the idea that enhanced dissolution is triggered by glacial high productivity, as it is also documented during the last deglaciation (Suárez-Ibarra et al., 2022, Figure 3C), even in deeper cores under the presence of modern non-corrosive Northern Component water. While inferring changes in paleoproductivity based on compositional assemblages from partially dissolved samples can be imprecise, our study addresses this issue by complementing the data with geochemical and sedimentological analyses. These additional analyses, like the $\delta^{18}O$ signal from the species *G. inflata* and *G. ruber* (both dissolution resistant according to experimental studies from Petró et al., 2018), as well as the BFAR and the TOC*AR, are less biased by dissolution.

Due to the OM enrichment in ^{12}C from photosynthesis (O'Leary, 1988; Ravelo and Hillaire-Marcel, 2007), remineralisation at the seafloor is expected to drive negative excursions in the endobenthic foraminiferal $\delta^{13}C$ values, as seen in MIS 5c and 4 (Figure 3E). Nevertheless, although $\delta^{13}C_{Uvig}$ is significantly anti correlated with our $PC1_P$ (ρ<0.05), the correlation value is weak (r=-0.31) and is likely impacted by additional changes in the dissolved inorganic carbon $\delta^{13}C$ of pore waters and/or the local bottom water mass geometry (Ravelo and Hillaire-Marcel, 2007; Hesse et al., 2014). Lopes et al. (2021) suggested an increased influence of more corrosive SCW at the core site during MIS 4 and 3, based on an apparent phasing between the $\delta^{13}C_{Uvig}$ record from core SIS-249 and the dust flux record from Dome C ice core (Lambert et al., 2008), as the dust-fertilisation in the Southern Ocean would be recorded in the $\delta^{13}C$ of the bottom water masses (Figure 3E). Although we do not exclude the possible influence of a higher proportion of SCW on carbonate preservation, our data show a relationship between the changes in the organic carbon cycle (periods of enhanced sea surface productivity associated with higher exportation of labile OM) and the deep-sea carbonate system. This highlights the need for further investigations applying a conservative or quasi-conservative water mass circulation tracer to elucidate the water masses mixing proportions at our site during the last glacial inception.

Furthermore, a third process that could have impacted the calcium carbonate preservation is the intensity of the Atlantic Meridional Overturning Circulation (AMOC). In a scenario with

10.3389/fevo.2023.1238334

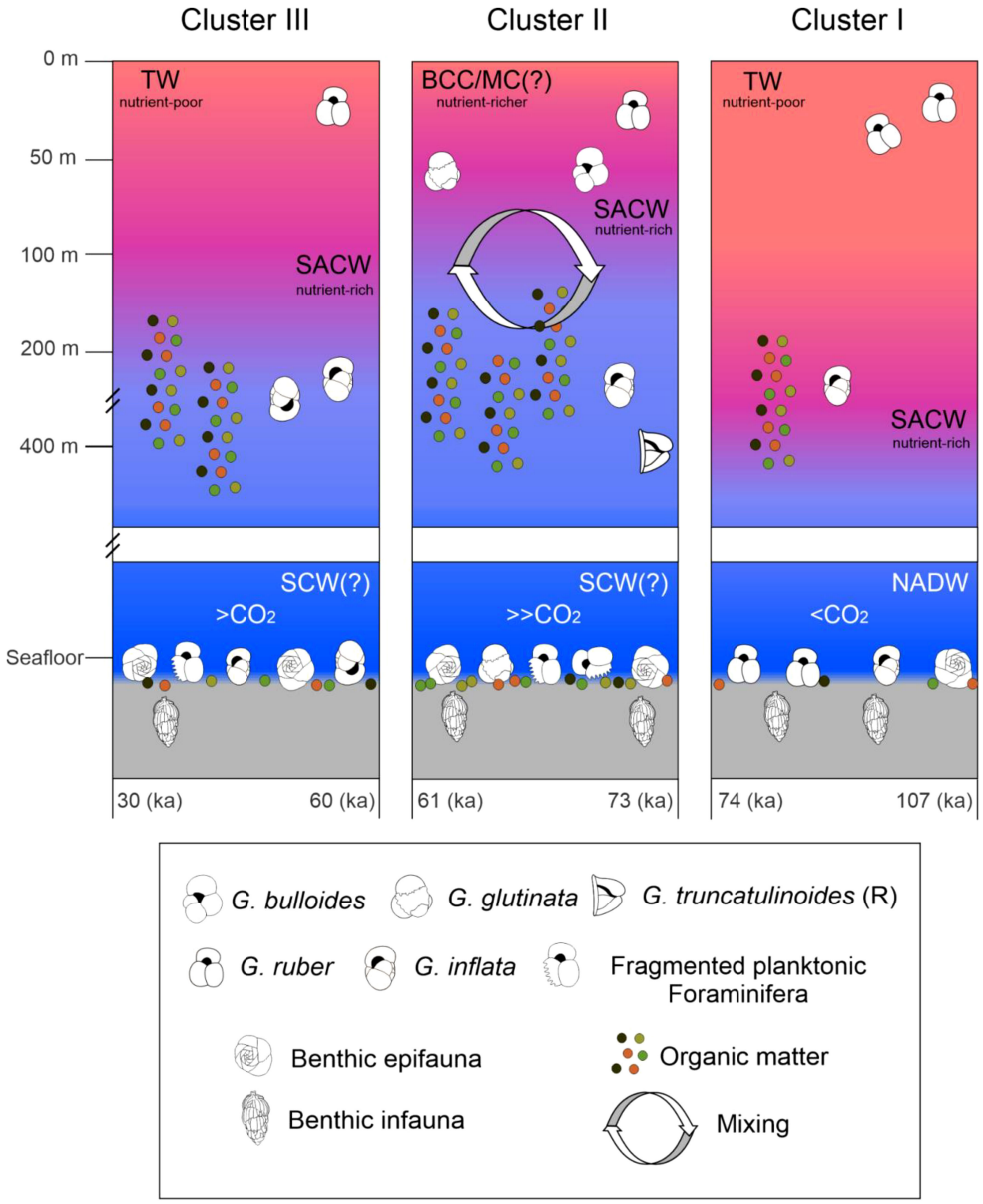

FIGURE 4
Schematic representation of main changes in sea surface and seafloor conditions recorded by core SIS-249 for the 107–30 ka interval, according to the foraminiferal assemblages and their respective three clusters. Interval I (107–74 ka) is dominated by species related to warm and oligotrophic water; species from interval II (73–61 ka) are related to eutrophic water, with high productivity and low stratification; and interval III (60–30 ka) is related to cooler water species. Interval II suggests higher levels of CO_2 at the seafloor mainly due to larger exports of OM. Benthic epifaunal and infaunal proportions, as well as TOC*AR.

a sluggish AMOC, the reduced water flow at the seafloor leads to an accumulation of respired CO_2, resulting in decreased water pH and subsequent corrosion of $CaCO_3$ (McManus et al., 2004; Thornalley et al., 2013; Howe et al., 2016b). Despite the lower temporal resolution of our $PC1_D$ record, it is evident that the positive excursions of $^{231}Pa/^{230}Th$ (Figure 3F), indicative of a sluggish AMOC (McManus et al., 2004; Böhm et al., 2015), do not align with the longer-term events of intense dissolution recorded by core SIS-249, which also seem to follow the 43 kyr-cycle. Furthermore, our findings are consistent with the conclusions of Suárez-Ibarra et al. (2022), who, using a dataset with higher temporal resolution, found that surface productivity was the primary factor driving calcium carbonate dissolution close to our study site.

Additionally, we would like to highlight that these processes, i) the biological pump and ii) water mass configuration, are not mutually exclusive and both may respond to the obliquity cycle. Under low obliquity values and decreased insolation at high latitudes, the (sub)polar fronts migrate equatorward: (i) displacing the north limit of the SSW belt closer to the study site, enhancing the wind-driven dust and continental river fertilisation, and boosting the biological pump; (ii) expanding the southern ice coverage, leading to an increased brine production and enhanced

SCW formation (Govin et al., 2009). This would result in the volumetric increase in the deep Atlantic of more corrosive SCWs which also act in part as a CO_2 storage reservoir.

Finally, although the enhanced remineralization causes part of the OM and biogenic carbonate to be recirculated back in the system instead of being exported to the sediments, we suggest an efficient biological pump in the mixed-layer, which removes inorganic carbon and points out the importance of the SBCM as a glacial carbon capture and sink of atmospheric CO_2 and thus part of the puzzle of glacial-interglacial CO_2 changes.

6 Conclusions

Based on our multiproxy analysis carried out in the sediments of core SIS-249, retrieved from the lower continental slope of the southwest Atlantic, southern Brazilian continental margin, we can conclude:

(i) In the study area, there was an increase in sea surface productivity from the last interglacial (MIS 5) to the subsequent glacial (MIS 4 and, partly, MIS 3). When compared to cores from the southeastern Brazilian continental margin, two possible fertilising mechanisms were identified: during glacial stadials the south was Fe-fertilised by enhanced dust delivery and riverine input due to the strengthening of southwesterly winds. During interstadials the southeastern region experienced expanded upwelling delivering subsurface nutrient rich waters to the surface.

(ii) Glacial increased continental aeolian-riverine fertilisation and reduced upper water column stratification led to an efficient removal of inorganic carbon via the biological pump, as evidenced by the high accumulation rates of total organic carbon, suggesting that the study area is capable to efficiently capture and sink atmospheric CO_2.

(iii) The degradation of the exported glacial organic matter can lead to decreased pH in bottom water, aiding dissolution and may play a major role in carbon sequestration irrespective of/addition to, deep water mass conditions.

Data availability statement

The datasets presented in this study can be found in online repositories. The names of the repository/repositories and accession number(s) can be found in the article/Supplementary Material.

Author contributions

Conceptualization – JS-I, TF, JC, MP; Data curation – JS-I, TF, CF; Formal Analysis – All; Funding acquisition – JS-I, JC, MP; Investigation – TF, MP; Methodology – JS-I, TF, CF, MP; Project administration – JC, MP; Resources – JS-I, JC, MP; Software – JS-I, CF, SC, MP; Supervision – TC, SC, TG-T, JC, MP; Validation – All; Visualization – JS-I, CF, SC, MP; Writing – original draft – JS-I, TF, CF; Writing – review & editing – All. All authors contributed to the article and approved the submitted version.

Funding

The author/s declare financial support was received for the research, authorship, and/or publication of this article. This work was funded by the Brazilian Coordination of Higher Education Staff Improvement–CAPES (grant number 88887.091729/2014-01), the Brazilian National Council for Scientific and Technological Development –CNPq (grant number 407922/2016-4) and the Charles University Grant Agency (GAUK, grant number 355422). JS-I thanks the STARS program (Přírodovědecká Fakulta, Univerzita Karlova), the ERASMUS+ program, the 4EU+ Alliance and the Johanna M. Resig Fellowship from the Cushman Foundation for Foraminiferal Research. TF thanks the CAPES and the DAAD for his MSc and PhD scholarships, respectively. CF thanks the CAPES for her PhD scholarship. TP acknowledges the AWI INSPIRES II program. BD appreciates financial support from FAPESP (grants 2022/01056-9, 2020/11452-3, and 2018/15123-4). MS thanks the STARS program (Přírodovědecká Fakulta, Univerzita Karlova). JC and MP acknowledge support from CNPq, grants 309394/2021-0 and 315684/2021-6, respectively.

Acknowledgments

The authors thank Rodrigo Portilho-Ramos, Thiago Santos, João Ballalai, Manuel F.G. Weinkauf and three reviewers for discussions through the development of this manuscript.

Conflict of interest

The authors declare that the research was conducted in the absence of any commercial or financial relationships that could be construed as a potential conflict of interest.

Publisher's note

Supplementary material

The Supplementary Material for this article can be found online at: https://www.frontiersin.org/articles/10.3389/fevo.2023.1238334/full#supplementary-material

References

Ahn, J., and Brook, E. J. (2008). Atmospheric CO2 and climate on millennial time scales during the last glacial period. *Science* 322, 83–85. doi: 10.1126/SCIENCE.1160832

Alves, E., Macario, K., Souza, R., Pimenta, A., Douka, K., Oliveira, F., et al. (2015). Radiocarbon reservoir corrections on the Brazilian coast from pre-bomb marine shells. *Quaternary Geochronology* 29, 30–35. doi: 10.1016/j.quageo.2015.05.006

Angulo, R. J., de Souza, M. C., Reimer, P. J., and Sasaoka, S. K. (2005). Reservoir effect of the southern and southeastern Brazilian coast. *Radiocarbon* 47, 67–73. doi: 10.1017/S0033822200052206

Archer, D., and Maier-Reimer, E. (1994). Effect of deep-sea sedimentary calcite preservation on atmospheric CO_2 concentration. *Nature* 367, 260–263. doi: 10.1038/367260a0

Arrhenius, G. (1952). Sediment cores from the east pacific. *Rep. Swedish Deep-Sea Expedition* 1947–1948 (5), 1–228.

Bé, A. W. H., and Hutson, W. H. (1977). Ecology of planktonic foraminifera and biogeographic patterns of life and fossil assemblages in the Indian ocean. *Micropaleontology* 23 (4), 369–414. doi: 10.2307/1485406

Berger, W. H., Bonneau, M.-C., and Parker, F. L. (1982). Foraminifera on the deep-sea floor: lysocline and dissolution rate. *Oceanologica Acta* 5 (2), 249–258.

Billups, K., Hudson, C., Kunz, H., and Rew, I. (2016). Exploring *Globorotalia truncatulinoides* coiling ratios as a proxy for subtropical gyre dynamics in the northwestern Atlantic Ocean during late Pleistocene Ice Ages. *Paleoceanography* 31, 553–563. doi: 10.1002/2016PA002927

Blaauw, M., and Christeny, J. A. (2011). Flexible paleoclimate age-depth models using an autoregressive gamma process. *Bayesian Anal.* 6, 457–474. doi: 10.1214/11-BA618

Böhm, E., Lippold, J., Gutjahr, M., Frank, M., Blaser, P., Antz, B., et al. (2015). Strong and deep atlantic meridional overturning circulation during the last glacial cycle. *Nature* 517, 73–76. doi: 10.1038/nature14059

Bottezini, S. R., Diniz, D., Ávila, A. S. P., and Leonhardt, A. (2022). Continental influence on the fertilization of marine waters during the Late Quaternary in the South of Brazilian Continental Margin. *Ocean Coast. Res.* 70, e22021. doi: 10.1590//2675-2824070.21072srb

Bottezini, S. R., Leonhardt, A., Diniz, D., and Ávila, A. S. P. (2021). Climatic and vegetational dynamics in Southern Brazil between 47.8 and 7.4 cal ka BP: a palynological analysis. *Rev. Bras. Paleontologia* 24, 345–356. doi: 10.4072/rbp.2024.4.05

Braga, E. S., Chiozzini, V. C., Berbel, G. B. B., Maluf, J. C. C., Aguiar, V. M. C., Charo, M., et al. (2008). Nutrient distributions over the Southwestern South Atlantic continental shelf from Mar del Plata (Argentina) to Itajaí (Brazil): Winter-summer aspects. *Continental Shelf Res.* 28, 1649–1661. doi: 10.1016/j.csr.2007.06.018

Broecker, W. S. (1982). Glacial to interglacial changes in ocean chemistry, Prog. *Oceanogr.* 11, 151–197. doi: 10.1016/0079-6611(82)90007-6

Broecker, W. S., and Peng, T. H. (1982). *Tracers in the Sea* (New York: Eldigio Press), 689.

Brovkin, V., Ganopolski, A., Archer, D., and Munhoven, G. (2012). Glacial CO_2 cycle as a succession of key physical and biogeochemical processes. *Clim. Past.* 8, 251–264. doi: 10.5194/cp-8-251-2012

Chalk, T. B., Foster, G. L., and Wilson, P. A. (2019). Dynamic storage of glacial CO_2 in the Atlantic Ocean revealed by boron $[CO_3^{2-}]$ and pH records. *Earth Planetary Sci. Lett.* 510, 1–11. doi: 10.1016/j.epsl.2018.12.022

Chiessi, C. M., Ulrich, S., Mulitza, S., Pätzold, J., and Wefer, G. (2007). Signature of the Brazil-Malvinas Confluence (Argentine Basin) in the isotopic composition of planktonic foraminifera from surface sediments. *Mar. Micropaleontology* 64, 52–66. doi: 10.1016/j.marmicro.2007.02.002

CLIMAP Project Members (1976). The surface of the ice-age earth. *Science* 191 (4232), 1131–1137. doi: 10.1126/science.191.4232.1131

Conan, S. M. H., and Brummer, G. J. A. (2000). Fluxes of planktic foraminifera in response to monsoonal upwelling on the Somalia Basin margin. *Deep Sea Res. Part II: Topical Stud. Oceanography* 47 (9-11), 2207–2227. doi: 10.1016/s0967-0645(00)00022-9

Conan, S. M. H., Ivanova, E. M., and Brummer, G. J. A. (2002). Quantifying carbonate dissolution and calibration of foraminiferal dissolution indices in the Somali Basin. *Mar. Geology* 182, 325–349. doi: 10.1016/S0025-3227(01)00238-9

Crivellari, S., Viana, P. J., de Carvalho Campos, M., Kuhnert, H., Lopes, A. B. M., da Cruz, F. W., et al. (2021). Development and characterization of a new in-house reference material for stable carbon and oxygen isotopes analyses. *J. Analytical Atomic Spectrometry* 36 (6), 1125–1134. doi: 10.1039/D1JA00030F

Curry, W. B., and Oppo, D. W. (2005). Glacial water mass geometry and the distribution of $\delta^{13}C$ of Sigma CO_2 in the western Atlantic Ocean. *Paleoceanography* 20, PA1017. doi: 10.1029/2004PA001021

de Almeida, K., Mello, R. M., Rodrigues, A. R., and Bastos, A. C. (2022). Bathymetric and regional benthic foraminiferal distribution on the Espírito Santo Basin slope, Brazil (SW Atlantic). *Deep Sea Res. Part I: Oceanographic Res. Papers* 181, 103688. doi: 10.1016/j.dsr.2022.103688

Delmonte, B., Andersson, P. S., Schöberg, H., Hansson, M., Petit, J. R., Delmas, R., et al. (2010). Geographic provenance of aeolian dust in East Antarctica during Pleistocene glaciations: preliminary results from Talos Dome and comparison with East Antarctic and new Andean ice core data. *Quaternary Sci. Rev.* 29 (1–2), 256–264. doi: 10.1016/j.quascirev.2009.05.010

Den Dulk, M., Reichart, G. J., van Heyst, S., Zachariasse, W. J., and van der Zwaan, G. J. (2000). Benthic foraminifera as proxies of organic matter flux and bottom water oxygenation? A case history from the northern Arabian Sea. *Palaeogeography Palaeoclimatology Palaeoecol.* 161, 337–359. doi: 10.1016/S0031-0182(00)00074-2

de Vargas, C., Renaud, S., Hilbrecht, H., and Pawlowski, J. (2001). Pleistocene adaptive radiation in *Globoratalia truncatulinoides*: genetic, morphologic, and environmental evidence. *Paleobiology* 27 (1), 104–125. doi: 10.1666/0094-8373(2001)027<0104:PARIGT>2.0.CO;2

Dias, B. B., Piotrowski, A. M., Barbosa, C. F., Venancio, I. M., Chiessi, C. M., and Albuquerque, A. L. S. (2021). Coupled changes in western south Atlantic carbón sequestration and particle reactive element cycling during millennial-scale Holocene climate variability. *Sci. Rep.* 11, 24378. doi: 10.1038/s41598-021-03821-8

Doss, W., and Marchitto, T. M. (2013). Glacial deep ocean sequestration of CO_2 driven by the eastern equatorial Pacific biologic pump. *Earth Planetary Sci. Lett.* 377-378, 45–54. doi: 10.1016/j.epsl.2013.07.019

Doughty, A. M., Kaplan, M. R., Peltier, C., and Barker, S. (2021). A maximum in global glacier extent during MIS 4. *Quaternary Sci. Rev.* 261, 106948. doi: 10.1016/j.quascirev.2021.106948

Duplessy, J. C., Shackleton, N. J., Fairbanks, R. G., Labeyrie, L., Oppo, D., and Kallel, N. (1988). Deepwater source variations during the last climatic cycle and their impact on the global deepwater circulation. *Paleoceanography* 3 (3), 343–360. doi: 10.1029/pa003i003p00343

Elderfield, H., Vautravers, M., and Cooper, M. (2002). The relationship between shell size and Mg/Ca, Sr/Ca, $\delta^{18}O$, and $\delta^{13}C$ of species of planktonic foraminifera. *Geochemistry Geophysics Geosystems* 3, 1–13. doi: 10.1029/2001GC000194

Emiliani, C. (1954). Depth habitats of some species of pelagic foraminifera as indicated by oxygen isotope ratios. *Am. J. Sci.* 252 (3), 149–158. doi: 10.2475/ajs.252.3.149

Feldmeijer, W., Metcalfe, B., Brummer, G.-J. A., and Ganssen, G. M. (2015). Reconstructing the depth of the permanent thermocline through the morphology and geochemistry of the deep dwelling planktonic foraminifer *Globorotalia truncatulinoides*. *Paleoceanography* 30, 1–22. doi: 10.1002/2014PA002687

Frenz, M., and Henrich, R. (2007). Carbonate dissolution revealed by silt grain-size distribution: Comparison of Holocene and Last Glacial Maximum Sediments from the Pelagic South Atlantic. *Sedimentology* 54, 391–404. doi: 10.1111/j.1365-3091.2006.00841.x

Frenz, M., Höppner, R., Stuut, J.-B. W., Wagner, T., and Henrich, R. (2003). "Surface sediment bulk geochemistry and grain-size composition related to the oceanic circulation along the south american continental margin in the southwest atlantic," in *The South Atlantic in the Late Quaternary*. Eds. G. Wefer, S. Mulitza and V. Ratmeyer. (Berlin, Heidelberg, New York, Tokyo: Springer-Verlag), 347–373. doi: 10.1007/978-3-642-18917-3_17

Frozza, C. F., Pivel, M. A. G., Suarez-Ibarra, J. Y., Ritter, M. N., and Coimbra, J. C. (2020). Bioerosion on late Quaternary planktonic Foraminifera related to paleoproductivity in the western South Atlantic. *Paleoceanography Paleoclimatology* 35, e2020PA003865. doi: 10.1029/2020pa003865

Garcia-Chapori, N., Laprida, C., Watanabe, S., Totah, V., and Violante, R. A. (2014). Mid-Late Pleistocene benthic foraminifera from Southwestern South Atlantic: driven by primary productivity or water mass properties? *Micropaleontology* 60, 195–210. doi: 10.47894/mpal.60.2.03

Gili, S., Gaiero, D. M., Goldstein, S. L., Chemale, F. Jr., Jweda, J., Kaplan, M. R., et al. (2017). Glacial/interglacial changes of Southern Hemisphere wind circulation from the geochemistry of South American dust. *Earth Planetary Sci. Lett.* 469, 98–109. doi: 10.1016/j.epsl.2017.04.007

Gonzales, M. V., de Almeida, F. K., Costa, K. B., Santarosa, A. C. A., Camillo, E., de Quadros, J. P., et al. (2017). Help INDEX: *Hoenglundina elegans* preservation index for marine sediments in the western South Atlantic. *J. Foraminiferal Res.* 47, 56–69. doi: 10.2113/gsjfr.47.1.56

Gooday, A. J. (1993). Deep-sea benthic foraminiferal species which exploit phytodetritus: characteristic features and controls on distribution. *Mar. Micropaleontology* 22 (3), 187–205. doi: 10.1016/0377-8398(93)90043-W

Gooday, A. J. (2003). Benthic foraminifera (Protista) as tools in deep-water palaeoceanography: environmental influences on faunal characteristics. *Adv. Mar. Biol.* 46, 1–90. doi: 10.1016/S0065-2881(03)46002-1

Gordon, A. L. (1989). Brazil-malvinas confluence-1984. *Deep Sea Res. Part A. Oceanographic Res. Papers* 36, 359–361. doi: 10.1016/0198-0149(89)90042-3

Gordon, A. L., and Greengrove, C. L. (1986). Geostrophic circulation of the Brazil-Falkland confluence. *Deep-Sea Res.* 33 (5), 573–585. doi: 10.1016/0198-0149(86)90054-3

Govin, A., Chiessi, C. M., Zabel, M., Sawakuchi, A. O., Heslop, D., Hörner, T., et al. (2014). Terrigenous input off northern South America driven by changes in Amazonian climate and the North Brazil Current retroflection during the last 250 ka. *Clim. Past* 10, 843–862. doi: 10.5194/cp-10-843-2014

Govin, A., Michel, E., Labeyrie, L., Waelbroeck, C., Dewilde, F., and Jansen, E. (2009). Evidence for northward expansion of Antarctic Bottom Water mass in the Southern Ocean during the last glacial inception. *Paleoceaonography* 24 (1), PA1202. doi: 10.1029/2008PA001603

Groeneveld, J., and Chiessi, C. M. (2011). Mg/Ca of *Globorotalia inflata* as a recorder of permanent thermocline temperatures in the South Atlantic. *Paleoceanography* 26, PA2203. doi: 10.1029/2010PA001940

Gu, F., Zonneveld, K. A., Chiessi, C. M., Arz, H. W., Pätzold, J., and Behling, H. (2017). Long-term vegetation, climate and ocean dynamics inferred from a 73,500 years old marine sediment core (GeoB2107-3) off southern Brazil. *Quaternary Sci. Rev.* 172, 55–71. doi: 10.1016/j.quascirev.2017.06.028

Guichard, S., Jorissen, F., Bertrand, P., Gervais, A., Martinez, P., Peypouquet, J. P., et al. (1997). Foraminifères benthiques et paléoproductivité: réflexions sur une carotte de l'*upwelling* (NW africain). *Comptes Rendus l'Académie Des. Sci. - Ser. IIA - Earth Planetary Sci.* 325, 65–70. doi: 10.1016/S1251-8050(97)83274-0

Hammer, Ø., Harper, D. A. T., and Ryan, P. D. (2001). PAST: Paleontological statistics software package for education and data analysis. *Palaeontologia Electronica* 4, 1–9.

Heaton, T. J., Köhler, P., Butzin, M., Bard, E., Reimer, R. W., Austin, W. E. N., et al. (2020). Marine20—The marine radiocarbon age calibration curve (0–55,000 cal BP). *Radiocarbon* 62, 779–820. doi: 10.1017/RDC.2020.68

Herguera, J. C., and Berger, W. H. (1991). Paleoproductivity from benthic foraminifera abundance: Glacial to postglacial change in the west equatorial Pacific. *Geology* 19 (12), 1173–1176. doi: 10.1130/0091-7613(1991)019%3C1173:PFBFAG%3E2.3.CO;2

Hesse, T., Wolf-Gladrow, D., Lohmann, G., Bijma, J., Mackensen, A., and Zeebe, R. E. (2014). Modeling $\delta^{13}C$ in benthic foraminifera: insights from model sensitivity experiments. *Mar. Micropaleontology* 112, 50–61. doi: 10.1016/j

Howe, J. N. W., Huang, K.-F., Oppo, D. W., Chiessi, C. M., Mulitza, S., Blusztajn, J., et al. (2018). Similar mid-depth atlantic water mass provenance during the last glacial maximum and heinrich stadial 1. *Earth Planetary Sci. Lett.* 490, 51–61. doi: 10.1016/j.epsl.2018.03.006

Howe, J. N. W., Piotrowski, A. M., Noble, T. L., Mulitza, S., Chiessi, C. M., and Baton, G. (2016a). North atlantic deep water production during the last glacial maximum. *Nat. Commun.* 7, 11765. doi: 10.1038/ncomms11765

Howe, J. N. W., Piotrowski, A. M., Oppo, D. W., Huang, K. F., Mulitza, S., Chiessi, C., et al. (2016b). Antarctic intermediate water circulation in the South Atlantic over the past 25,000 years. *Paleoceanography* 31, 1302–1314. doi: 10.1002/2016PA002975

Husson, D. (2014). *MathWorks File Exchange: RedNoise_ConfidenceLevels*. Available at: https://www.mathworks.com/matlabcentral/fileexchange/45539-rednoise_confidencelevels.

Jorissen, F. J., Fontanier, C., and Thomas, E. (2007). Paleoceanographical proxies based on deep-sea benthic foraminiferal assemblage characteristics. *Developments Mar. Geology* 1, 263–325. doi: 10.1016/S1572-5480(07)01011-1

Kučera, M. (2007). Planktonic foraminifera as tracers of past oceanic environments. *Developments Mar. Geology* 1, 213–262. doi: 10.1016/S1572-5480(07)01011-1

Lambert, F., Delmonte, B., Petit, J. R., Bigler, M., Kaufmann, P. R., Hutterli, M. A., et al. (2008). Dust-climate couplings over the past 800,000 years from the EPICA Dome C ice core. *Nature* 452, 616–619. doi: 10.1038/nature06763

Lamy, F., Arz, H.W., Kilian, R., Lange, C. B., Lembke-Jene, L., Wengler, M., et al. (2015). Glacial reduction and millennial-scale variations in Drake Passage through flow. *Proc. Natl. Acad. Sci.* 112, 13496–13501. doi: 10.1073/pnas.1509203112

Laskar, J., Robutel, P., Joutel, F., Gastineau, M., Correia, A. C. M., and Levrard, B. (2004). A long term numerical solution for the insolation quantities of the Earth. *A A* 428, 261–285. doi: 10.1051/0004-6361:20041335

Le, J., and Shackleton, N. J. (1992). Carbonate dissolution fluctuations in the western equatorial Pacific during the late Quaternary. *Paleoceanography* 7, 21–42. doi: 10.1029/91PA02854

Lessa, D., Morard, R., Jonkers, L., Venancio, I. M., Reuter, R., Baumeister, A., et al. (2020). Distribution of planktonic foraminifera in the subtropical South Atlantic: depth hierarchy of controlling factors. *Biogeosciences* 17, 4313–4342. doi: 10.5194/bg-17-4313-2020

Lessa, D. V. O., Ramos, R. P., Barbosa, C. F., da Silva, A. R., Belem, A., Turcq, B., et al. (2014). Planktonic foraminifera in the sediment of a western boundary upwelling system off Cabo Frio, Brazil. *Marine Micropaleontology*. *106* 55–68. doi: 10.1016/j.marmicro.2013.12.003

Lessa, D. V. O., Santos, T. P., Venancio, I. M., and Albuquerque, A. L. S. (2017). Offshore expansion of the Brazilian coastal upwelling zones during Marine Isotope Stage 5. *Global Planetary Change* 158, 13–20. doi: 10.1016/j.gloplacha.2017.09.006

Lessa, D. V. O., Santos, T. P., Venancio, I. M., Santarosa, A. C. A., dos Santos Junior, E. C., Toledo, F. A. L., et al. (2019). Eccentricity-induced expansions of Brazilian coastal upwelling zones. *Global Planetary Change* 179, 33–42. doi: 10.1016/j.gloplacha.2019.05.002

Lessa, D. V., Venancio, I. M., dos Santos, T. P., Belem, A. L., Turcq, B. J., Sifeddine, A., et al. (2016). Holocene oscillations of southwest atlantic shelf circulation based on planktonic foraminifera from an upwelling system (Off cabo frio, southeastern Brazil). *Holocene* 26 (8), 1175–1187. doi: 10.1177/0959683616638433

Li, M., Hinnov, L. A., and Kump, L. R. (2019). Acycle: Time-series analysis software for paleoclimate projects and education. *Comput. Geosciences* 127, 12–22. doi: 10.1016/j.cageo.2019.02.011

Lisiecki, L. E., and Raymo, M. E. (2005). A Pliocene–Pleistocene stack of 57 globally distributed benthic $\delta^{18}O$ records. *Paleoceanography* 20, PA1003. doi: 10.1029/2004PA001071

Locarnini, R. A., Mishonov, A. V., Antonov, J. I., Boyer, T. P., Garcia, H. E., Baranova, O. K., et al. (2013). "World ocean atlas 2013, volume 1: temperature,", vol. 73 . Eds. S. Levitus and A. Mishonov (NOAA Atlas NESDIS), (Maryland, USA: World ocean atlas 2013) 1, 40.

Lohmann, G. P., and Schweitzer, P. N. (1990). Globorotalia truncatulinoides' Growth and chemistry as probes of the past thermocline: 1. Shell size. *Paleoceanography* 5 (1), 55–755. doi: 10.1029/PA005i001p00055

Lopes, R. P., Bonetti, C., Dos Santos, G. S., Pivel, M. A. G., Petró, S. M., Caron, F., et al. (2021). Late Pleistocene sediment accumulation in the lower slope off the Rio Grande terrace, southern Brazilian Continental Margin. *Quaternary Int.* 571, 97–116. doi: 10.1016/j.quaint.2020.12.022

Mahiques, M. M., Fukumoto, M. M., Silveira, I. C. A., Figueira, R. C. L., Bícego, M. C., Lourenço, R. A., et al. (2007). Sedimentary changes on the southeastern Brazilian upper slope during the last 35,000 years. *Acad. Bras. Ciênc.* 79 (1), 171–181. doi: 10.1590/S0001-37652007000100018

Martin, J. H. (1990). Glacial-interglacial CO_2 change: the iron hypothesis. *Paleoceanography* 5 (1), 1–13. doi: 10.1029/PA005i001p00001

Matano, R. P., Combes, V., Piola, A. R., Guerrero, R., Palma, E. D., Strub, P. T., et al. (2014). The salinity signature of the cross-shelf exchanges in the Southwestern Atlantic Ocean: Numerical simulations. *J. Geophysical Research: Oceans* 119, 7949–7968. doi: 10.1002/2014JC010116

McManus, J. F., Francois, R., Gherardi, J.-M., Keigwin, L. D., and Brown-Leger, S. (2004). Collapse and rapid resumption of atlantic meridional circulation linked to deglacial climate changes. *Nature* 428 (6985), 834–837. doi: 10.1038/nature02494

Menking, J. A., Shackleton, S. A., Bauska, T. K., Buffen, A. M., Brook, E. J., Barker, S., et al. (2022). Multiple carbon cycle mechanisms associated with the glaciation of Marine Isotope Stage 4. *Nat. Commun.* 13, 5443. doi: 10.1038/s41467-022-33166-3

Mohtadi, M., Max, L., Hebbeln, D., Baumgart, A., Krück, N., and Jennerjahn, T. (2007). Modern environmental conditions recorded in surface sediment samples off W and SW Indonesia: Planktonic foraminifera and biogenic compounds analyses. *Mar. Micropaleontology* 65 (1–2), 96–112. doi: 10.1016/j.marmicro.2007.06.004

Möller, O. O., Piola, A. R., Freitas, A. C., and Campos, E. J. D. (2008). The effects of river discharge and seasonal winds on the shelf off southeastern South America. *Continental Shelf Res.* 28, 1607–1624. doi: 10.1016/j.csr.2008.03.012

Nadal De Masi, M. A. (1999). *Prehistoric hunter-gatherer mobility on the southern Brazilian coast: Santa Catarina Island* (Stanford University), 186. PhD dissertation.

Naidu, P. D., and Malmgren, B. A. (1995). Do benthic foraminifer records represent a productivity index in oxygen minimum zone areas? An evaluation from the Oman Margin, Arabian Sea. *Mar. Micropaleontology* 26, 49–55. doi: 10.1016/0377-8398(95)00014-3

O'Leary, M. H. (1988). Carbon Isotopes in Photosynthesis: Fractionation techniques may reveal new aspects of carbon dynamics in plants. *BioScience* 38 (5), 328–336. doi: 10.2307/1310735

Paillard, D. (2021). "Climate and astronomical cycles," in *Paleoclimatology*. Ed. G. Ramstein, et al (Switzerland: Springer Nature). doi: 10.1007/978-3-030-24982-3_28

Paillard, D., Labeyrie, L., and Yiou, P. (1996). Macintosh program performs time-series analysis. *Eos Trans. AGU* 77 (39), 379–379. doi: 10.1029/96EO00259

Parker, F. L., and Berger, W. H. (1971). Faunal and solution patterns of planktonic Foraminifera in surface sediments of the South Pacific. *Deep-Sea Res.* 18 (1), 73–107. doi: 10.1016/0011-7471(71)90017-9

Patterson, R. T., and Fishbein, A. (1989). Re-examination of the statistical methods used to determine the number of point counts needed for micropaleontological quantitative research. *Paleontological Soc.* 63, 245–248. doi: 10.1017/S0022336000019272

Peeters, F. J. C., Brummer, G. J. A., and Ganssen, G. (2002). The effect of upwelling on the distribution and stable isotope composition of *Globigerina bulloides* and *Globigerinoides ruber* (planktic foraminifera) in modern surface waters of the NW Arabian Sea. *Global Planetary Change* 34 (3–4), 269–291. doi: 10.1016/S0921-8181(02)00120-0

Peeters, F., Ivanova, E., Conan, S., Brummer, G.-J., Ganssen, G., Troelstra, S., et al. (1999). A size analysis of planktic Foraminifera from the Arabian Sea. *Mar. Micropaleontology* 36 (1), 31–61. doi: 10.1016/S0377-8398(98)00026-7

Pereira, L. S., Arz, H. W., Pätzold, J., and Portilho-Ramos, R. C. (2018). Productivity evolution in the South Brazilian Bight during the last 40,000 years. *Paleoceanography Paleoclimatology* 33, 1339–1356. doi: 10.1029/2018PA003406

Peterson, R. G., and Stramma, L. (1991). Upper-level circulation in the south atlantic ocean. *Prog. Oceanography* 26, 1–73. doi: 10.1016/0079-6611(91)90006-8

Petró, S. M., Pivel, M. A. G., and Coimbra, J. C. (2018). Foraminiferal solubility rankings: A contribution to the search for consensus. *J. Foraminiferal Res.* 48 (4), 301–313. doi: 10.2113/gsjfr.48.4.301

Petró, S. M., Pivel, M. A. G., and Coimbra, J. C. (2021). Evidence of supra-lysoclinal dissolution of pelagic calcium carbonate in the late Quaternary in the western South Atlantic. *Mar. Micropaleontology* 166, 102013. doi: 10.1016/j.marmicro.2021.102013

Pinho, T. M. L., Chiessi, C. M., Portilho-Ramos, R. C., Campos, M. C., Crivellari, S., Nascimento, R. A., et al. (2021). Meridional changes in the South Atlantic Subtropical Gyre during Heinrich Stadials. *Sci. Rep.* 11 (1), 9419. doi: 10.1038/s41598-021-88817-0

Piola, A. R., Campos, E. J., Möller, O. O. Jr., Charo, M., and Martinez, C. (2000). Subtropical shelf front off eastern South America. *J. Geophysical Research: Oceans* 105 (C3), 6565–6578. doi: 10.1029/1999JC000300

Piola, A. R., Matano, R. P., Palma, E. D., Möller, O. O. Jr., and Campos, E. J. (2005). The influence of the Plata River discharge on the western South Atlantic shelf. *Geophysical Res. Lett.* 32, L01603. doi: 10.1029/2004GL021638

Portilho-Ramos, R. C., Ferreira, F., Calado, L., Frontalini, F., and Toledo, M. B. (2015). Variability of the upwelling system in the southeastern Brazilian margin for the last 110,000 years. *Global Planetary Change* 135, 179–189. doi: 10.1016/j.gloplacha.2015.11.003

Portilho-Ramos, R. C., Pinho, T. M. L., Chiessi, C. M., and Barbosa, C. F. (2019). Understanding the mechanisms behind high glacial productivity in the southern Brazilian margin. *Climate Past* 15, 943–955. doi: 10.5194/cp-15-943-2019

Quillévéré, F., Morard, R., Escarguel, G., Douady, C. J., Ujiié, Y., de Garidel-Thoron, T., et al. (2013). Global scale same-specimen morpho-genetic analysis of *Truncorotalia truncatulinoides*: A perspective on the morphological species concept in planktonic foraminifera. *Palaeogeography Palaeoclimatology Palaeoecol.* 391, 2–12. doi: 10.1016/j.palaeo.2011.03.013

Ravelo, A. C., and Hillaire-Marcel, C. (2007). "The use of oxygen and carbon isotopes of foraminifera in paleoceanography," in *Proxies in Late Cenozoic Paleoceanography*. Eds. C. Hillaire-Marcel and A. Verna (Amsterdam: Developments in Marine Geology, Elsevier), 735–764.

Renaud, S., and Schmidt, D. N. (2003). Habitat tracking as a response of the planktic foraminifer *Globorotalia truncatulinoides* to environmental fluctuations during the last 140 kyr. *Mar. Micropaleontology* 49, 97–122. doi: 10.1016/S0377-8398(03)00031-8

Rickaby, R. E. M., Elderfield, H., Roberts, N., Hillenbrand, C.-D., and Mackensen, A. (2010). Evidence for elevated alkalinity in the glacial Southern Ocean. *Paleoceanography* 25 (1), PA1209. doi: 10.1029/2009PA001762

Rodrigues, A. R., Pivel, M. A. G., Schmitt, P., Almeida, F. K., and Bonetti, C. (2018). Infaunal and epifaunal benthic foraminifera species as proxies of organic matter paleofluxes in the Pelotas Basin, south-western Atlantic Ocean. *Mar. Micropaleontology* 144, 38–49. doi: 10.1016/j.marmicro.2018.05.007

Santos, T. P., Lessa, D. V. O., Venancio, I. M., Chiessi, C. M., Mulitza, S., Kuhnert, H., et al. (2017a). Stable oxygen isotope record during Termination II in sediment core GL1090. *PANGAEA*. doi: 10.1594/PANGAEA.884583

Santos, T. P., Lessa, D. O., Venancio, I. M., Chiessi, C. M., Mulitza, S., Kuhnert, H., et al. (2017b). The impact of the AMOC resumption in the western South Atlantic thermocline at the onset of the Last Interglacial. *Geophysical Res. Lett.* 44, 11–547. doi: 10.1002/2017GL074457

Sautter, L. R., and Thunell, R. C. (1991). Planktonic foraminiferal response to upwelling and seasonal hydrographic conditions; sediment trap results from San Pedro Basin, Southern California Bight. *J. Foraminiferal Res.* 21 (4), 347–363. doi: 10.2113/gsjfr.21.4.347

Schiebel, R., and Hemleben, C. (2017). *Planktic Foraminifers in the Modern Ocean*. (Berlin: Springer), 359.

Schlitzer, R. (2000). Electronic atlas of WOCE hydrographic and tracer data now available. *Eos Trans. Am. Geophysical Union* 81, 45–45. doi: 10.1029/00EO00028

Schlitzer, R. (2020). *Ocean Data View*. Available at: https://odv.awi.de.

Schulz, M., and Mudelsee, M. (2002). REDFIT: estimating red-noise spectra directly from unevenly spaced paleoclimatic time series. *Comput. Geosci.* 28 (3), 421–426. doi: 10.1016/S0098-3004(01)00044-9

Shackleton, S., Menking, J. A., Brook, E., Buizert, C., Dyonisius, M. N., Petrenko, V. V., et al. (2021). Evolution of mean ocean temperature in Marine Isotope Stage 4. *Climate Past* 17, 2273–2289. doi: 10.5194/cp-17-2273-2021

Sigman, D. M., and Boyle, E. A. (2000). Glacial/Interglacial variations in atmospheric carbon dioxide. *Nature* 407, 859–869. doi: 10.1038/35038000

Sigman, D. M., Hain, M. P., and Haug, G. H. (2010). The polar ocean and glacial cycles in atmospheric CO2 concentration. *Nature* 466, 47–55. doi: 10.1038/nature09149

Skinner, L. C. (2009). Glacial-interglacial atmospheric CO2 change: a possible "standing volume" effect on deep-ocean carbon sequestration. *Climate Past* 5, 537–550. doi: 10.5194/cp-5-537-2009

Smart, C. W., King, S. C., Gooday, A. J., Murray, J. W., and Thomas, E. (1994). A benthic foraminiferal proxy of pulsed organic matter paleofluxes. *Mar. Micropaleontology* 23 (2), 89–99. doi: 10.1016/0377-8398(94)90002-7

Souto, D. D., Lessa, D. V. O., Albuquerque, A. L. S., Sifeddine, A., Turcq, B. J., and Barbosa, C. F. (2011). Marine sediments from southeastern Brazilian continental shelf: A 1200 year record of upwelling productivity. *Palaeogeography Palaeoclimatology Palaeoecol.* 299, 49–55. doi: 10.1016/j.palaeo.2010.10.032

Stephens, B. B., and Keeling, R. F. (2000). The influence of Antarctic sea ice on glacial-interglacial CO_2 variations. *Nature* 404, 171–174. doi: 10.1038/35004556

Stramma, L., and England, M. (1999). On the water masses and mean circulation of the South Atlantic Ocean. *J. Geophysical Research: Oceans* 104 (C9), 20863–20883. doi: 10.1029/1999JC900139

Suárez-Ibarra, J. Y., Frozza, C. F., Palhano, P. L., Petró, S. M., Weinkauf, M. F. G., and Pivel, M. A. G. (2022). Calcium carbonate dissolution triggered by high productivity during the last glacial-interglacial interval in the deep western south atlantic. *Front. Earth Sci.* 10. doi: 10.3389/feart.2022.830984

Suárez-Ibarra, J. Y., Frozza, C. F., Petró, S. M., and Pivel, M. A. G. (2021). Fragment or broken? Improving the planktonic foraminifera fragmentation assessment. *PALAIOS* 36, 165–172. doi: 10.2110/palo.2020.062

Takahashi, K., and Bé, A. W. H. (1984). Planktonic Foraminifera: factors controlling sinking speeds. *Deep-Sea Res. Part Oceanogr Res. Pap.* 31, 1477–1500. doi: 10.1016/0198-0149(84)90083-9

Thornalley, D. J. R., Barker, S., Becker, J., Hall, I. R., and Knorr, G. (2013). Abrupt changes in deep Atlantic circulation during the transition to full glacial conditions. *Paleoceanography paleoclimatology* 28 (2), 253–262. doi: 10.1002/palo.20025

Toggweiler, J. R., Russell, J. L., and Carson, S. R. (2006). Midlatitude westerlies, atmospheric CO_2, and climate change during the ice ages. *Paleoceanography* 21, PA2005. doi: 10.1029/2005PA001154

Toledo, F., Costa, K. B., Pivel, M. A. G., and Campos, E. J. D. (2008). Tracing past circulation changes in the western South Atlantic based on planktonic Foraminifera. *Rev. Bras. Paleontologia* 11, 169–178. doi: 10.4072/rbp.2008.3.03

Ujiié, Y., de Garidel-Thoron, T., Watanabe, S., Wiebe, P., and de Vargas, C. (2010). Coiling dimorphism within a genetic type of the planktonic foraminifer *Globorotalia truncatulinoides*. *Mar. Micropaleontology* 77, 145–153. doi: 10.1016/j.marmicro.2010.09.001

Ujiié, Y., and Lipps, J. H. (2009). Cryptic diversity in planktic foraminifera in the Northwest Pacific Ocean. *J. Foraminiferal Res.* 39 (3), 145–154. doi: 10.2113/gsjfr.39.3.145

Venancio, I. M., Gomes, V. P., Belem, A. L., and Albuquerque, A. L. S. (2016). Surface-to-subsurface temperature variations during the last century in a western boundary upwelling system (Southeastern, Brazil). *Continental Shelf Res.* 125, 97–106. doi: 10.1016/j.csr.2016.07.003

Weber, M. E., Kuhn, G., Sprenk, D., Rolf, C., Ohlwein, C., and Ricken, W. (2012). Dust transport from Patagonia to Antarctica e A new stratigraphic approach from the Scotia Sea and its implications for the last glacial cycle. *Quat. Sci. Rev.* 36, 177–188. doi: 10.1016/j.quascirev.2012.01.016

Zaric, S., Donner, B., Fischer, G., Mulitza, S., and Wefer, G. (2005). Sensitivity of planktic foraminifera to sea surface temperature and export production as derived from sediment trap data. *Mar. Micropaleontology* 55 (1–2), 75–105. doi: 10.1016/j.marmicro.2005.01.002

Ziegler, M., Diz, P., Hall, I.R., and Zahn, R. (2013). Millennial-scale changes in atmospheric CO2 levels linked to the Southern Ocean carbon isotope gradient and dust flux. *Nat. Geosci.* 6, 457–461. doi: 10.1038/ngeo1782

RRH: TEST SIZE: PRODUCTIVITY VS. DISSOLUTION

LRH: SUÁREZ-IBARRA ET AL.

PLANKTONIC FORAMINIFERA TEST SIZE DICTATED BY CONDITIONS IN LIFE AND POST-MORTEM

JAIME Y. SUÁREZ-IBARRA[1*], INGRID VIEIRA[2], CRISTIANE F. FROZZA[2], SONIA CHAABANE[3,4,5], PÂMELA L. PALHANO[2], VOJTĚCH KOVÁŘ[1], THOMAS B. CHALK[3], GEISE S. ANJOS-ZERFASS[6], THIBAULT DE GARIDEL-THORON[3], KATARÍNA HOLCOVÁ[1], MARÍA A.G. PIVEL[7]

*Corresponding author, jysuarezibarra@gmail.com, suarezij@natur.cuni.cz

[1] Institute of Geology and Palaeontology, Faculty of Science, Charles University, Prague, Czech Republic

[2] Programa de Pós-Graduação em Geociências, Instituto de Geociências, Universidade Federal do Rio Grande do Sul, Porto Alegre, Brazil

[3] Aix-Marseille Université, CNRS, IRD, INRAE, CEREGE, Europôle Méditerranéen de l'Arbois, Aix-en-Provence, France

[4] Department of Climate Geochemistry, Max Planck Institute for Chemistry, Mainz, Germany,

[5] Fondation pour la recherche sur la biodiversité (FRB-CESAB), Montpellier, France

[6] Petrobras, Leopoldo Américo Miguez de Mello Research, Development and Innovation Center, Rio de Janeiro, Brazil

[7] Centro de Estudos de Geologia Costeira e Oceanica (CECO), Instituto de Geociências, Universidade Federal do Rio Grande do Sul, Porto Alegre, Brazil.

ABSTRACT

In this study, we quantify the impact of environmental conditions (temperature, productivity, and salinity) and taphonomic (carbonate dissolution) processes in the test (shell) size variation of planktonic foraminifera. To do so, we measure the cross-sectional area of over 16,000 tests from core SAT-048A, recovered from the Western South Atlantic. Core SAT-048A spans the last 45 ka BP and is in a highly dynamic (palae)oceanographic setting. We perform multiple linear correlation analyses which reveal significant relations between the test sizes and the studied environmental parameters, notably, smaller sizes during periods of intensified upwelling which is consequent with enhanced carbonate dissolution. We hypothesise that smaller sizes of *Globigerinoides ruber albus* might result from slower metabolic rates of its symbionts under high productivity conditions where increased suspended particles attenuate the incoming light. *G. ruber albus* is sometimes considered dissolution-prone species, thus its apparent smaller sizes may (also) be due to carbonate dissolution. The remineralisation of exported organic matter decreases the pH of the seawater, meaning carbonate tests can fragment, a process often signposted by the loss of the thinner and more fragile terminal chamber(s). We document an intricate interplay between living and post-mortem conditions, noting that they are additive in the fossil record. This paper provides a framework to understand the differential effect of dissolution on calcite tests which without proper identification can lead to underestimation of test sizes (by ~25±9%) and planktonic foraminifera fragmentation, potentially-impacting all foraminifera-based ecology and geochemical proxies. Finally, we highlight the use of different size descriptors and environmental parameters to better comprehend the effect of living and post-mortem conditions in the test size variation of planktonic foraminifera.

Keywords: productivity, fragmentation, taphonomy, morphometry, carbonate dissolution

INTRODUCTION

Since their emergence in the Jurassic, planktonic foraminifera have evolved in terms of morphology and species diversity (Schmidt et al., 2004a; BouDagher-Fadel, 2018; Rillo et al., 2019; Yasuhara et al. 2020), associated with variations in global oceanographic conditions (e.g., Kucera and Malmgren, 1998; Hart et al., 2003; Aze et al., 2011; Knappertsbusch, 2016; Schmidt et al., 2016; Woodhouse et al., 2023) and local changes (e.g., variations in salinity, nutrient availability, Naidu and Malmgren, 1995; Mojtahid et al., 2015; Weinkauf et al., 2019; Zarkogiannis et al., 2020). Variations in morphological characteristics of planktonic foraminiferal tests, such as size, porosity, chamber architecture, and wall thickness, have been shown to be controlled by environmental factors (e.g., Hecht, 1976a; Hecht et al., 1976; Schmidt et al., 2004a; Kaiho et al., 2006; Birch et al., 2012; Davis et al., 2013; Marshall et al., 2015; Wade et al., 2016; Burke et al., 2018; Duque-Castaño et al., 2019; Todd et al., 2020; Adebayo et al., 2023). Furthermore, although there is a demonstrated ecophenotypic plasticity (the ability of an organism to exhibit different phenotypic traits in response to changes in environmental conditions; e.g., West-Eberhard, 1989; Darling and Wade, 2008; Weiner et al., 2015; Aurahs et al., 2011; Davis et al., 2020), and the existence of (pseudo)cryptic diversity might also account for some morphological variability (e.g., Darling et al., 2006; Ujiié and Lipps, 2009; Ujiié et al., 2010; Weiner et al., 2015; Morard et al., 2016), there is potential to develop these morphological

64 changes as proxies for past environmental conditions (Wade and Olsson, 2009; Weinkauf et al.,
65 2019).

66 It has been documented that sea surface temperature controls the test size of planktonic
67 foraminifera on a global scale, exhibiting a positive linear relationship (Schmidt et al., 2004b).
68 Nevertheless, this relation is disrupted in areas with turbulent hydrographic conditions, such as
69 ocean fronts or upwelling zones, likely associated with environmental variability disrupting
70 ecosystems (Ortiz et al., 1995; Renaud and Schmidt, 2003; Schmidt et al., 2003, 2004a;
71 Zarkogiannis et al., 2020). Though planktonic foraminifera species have different ecological
72 preferences (Kucera, 2007; Schiebel and Hemleben, 2017; Chaabane et al., 2023a,b), key studies
73 have investigated the size variations by considering entire associations rather than individual
74 species (e.g., Schmidt et al., 2003, 2004a; Todd et al., 2020). Furthermore, when analysing
75 species-specific test size responses to environmental parameters, results vary (e.g., Moller et al.,
76 2013; Brombacher et al., 2018b, Rillo et al., 2020; Adebayo et al., 2023). For instance, using a
77 similar dataset, Rillo et al. (2020) emphasised the challenge of consistently predicting test size
78 variation in planktonic foraminifera based on environmental conditions, while Adebayo et al.
79 (2023) highlight the importance of environmental parameters (specifically local carbonate
80 chemistry and temperature) in influencing test size variation at both the species and assemblage
81 level.

82 Pioneer experiments dissolving planktonic foraminiferal tests documented a reduction in
83 the size frequency distribution (Berger, 1967; Hecht et al., 1975), potentially associated with the
84 preferential removal and/or destruction of the thinner terminal chambers (Berger, 1970; Bé et al.,
85 1975). In addition, studies using X-ray microcomputed tomography (e.g., Iwasaki et al., 2015;
86 2019; Fox et al., 2020) and measuring test weight (e.g., Moy et al., 2009; de Moel et al., 2009)

have recorded a thinning in carbonate walls due to increased dissolution, which can lead to fragmentation. Nevertheless, it has not been yet fully explored how the carbonate dissolution processes can affect the size variation. The Last Glacial period in the Western South Atlantic is an interesting interval to be studied, as intense dissolution processes have been documented (Petró et al., 2021) in response to increased surface primary productivity (e.g., Suárez-Ibarra et al., 2022, 2023, also discussed in Section 2) and changing bottom water conditions (Howe et al., 2016a,b; Oppo et al., 2023).

In this study we aim to quantify the influence of living environmental conditions (i.e., temperature, productivity, and salinity) and post-mortem processes (i.e., dissolution) in the test size variation of Quaternary planktonic foraminifera, investigating the possible mechanisms behind the size changes. To do so, we analysed core SAT-048A, recovered from the Western South Atlantic, which spans 5–43 ka BP, where large variations in upper water column conditions and carbonate preservation have been documented.

REGIONAL SETTING

In the offshore portion of the southernmost Brazilian continental margin, Western South Atlantic, there is the influence of the southward Brazil Current, flowing along the shelf break and transporting, in the upper 200 meters, warm (>20°C), saline (>36 psu) and nutrient-poor Tropical Water (Silveira et al., 2000; Rodrigues and Lorenzzetti, 2001) (**Figure 1**). At the pycnocline layer, the Brazil Current transports progressively cooler (6–20°C), less saline (34.6–36 psu) and nutrient-rich South Atlantic Central Water. At ~38°S, the Brazil Current meets a northward-flowing branch of the Antarctic Circumpolar Current, the Malvinas Current, which transports

Subantarctic Water, which is cooler (4–16°C) and fresher (<34.2 psu) (Piola and Matano, 2009). The confluence of these two currents, with contrasting properties, produces a highly dynamic zone of with eddies and turbulent meanders known as the Brazil-Malvinas Confluence, which displays seasonal and interannual migration (Gordon, 1989; Palma and Matano, 2009). After the Brazil and Malvinas currents converge, their waters flow eastward transported by the South Atlantic Current (Gordon, 1989; Palma and Matano, 2009; Piola and Matano, 2009).

The study region is also influenced by the influx of continental water outflow from the cooler (>10°C) and fresher (<33.5 psu) De la Plata River plume, which can extend up to ~27°S during the winter months (Piola et al., 2005; Möller et al., 2008). The plume may modify parameters such as sea surface temperature, nutrient availability (**Figure 1**) and sea surface salinity at the southern portion of the Brazilian continental margin. The extent of the northward intrusion of these cooler and fresher waters is mostly dependent on the wind pattern rather than river discharge (Pimenta et al., 2005; Piola et al., 2005). During austral winter, SW winds carry the plume northward while during austral summer the dominant NE winds restrict the Plume closer to the river mouth, at around 32°S (Möller et al., 2008).

MATERIAL AND METHODS

CORE INFORMATION

This study is based on the analysis of 16,022 specimens, recovered from 49 sediment samples from core SAT-048A (29º11'S, 47º15'W, 1,542 mbsl). Core SAT-048A was retrieved by *FUGRO Brasil – Serviços Submarinos e Levantamentos Ltda* for the *Agência Nacional do*

Petróleo, Gás Natural e Biocombustíveis (Brazilian National Agency of Petroleum, Natural Gas and Biofuels) at the south Brazilian continental margin, Western South Atlantic. The sediment samples were sieve-washed over a 63 μm mesh and oven-dried at 55°C. Before being classified, planktonic foraminiferal specimens were dry sieved on a 150 μm mesh. The taxonomical classification follows Schiebel and Hemleben (2017) and Brummer and Kucera (2022). For the *Globigerinoides* clade, we follow Morard et al. (2019). We use the age model published by Suárez-Ibarra et al. (2022) which briefly comprises ten ^{14}C AMS dates plus the Laschamp geomagnetic excursion, run using the package "bacon" (Blaauw and Christen, 2011; version 2.4.2) for the free software R (R Core Team, 2020, version 4.1.2) (**supplementary material**).

IMAGE ACQUISITION, SIZE MEASUREMENTS AND DATA TREATMENT

For the image acquisition, tests are positioned with their umbilical side facing upwards. Photographs are manually taken using the Zen 2.6 lite software (blue edition) and a Zeiss stereomicroscope, model Discovery V8 Stereo with an Axiocam 105 colour digital camera attached. The basic resolution of the Axiocam is 2560 (H) x 1920 (V), 5.0 Mpixels and, the size of the pixel is 2.2 μm x 2.2 μm. To measure the tests, we use the software ImageJ (Abràmoff et al., 2004; version 1.53c) freely available at https://imagej.nih.gov/ij/. To obtain the measurements in ImageJ, images are converted to grayscale (8 bits), then to binary images and cropped to remove undesired particles or marks.

To quantify the test morphometric variation, we normalise the cross-sectional area of the foraminifera (μm) by calculating its square root, hereafter referred to as *size*. We chose the cross-sectional area as it has been shown to be a robust, repeatable, and standardised 2D metric

consistently correlated with 3D volumetric measurements (Brombacher et al., 2017, 2018a), these can then both be represented in 1D using the square root metric. In this study, we focus our analyses on the species *Globigerinoides ruber albus* (4,987 specimens), *Globigerinita glutinata* (3,008 specimens), and *Globigerina bulloides* (2,911 specimens). These species were selected because they yielded enough specimens for statistical analyses and are important taxa in the study area (Boltovskoy et al., 1996). In addition, to provide an overview of the planktonic foraminifera morphometric assemblage, we included 5,121 specimens belonging to the (sub)species *Globigerinoides ruber ruber*, *Globorotalia inflata*, *Neogloboquadrina incompta* and *Globigerinella calida*. Collectively, these seven (sub)species represent (on average) 82±4 % (at 1SD, interval ranges: 68–94%) of the whole assemblage per sample and are hereafter referred to as the "*partial assemblage*". To assure statistical significance, we aim for a minimum of 20–25 specimens per species per sample (**Table 1**), as suggested by Kucera (2007) and Brombacher et al. (2017), though also included in our analysis are four *G. bulloides* samples (within the 9.4–5.8 ka BP time interval) with only 15 to 18 specimens.

To assess the error in determining the cross-sectional area, we measured one slide containing 77 large and small specimens six times: two replicas each of three different illumination angles. We determined the variation among the six analysed replicates for each of the 77 individual specimens. To do so, we calculated the percentage (%) of variation by comparing the standard deviation of the measurements to the mean value for each specimen. The repeated measurements showed high reproducibility and accuracy, with a mean variation of 3.05±1.39% at 1SD.

Furthermore, as planktonic foraminifera are subjected to a sieving process, typically with mesh sizes of over 150 or 125 μm, smaller and/or juvenile specimens are usually excluded from

179 the assemblages (e.g., Di Donato et al., 2014). As a result, the frequency distribution of test sizes
180 is artificially truncated and skewed towards larger sizes (Schmidt et al., 2004a). Given this issue,
181 morphometric analyses focus on the largest portion of the assemblages, as described by the 95th
182 percentile (e.g., Todd et al., 2020; Rillo et al., 2020; Adebayo et al., 2023). Nevertheless, we
183 conducted a sensitivity test on the size cut-off descriptor to better capture the size changes of the
184 species-specific population dynamics. We found two patterns with similar variations: i) the
185 mean, median, and 65th percentiles and ii) the 75th, 85th and 95th percentiles. To have a better idea
186 of the variation trough time, we analysed the 95th percentile and mean values.
187
188 QUANTIFYING THE EFFECTS OF ENVIRONMENTAL PARAMETERS IN THE TEST SIZE VARIATION
189
190 To quantify potential effects of palaeoenvironmental parameters on the test size variation
191 of the selected planktonic foraminifera, we run 16 multiple linear correlations on the size (mean
192 and 95th percentile of the square root of the cross-sectional area), as a dependent variable, against
193 the reconstructed environmental parameters: i) sea subsurface temperature estimates (at 25 and 75
194 m depth), ii) sea subsurface salinity estimates (at 25 m depth), iii) reconstructed primary
195 productivity, and iv) calcium carbonate preservation (iii and iv from Suárez-Ibarra et al., 2022).
196 Correlation analyses were run using the free software R (R stats package, R Core Team, 2020,
197 version 4.1.2). Finally, to further test the hypotheses of ecological optimum, we run Pearson and
198 Spearman's rank correlation analyses between the sizes and the respective relative abundances of
199 each analysed taxa.
200 To estimate past sea subsurface temperatures at 25 and 75 m depths (T_{25m} and T_{75m},
201 respectively), relative abundances of whole assemblages (26 planktonic foraminifera

morphospecies) from core SAT-048A were used (Suárez-Ibarra et al., 2020), using the Modern Analog Technique (Hutson, 1980) within the statistical software PAST (version 3.2; Hammer et al., 2001). The calibration was performed using 1,538 core top samples from the Atlantic Ocean (including 421 samples from the South Atlantic), recovered from the ForCenS database (Siccha and Kucera, 2017) and García-Chapori and Laprida (2020) for the Brazil-Malvinas Confluence. Mean annual temperatures for 25 and 75 m depth were extracted from the World Ocean Atlas 2013 (Locarnini et al., 2013, at a resolution of 0.25°), using the Ocean Data View software (Schlitzer, 2021).

To infer changes in past sea subsurface salinity at 25 meters depth (S_{25m}), we reconstructed the ice volume corrected-oxygen stable isotopes of the seawater ($\delta^{18}O_{sw}$). We based our reconstructions on the core-top calibration of Farmer et al. (2007) for *Globigerinoides ruber ruber* (pink *ruber*):

$$T = 14.7 - 4.86\ (\delta^{18}O_c - \delta^{18}O_{sw})$$

where T is our MAT-temperature at 25 meters depth, $\delta^{18}O_c$ (‰ Vienna Pee Dee Belemnite, VPDB) is the oxygen stable isotope value from *G. ruber ruber,* and $\delta^{18}O_{sw}$ is the oxygen stable isotope of the seawater (‰ Vienna Standard Mean Ocean Water, VSMOW) related to salinity. The 1SD for α, (°C) and β (°C/‰) factors are ±1.6 and ±0.57, respectively (Farmer et al., 2007). To convert VPDB to VSMOW, an offset of 0.27‰ was applied. In addition, to subtract the ice volume effect, we computed the $\delta^{18}O$ values from Shakun et al. (2015) to the corresponding ages. For the oxygen stable isotope analyses, approximately 12–15 specimens from the planktonic species *G. ruber ruber* ($\delta^{18}O_{G.\ ruber\ ruber}$) were selected from the 250 μm fraction. The analyses were performed with a Thermo Scientific MAT-253 mass spectrometer, coupled to a Kiel IV carbonate device, by the Laboratory of Stable Isotopes of the

University of California, Santa Cruz (SIL-UCSC). All results are expressed relative to the Vienna Pee-Dee Belemnite (VPDB) standard.

SCANNING ELECTRON MICROSCOPE IMAGES AND X-RAY 3D MODELS

To further characterise the planktonic foraminifera test preservation, we use scanning electron microscope (SEM) imaging in secondary electron mode, with an accelerating voltage of 12 kV and the working distance ranged from 7 to 12 mm. SEM images of gold-coated samples were acquired at the *Laboratório de Geologia Isotópica at Universidade Federal do Rio Grande do Sul*, Brazil (LGI-CPGq-IGEO-UFRGS). Five open-access CT-scan foraminifera models were processed using Dragonfly 2022.2 [Computer software]. Comet Technologies Canada Inc., Montreal, Canada; software available at https://www.theobjects.com/dragonfly. This includes the digital 'removal' of the last chamber and a comparison of volumes of the original and modified models. Sources of the models are listed in Table 6.

RESULTS

PLANKTONIC FORAMINIFERA TEST SIZES AND ABUNDANCES

The partial assemblage and *G. ruber albus* sizes show generally higher values (as described by the mean and 95th percentile) compared to those of *G. bulloides* and *G. glutinata* (**Figure 2**). The smallest size for the partial assemblage (267 μm, in the largest 95th percentile) and *G. ruber albus* (231 μm, largest 95th percentile) occur at the base of the core (40 ka BP). Later, the partial

assemblage and *G. ruber albus* sizes display an increasing trend towards the present, with a brief declining trend during the 22–16 ka BP time interval. The largest size for the assemblage was 406 μm, recorded at 7 ka BP, while the largest size for *G. ruber albus* measured 400 μm and occurred at 22 ka BP.

From 41 to 23 ka BP, *G. glutinata* sizes exhibit an increasing trend, followed by a period of relatively stable values. After 23 ka BP, the size variability shows high amplitude changes. After relatively lower values from 21 to 16 ka BP, there is an increasing trend in size up to the present. Between 36 and 11 ka BP, *G. glutinata* sizes are consistently smaller than those of *G. bulloides*. The smallest size of *G. glutinata* is also observed at the base of the core 41 ka BP (208 μm, 95th percentile), making it the smallest of the three principal species. The largest *G. glutinata* size is recorded at 7 ka BP (271 μm, 95th percentile) and at 22 ka BP, similar size to that of *G. ruber albus*.

During the 42–36 ka BP time interval, *G. bulloides* size exhibits a decreasing trend. The absolute smallest size is recorded during the Holocene at 7 ka BP (217 μm, 95th percentile). Between 36 and 35 ka BP, a rapid increase in *G. bulloides* size is observed, followed by a phase of constant larger sizes to 12 ka BP. The peak size of 292 μm (95th percentile) is recorded at 22 ka BP, coinciding with the moment when *G. ruber albus* and *G. glutinata* also exhibit their largest sizes. From 12 ka BP onward, sizes gradually decrease till they reach their minimum value at 7 ka BP.

SUBSURFACE PALAEOTEMPERATURE AND PALAEOSALINITY ESTIMATES

The Modern Analogue Technique is used to obtain palaeotemperature curves for depths of 25 metres (T_{25m}) and 75 metres (T_{75m}), as shown in **Figure 3B**. During MIS 3 and MIS 2, T_{75m} exhibits near constant values, followed by a warming trend after 16 ka BP. The palaeotemperature values recorded at this depth during MIS 1 are the highest, peaking at 24°C around 12 ka BP. Throughout the record, T_{25m} displays more fluctuations, starting with 22° C and recording a peak of 24°C between 35 and 30 ka BP. From 30 ka BP to the onset of the Last Glacial Maximum, stable values around 22°C are observed. During the Last Glacial Maximum, the lowest temperature reached approximately 18°C at 22 ka BP. Afterwards, temperatures rose toward 5 ka BP, with the highest temperature of 26°C recorded at the onset of the Holocene.

In general, the $\delta^{18}O_{G.\ ruber\ ruber}$ displays a decreasing trend towards the recent, with values ranging from -1.6 to 0.8‰. Our salinity proxy (S_{25m}) showed variations throughout the record (**Figure 3D**). During MIS 3, the values remained stable, and the beginning of MIS 2 presented lower values than MIS 3. Lower S_{25m} values were observed from 21 to 17 ka BP, followed by a tendency for salinity to increase after that, returning to stable values close to 1‰ (vs. VSMOW).

STATISTICAL ANALYSES

The results of the multiple linear correlations used to quantify the palaeoenvironmental effects on the test size variation are shown in **Table 2**. All four models negatively associate the changes in the size of partial assemblage with palaeoproductivity ($PC1_P$), with adjusted coefficient of determinations (R^2) of 0.68, 0.67, 0.59 and 0.55. For *G. ruber albus,* one model negatively relates the size (mean) with temperature ($T_{75m,}$ R^2 =0.55), two negatively link (mean) size with productivity (R^2 =0.55 and 0.45), and three models negatively associate test size with dissolution

intensity (R^2 =0.55, 0.43 and 0.39). For *G. glutinata,* two models link size (mean) with dissolution (R^2 =0.24 and 0.22). Finally, for *G. bulloides*, one model positively associates (mean) size with temperature (T_{25m}, R^2 =0.25), and two models negatively relate size with temperature (T_{75m}) and productivity (R^2 =0.21 and 0.16).

From the six Pearson correlations (**Table 3, Figure S2**), only one associates the (mean) size with its relative abundance (*G. glutinata*), with an R of -0.28 (*p*-value =0.05). None of the Spearman's rank correlations are significant (**Table S3**).

DISCUSSION

Our results show that the relation between test size changes and environmental parameters might not be recorded in all size descriptors concurrently (**Table 2**). For instance, if only the 95th percentile had been analysed, the relation of temperature, and productivity with the test size of the studied species would have been underestimated. Although size frequency distribution is artificially cut off due to the sieving process (Schmidt et al., 2004a), our results highlight the necessity to analyse the test size variation with different statistical descriptors, especially when the number of analysed specimens per sample is low, for instance, datasets produced manually (e.g., this study) *vs*. those automatically produced (e.g., Schmidt et al., 2004a; Adebayo et al., 2023). This phenomenon arises as the 95th percentile might represent as few as eight individuals, not fully capturing the size changes of the whole species population.

In the same way, using temperature reconstructions at different depths affects the significance and direction of how MAT relates to planktonic foraminifera test size, for instance with *G. ruber albus* and *G. bulloides* (**Table 2**). Given the pronounced temperature changes in

316 the upper water column, it is necessary to test multiple temperature reconstructions to fully
317 understand their effect in driving the sizes of planktonic foraminifera tests. Thus, to fully
318 understand the palaeoenvironmental effects on the test sizes, we recommend running sensitivity
319 tests on the size descriptors and using different parameters to reconstruct past environmental
320 variables, when possible.
321
322 LIVING CONDITIONS: THE EFFECTS OF TEMPERATURE, PRODUCTIVITY, AND SALINITY
323
324 High relative abundances of planktonic foraminifera are often interpreted as evidence of
325 ecological optima, and are expected to result in large test sizes (Hecht, 1976b; Schmidt et al.,
326 2004b; Weinkauf et al., 2013, for a deeper discussion see Adebayo et al., 2023). Nonetheless,
327 just one of the 12 models (6 Pearson and 6 Spearman, **tables 3 and S2, Figure S2**) negatively
328 associates size with the species' relative abundance and this association is weak. The absence of
329 correlation suggests that high relative abundances might not be the best indicators for optimum
330 ecological conditions but rather environmental parameters, as previously documented by
331 Schmidt et al. (2004b) and Adebayo et al. (2023).
332 The multiple linear correlation analyses between the size of partial assemblage and
333 environmental parameters (**Table 2**) point to productivity being the main driver of size variations
334 through time. While the relationship between planktonic foraminifera test sizes and temperature
335 has been extensively documented (e.g., Deuser et al., 1981; Schmidt et al., 2004a; Lombard et
336 al., 2009; Davis et al., 2013), given the significant variations in nutrient availability in the study
337 area, it was anticipated that the size variation of the partial assemblage would be more closely
338 associated with productivity than with temperature (e.g., Ortiz et al., 1995; Renaud and Schmidt,

2003; Schmidt et al., 2004a; Zarkogiannis et al., 2020), although we note both parameters are affected by the upwelling of subsurface nutrient rich waters (e.g., Gu et al., 2017; Pereira et al., 2018; Alvarenga et al., 2022; Suárez-Ibarra et al., 2022, 2023).

From **Figure 2**, it is possible to infer that changes in partial assemblage mainly represent changes in the size of *G. ruber albus* (the most abundant species within the samples), as the size of *G. glutinata* and *G. bulloides* does not appreciably vary along the record. Given the reduction in test sizes from tropical to polar biogeographic provinces, the analysis of species-specific size response becomes necessary, as changes in the test sizes of planktonic foraminifera assemblages also denote changes in species proportions (Schmidt et al., 2004b).

To analyse the drivers of *G. ruber albus* size changes, it is necessary to consider its ecological preferences. *G. ruber* (both *albus* and *ruber*) is abundant in oligotrophic (low productivity) conditions, prevailing in our study area in the modern (Sousa et al., 2014). However, glacial upwelling events (which increased the number of suspended particles) may have resulted in reduced size of *G. ruber albus* tests. This likely associated with the need of its symbionts for light to carry out metabolic activities, and/or a decrease in the symbiotic host respiration rate, resulting in the competitive advantage of smaller tests (Schmidt et al. 2004b; Bijma et al., 1990; Bijma et al., 1992; Kemle-von-Mücke and Hemleben, 1999). As upwelling reduces subsurface temperatures, the negative size response of the *G. ruber albus* to T_{75m} can be explained by the species' preference for warm and oligotrophic subtropical waters, despite its high tolerance to different environmental conditions (Bijma et al., 1990; Kemle-von-Mücke and Hemleben, 1999; Schiebel and Hemleben, 2017). In the same way, albeit weakly, *G. bulloides* sizes also respond negatively to cooler deep temperatures (75 m depth) and positively (mean size, **Table 2**) to shallower warmer temperatures, likely related to quick reproduction during

productive periods (Naidu and Malmgren, 1995; Conan and Brumer, 2000; Schiebel et al., 2001; Schmidt et al., 2004a; Souto et al., 2011).

Yet, another reason that could account for the reduced *G. ruber* sizes is carbonate dissolution, triggered by upwelling events (Suárez-Ibarra et al., 2022, 2023), explored in the following subsection.

POST-MORTEM CONDITIONS: REDUCTION IN TEST SIZE DUE TO DISSOLUTION

As our Holocene assemblages are dominated by *G. ruber albus* (**Figure 2**), and Holocene conditions are similar to modern ones, our planktonic foraminifera assemblages should belong to the subtropical province (Boltovskoy et al., 1996; Kucera, 2007). To compare our size measurements (square root of cross-sectional area) with those from Schmidt et al. (2004b, maximum diameter), we run a Pearson's correlation between the square root of cross-sectional area and maximum diameter of 422 random specimens, belonging to different species (**Figure 4**). Strong and significantly correlated ($R=0.995$, p-value<0.01), the regression equation ($Y = 1.29X * 6.73$) allows us to calculate the maximum diameters of our measurements. Our highest Holocene size value for the partial assemblage (406 μm, 95th percentile, **Figure 2**) would correspond to 517 μm, a typical value for the subtropical-tropical bioprovinces (Schmidt et al., 2004b). Yet, the minimum 95th percentile value for partial assemblage (267 μm) at 40 ka BP would correspond to polar-subpolar bioprovinces (338 μm), and not to the glacial upwelling conditions for our study area.

As a response to the enhanced upwelling events, higher quantities of exported labile glacial organic matter (Rodrigues et al., 2018) underwent remineralisation. This process released

385 CO_2, which in turn, led to a reduction in the pH of the surrounding water, affecting the
386 planktonic foraminiferal tests (Schulte and Bard, 2003; Petró et al., 2021; Suárez-Ibarra et al.,
387 2022, 2023). Although *G. ruber albus* is not particularly susceptible to dissolution in our study
388 area (according to experiments using weak acetic acid over 200 days, Petró et al., 2018), there is
389 a high discrepancy among rankings (Adelseck, 1977; Thunell and Honjo, 1981; Boltovskoy and
390 Totah, 1992, Petró et al., 2018). However, it is typically considered in the literature that *G. ruber*
391 *albus* is a dissolution-prone species (Berger, 1967; Berger, 1970; Bé et al., 1975; Hecht et al.,
392 1975; Kucera, 2007). If the size of *G. ruber albus* reflects the size of the partial assemblage, then
393 dissolution could account for the discrepancy between the size of our assemblages and those
394 from Schmidt et al. (2004b). The mentioned reasoning is supported by the correlation models
395 (**Table 2)**, which point dissolution ($PC1_D$) driving the test size changes in *G. ruber albus*.
396 Similarly, studying Holocene mid-depth Mediterranean sediment samples, Principato et
397 al. (2006) documented enhanced carbonate corrosion during organic matter-rich intervals
398 (sapropels accumulation), conditions that lead to pteropod dissolution, decreased test weight of
399 *G. ruber* and reduced total counts of planktonic foraminifera per sample (~10–7 ka BP).
400 Conversely, during the same sapropel accumulation events in low-depth Mediterranean samples,
401 larger sizes of *G. ruber albus* were observed with no signs of dissolution (Mojtahid et al., 2015).
402 As test weights and sizes are commonly positively correlated, Mojtahid et al. (2015) suggested
403 that dissolution could account for the reduced *G. ruber* test weights from Principato et al. (2006).
404 Therefore, we also hypothesise that biologically mediated carbonate dissolution under high
405 organic matter export can account for at least part of our decreased *G. ruber* test sizes (95^{th}
406 percentile).

To explore the idea that dissolution impacted the *G. ruber albus* tests, a second "screening" on selected tests using scanning electron microscope (SEM) was carried out. Although the taxonomic identification utilised only planktonic foraminifera tests with no signs of broken chambers, we found the presence of scars in the last whorl of some *G. ruber albus*. As the use of SEM images is not viable for classic taxonomic counts (minimum of 300 specimens, Patterson and Fishbein, 1989), and they are not visible with the use of stereomicroscopes, these scars are rarely identified (**Figure 5**). With poor carbonate preservation, planktonic foraminifera tests undergo fragmentation, decreasing the relative abundances of species susceptible to dissolution. Nevertheless, if dissolution-prone species experience a systematic test break-down, the relative abundances of these susceptible species can actually remain high as the broken tests might look like multiple smaller whole individuals (**Figure 5**).

The misidentification of broken tests that look like "whole specimens" (**Figure 5E**) can also lead to a sub quantification of size variations, as already noted by Berger (1967) and Hecht et al. (1975). In his pioneer investigations into the selective dissolution of planktonic foraminifera, Berger (1968) noted that terminal chambers tend to be initially lost (also Zarkogiannis et al., 2020). As the final chamber(s) tend to be thinner than the previous ones due to the over-calcifying process (e.g., Erez, 2003; Schmidt et al., 2008; Iwasaki et al., 2019; Fehrenbacher and Martin, 2014), dissolution might lead to the removal of the terminal chamber(s), leaving nothing, or remnant scars only evident under SEM imaging. This process can be enhanced in *G. ruber albus* by secondary openings that reduce the contact surface between chambers (Schiebel and Hemleben, 2017). Subsequently, the remaining test, often resembling a smaller, densely shelled individual, can be identified as a "whole specimen"

(Berger, 1970), being a potential explanation on how dissolution overprints the test size variation of *G. ruber albus* in our data.

Can a *G. ruber albus* test look like a whole specimen after the removal of the final chamber(s) as suggested by Berger (1970)? To answer this question, we use X-ray computed micro-tomography (micro-CT) on individuals that are expected to have completed their ontogenetic cycles. From five open-source 3D models, we visualise how the last whorl of planktonic foraminiferal tests of *G. ruber albus* that lost their final chamber present themselves. In **Figure 6**, it is possible to see how virtual-artificially fragmented tests of *G. ruber albus* look before and after the removal of the terminal chamber(s). As the trochospiral growing pattern of *G. ruber albus* builds new chambers in relative similar positions through its life cycle, the umbilical views of a whole and a broken test are similar (**Figure 6**).

Furthermore, as expected, the cross-sectional area of the whole individual is reduced by ~25±9%, with the removal of the terminal chamber (**Table 6**). If our calculated lowest maximum diameter (~338 μm) is increased by 25±9%, the obtained values (422±30 μm) are within the temperate and upwelling bioprovinces (Schmidt et al., 2004b), more in agreement with the reconstructed conditions experienced during the last glacial in the studied area. Nevertheless, as carbonate dissolution is impacted by surface productivity in our study area, it is not possible to disentangle the effects of both environmental parameters. To further test the hypothesis of a taphonomical influence on the size changes of *G. ruber albus*, it would be necessary to analyse an environmental setting where dissolution varies independently from productivity.

Finally, the misidentification of broken tests as whole individuals seems to be a common phenomenon, noticeable in the SEM images available at the taxonomic database of planktonic

foraminifera Mikrotax (Huber et al., 2016). In the **Table S3,** we compiled a list of 26 planktonic foraminifera individuals showing scars of (potentially) removed terminal chamber(s).

CONCLUSIONS

By examining the size variations in planktonic foraminifera tests from the Western South Atlantic, we have documented an intricate interplay between ecological (such as productivity and temperature) and taphonomic processes. Ecologically, we document that productivity plays a significant role in driving the test sizes of planktonic foraminifera (partial) assemblages in upwelling oceanographic settings. We observe a correlation between the test size of *Globigerinoides ruber albus* and productivity, with smaller tests during increased productivity, likely due to reduced metabolic activity of the symbionts under upwelling periods. Additionally, we hypothesise that temperature fluctuations, especially through the upper water column, may have influenced the size of certain species, further emphasising the need to consider diverse temperature reconstructions when analysing size variations. On the taphonomic front, we document a test size reduction (~25±9%), attributed to test fragmentation during enhanced dissolution. The lack of ease in identifying the presence of scars and signs of test fragmentation, potentially leads to the misidentification of broken tests as whole individuals. Our findings highlight the importance of considering multiple environmental parameters when interpreting size variations in planktonic foraminifera tests. Finally, this paper underscores the necessity of understanding the subtle imprints of carbonate dissolution on the planktonic foraminiferal record, as it has the capacity to bias foraminiferal-based ecology and geochemical proxies. ~~In~~

ACKNOWLEDGEMENTS

The authors thank the Charles University Grant Agency (GAUK, grant number 355422) and the Coordination for the Improvement of Higher Education Personnel (CAPES) for supporting the IODP Program and for financial support through Grant 88887.091727/2014-01. We thank Dr. Anieke Brombacher, Dr. Manuel Weinkauf and Prof. Dr. Fernando Erthal for important insights during the preparation of this study. JYSI thanks the Johanna M Resig Fellowship from the Cushman Foundation for Foraminiferal Research, the STARS and COOPERATIO program (Přírodovědecká Fakulta, Univerzita Karlova) and the ERASMUS+ program. IV thanks the CAPES for her MSc scholarship. CFF thanks the Brazilian National Council for Scientific and Technological Development (CNPq) for her PhD scholarship. MAGP gratefully acknowledges the CNPq for grant number 315684/2021-6.

The dataset utilised in this study was submitted to Pangaea.

REFERENCES

Abràmoff, M. D., Magalhães, P. J., and Ram, S. J., 2004, Image processing with ImageJ Part II: Biophotonics International, v.11, p. 36–43.

Adebayo, M. B., Bolton, C. T., Marchant, R., Bassinot, F., Conrod, S., and de Garidel-Thoron, T., 2023, Environmental controls of size distribution of modern planktonic foraminifera in the Tropical Indian Ocean: Geochemistry, Geophysics, Geosystems, v. 24(4), p. e2022GC010586, DOI: 10.1029/2022GC010586.

Adelseck, C. G., 1977, Dissolution of deep-sea carbonate : preliminary calibration of preservational and morphologic aspects: Deep Sea Research, v. 24, p. 1167–1170, DOI: 10.1016/0146-6291(77)90520-3.

Alvarenga, A., Paladino, M. I., Gerotto, A., DeMenocal, P., Iwai, F. S., Sousa, S. H. M., Figueira, R. C. L., Mahiques, M. M., and Nagai, R., 2022, S/SE Brazilian continental margin sea surface temperature and productivity changes over the last 50 kyr: Palaeogeography, Palaeoclimatology, Palaeoecology, v. 601 p. 111144, DOI:10.1016/j.palaeo.2022.111144.

Aurahs, R., Treis, Y., Darling, K., and Kucera, M., 2011, A revised taxonomic and phylogenetic concept for the planktonic foraminifer species Globigerinoides ruber based on molecular and morphometric evidence: Marine Micropaleontology, v. 79, p. 1–14, DOI: 10.1016/j.marmicro.2010.12.001.

Aze, T., Ezard, T. H. G., Purvis, A., Coxall, H. K., Stewart, D. R. M., Wade, B. S., and Pearson, P. N., 2011, A phylogeny of Cenozoic macroperforate planktonic foraminifera from fossil data: Biological Reviews, v. 86(4), p. 900-927, DOI: 10.1111/j.1469-185X.2011.00178.x.

Bé, A. W. H., Morse, J. W., and Harrison, S. M., 1975, Progressive dissolution and ultrastructural breakdown of planktonic foraminifera. Dissolution of Deep-Sea Carbonates, Edi., Sliter, W.V., Bé, A.W.H., Berger, W.H. Special Publication 13, Cushman Foundation for Foraminiferal Research.

Berger, W. H., 1967, Foraminiferal Ooze: Solution at Depths: Science, v. 156(3773), p. 383–385, DOI:10.1126/science.156.3773.383.

Berger, W. H., 1970, Planktonic Foraminifera: Selective solution and the lysocline: Marine Geology, v. 8, p. 111–138, DOI: 10.1016/0025-3227(70)90001-0.

518 Bijma, J., Faber, W. W., and Hemleben, C., 1990, Temperature and salinity limits for growth and
519 survival of some planktonic foraminifers in laboratory cultures: Journal of. Foraminiferal
520 Research, v. 20, p. 95–116, DOI: 10.2113/gsjfr.20.2.95.
521 Bijma, J., Hemleben, C., Oberhaensli, H., and Spindler, M., 1992, The effects of increased water
522 fertility on tropical spinose planktonic foraminifers in laboratory cultures: Journal of
523 Foraminiferal. Research, v. 22, p. 242–256, DOI: 10.2113/gsjfr.22.3.242.
524 Birch, H. S., Coxall, H. K., and Pearson, P. N., 2012, Evolutionary ecology of Early Paleocene
525 planktonic foraminifera: size, depth habitat and symbiosis: Paleobiology, v. 38, p. 374–390,
526 DOI: 10.1666/11027.1.
527 Blaauw, M., and Christeny, J. A., 2011, Flexible paleoclimate age-depth models using an
528 autoregressive gamma process: Bayesian Anal. 6, p. 457–474, DOI: 10.1214/11-BA618.
529 Boltovskoy, E., and Totah, V.I., 1992, Preservation index and preservation potential of some
530 foraminiferal species: Journal of Foraminiferal Research, v. 22, p. 267–273.
531 Boltovskoy, E., Boltovskoy, D., Correa, N., and Brandini, F., 1996, Planktic foraminifera from
532 the southwestern Atlantic (30°-60°S): Species-specific patterns in the upper 50 m: Marine
533 Micropaleontology, v. 28, p. 53–72, DOI:10.1016/0377-8398(95)00076-3.
534 BouDagher-Fadel, M.K., 2018, Biostratigraphic and Geological Significance of Planktonic
535 Foraminifera, Updated 2nd ed, UCL Press, London, UK, 298 pp.
536 Brandini, P. F., Nogueira, M., Simião, M., Codina, C. U., J., and Noernberg, M., 2014, Deep
537 chlorophyll maximum and plankton community response to oceanic bottom intrusions on
538 the continental shelf in the South Brazilian Bight: Continetal Shelf Research, v. 89, p. 61–
539 75, DOI: 10.1016/j.csr.2013.08.002.

Brombacher, A., Wilson, P. A., and Ezard, T. H. G., 2017, Calibration of the repeatability of foraminiferal test size and shape measures with recommendations for future use: Marine Micropaleontology, v. 133, p. 21–27, DOI: 10.1016/j.marmicro.2017.05.003.

Brombacher, A., Leanne, E. E., Pincelli, M. H., Wilson P. A., and Ezard, T. H. G., 2018a, Calibration of test diameter and area as proxies for body size in the planktonic foraminifer *Globoconella Puncticulata*: Journal of Foraminiferal Research, v. 48 (3), p. 241–245, DOI: 10.2113/gsjfr.48.3.241.

Brombacher, A., Wilson, P. A., Bailey, I. and Ezard T. H. G., 2018b, Temperature is a poor proxy for synergistic climate forcing of plankton evolution: Procedings in Royal Society B (Biological Sciences), v. 285, p. 20180665, DOI: 10.1098/rspb.2018.0665.

Brummer, G. J. A., and Kucera, M., 2022, Taxonomic review of living planktonic foraminifera: Journal of Foraminiferal Research, v. 41(1), p. 29-74, DOI: 10.5194/jm-41-29-2022.

Burke, J. E., Renema, W., Henehan, M. J., Elder, L. E., Davis, C. V., Maas, A. E., Foster, G. L., Schiebel, R., and Hull, P.M., 2018, Factors influencing test porosity in planktonic foraminifera. Biogeosciences, v. 15, p. 6607–6619. DOI: 10.5194/bg-15-6607-2018.

Chaabane, S., de Garidel-Thoron, T., Giraud, X. et al., 2023a, The FORCIS database: A global census of planktonic Foraminifera from ocean waters: Science Data, v. 10, 354, DOI: 10.1038/s41597-023-02264-2.

Chaabane, S., de Garidel-Thoron, T., Meilland, J., Sulpis, O., Chalk, T., Brummer, G. J., Mortyn, P. G., Giraud, X., Howa, H., Casajus, N., Kuroyanagi, A., Beaugrand, G., and Schiebel, R., 2023b, Modern planktonic Foraminifera: migrating is not enough. 27 October 2023, PREPRINT (Version 1) available at Research Square. DOI: 10.21203/rs.3.rs-3485983/v1.

562 Conan, S. M. -H., and Brummer, G. J. A., 2000, Fluxes of planktic foraminifera in response to
563 monsoonal upwelling on the Somalia Basin margin: Deep Sea Research Part II: Topical
564 Studies in Oceanography, v. 47(9-11), p. 2207–2227, DOI: 10.1016/s0967-0645(00)00022-
565 9.
566 Darling, K.F., and Wade, C.M., 2008, The genetic diversity of planktic foraminifera and the
567 global distribution of ribosomal RNA genotypes: Marine Micropaleontology, v. 67, p. 216–
568 238, DOI: 10.1016/j.marmicro.2008.01.009.
569 Davis, C. V., Badger, M. P. S., Bown, P. R., and Schmidt, D. N., 2013, The response of
570 calcifying plankton to climate change in the Pliocene: Biogeosciences, v. 10, p. 6131–6139,
571 DOI: 10.5194/bg-10-6131-2013.
572 Davis, C. V., Livsey, C. M., Palmer, H. M., Hull, P. M., Thomas, E. H. G., Hill, T.M., and
573 Benitez-Nelson, C. R., 2020, Extensive morphological variability in asexually produced
574 planktic foraminifera: Science Advance, v. 6, p. 1–7, DOI: 10.1126/sciadv.abb8930.
575 Deuser, W. G., Ross, E. H., Hemleben, C., and Spindler, M., 1981, Seasonal changes in species
576 composition, numbers, mass, size, and isotopic composition of planktonic foraminifera
577 settling into the deep sargasso sea: Palaeogeography, Palaeoclimatology, Palaeoecology, v.
578 33, p. 103–127, DOI: 10.1016/0031-0182(81)90034-1.
579 Di Donato, V., Daunis-i-Estadella, J., Martín-Fernández, J. A., and Esposito, P., 2014, Size
580 fraction effects on planktonic foraminifera assemblages: a compositional contribution to
581 the Golden Sieve Rush: Mathematical Geosciences, v. 47, p. 455–470, DOI:
582 10.1007/s11004-014-9529-y.
583 Duque-Castaño, M. L., Leonhardt, A., and Pivel, M. A. G., 2019, Morphometric analysis in the
584 shells of the planktonic foraminifera *Orbulina universa*: a source for paleoceanographic

information: Brazilian Journal of Oceanography, v. 67, p. 134—142. DOI: 10.1590/s1679-87592019025206701.

Erez, J., 2003, The source of ions for biomineralization in foraminifera and their implications for paleoceanographic proxies: Reviews in Mineralogy and Geochemistry, v.54(1), p. 115–149. DOI: 10.2113/0540115.

Farmer, E. C., Kaplan, A., Menocal, P. B. de, and Lynch-Stieglitz, J., 2007, Corroborating ecological depth preferences of planktonic foraminifera in the tropical Atlantic with the stable oxygen isotope ratios of core top specimens: Paleoceanography, v.22, p. PA3205, DOI: 10.1029/2006PA001361.

Fehrenbacher, J. S., and Martin, P. A., 2014, Exploring the dissolution effect on the intrashell Mg/Ca variability of the planktic foraminifer *Globigerinoides ruber*: Paleoceanography and paleoclimatology, v. 29(9), p. 854-868, DOI: 10.1002/2013PA002571.

Foraminarium (2021a). *Globigerinoides ruber* (fossil). CC BY 4.0 DEED Attribution 4.0 International. Available at: https://sketchfab.com/3d-models/globigerinoides-ruber-fossil-34129111b1054068aaeeee6779316325.

Foraminarium (2021b). *Globigerinoides elongatus*1. CC BY 4.0 DEED Attribution 4.0 International. Available at: https://sketchfab.com/3d-models/globigerinoides-elongatus1-e94239e09fe042e88220679f9d8d9d36.

Foraminarium (2021c). *Globigerinoides ruber* (modern; plankton tow). CC BY 4.0 DEED Attribution 4.0 International. Available at: https://sketchfab.com/3d-models/globigerinoides-ruber-modern-plankton-tow-0f01d43975b54d22b5f1e8508c72d070.

Foraminarium (2022). *Globigerinoides ruber* Miocene Age. CC BY 4.0 DEED Attribution 4.0 International. Available at: https://sketchfab.com/3d-models/globigerinoides-ruber-miocene-age-a0b6a683aeb84ead995018ecced7dabc.

Fox, L., Stukins, S., Hill, T. et al., 2020, Quantifying the Effect of Anthropogenic Climate Change on Calcifying Plankton: Science Reports, v. 10, p. 1620, DOI: 10.1038/s41598-020-58501-w.

Frozza, C. F., Pivel, M. A. G., Suárez-Ibarra, J. Y., Ritter, M. N., and Coimbra, J. C., 2020, Bioerosion on Late Quaternary Planktonic Foraminifera Related to Paleoproductivity in the Western South Atlantic: Paleoceanography and Paleoclimatology, v. 35, p. 1–16. DOI: 10.1029/2020PA003865.

García-Chapori, N., and Laprida, C., 2021, Planktonic foraminifera assemblages from the Brazil–Malvinas Confluence: palaeoceanographic implications of sub-surface temperature reconstructions in the western South Atlantic: Lethaia, v. 54(4), p. 477–494, DOI: 10.1111/let.12416.

Gordon, A.L., 1989, Brazil-Malvinas Confluence-1984: Deep Sea Research Part A (Oceanographic Research Papers), v.36, p. 359–361, DOI: 10.1016/0198-0149(89)90042-3.

Gu, F., Zonneveld, K. A., Chiessi, C. M., Arz, H. W., Pätzold, J., and Behling, H., 2017, Long-term vegetation, climate and ocean dynamics inferred from a 73,500 years old marine sediment core (GeoB2107-3) off southern Brazil: Quaternary Science Reviews, v. 172, p. 55–71, DOI: 10.1016/j.quascirev.2017.06.028.

Hammer, Ø., Harper, D.A.T., and Ryan, P.D., 2001, Past: Paleontological Statistics Software Package for Education and Data Analysis. Palaeontol. Electron. 4, p. 1–9.

Hart, M.B., Hylton, M.D., Oxford, M.J., Price, G.D., Hudson, W., and Smart, C.W., 2003, The search for the origin of the planktic Foraminifera: Journal of Geological Society of London, v. 160, p. 341–343, DOI: 10.1144/0016-764903-003.

Hecht, A. D., Eslinger, E. V., and Garmon, L. B, 1975, Experimental studies on the dissolution of planktonic foraminifera. Dissolution of Deep-Sea Carbonates, Edi., Sliter, W. V., Bé, A. W. H., Berger, W. H. Special publication 13, Cushman Foundation for Foraminiferal Research.

Hecht, A.D, 1976a, Size variations in planktonic foraminifera: Implications for quantitative paleoclimatic analysis: Science, v.192 (4246), p. 1330-1332, DOI: 0.1126/science.192.4246.1330.

Hecht, A.D., 1976b, An ecologic model for test size variation in Recent planktonic foraminifera; applications to the fossil record: Journal of Foraminiferal Research, v. 6(4), p. 295-311, DOI: 10.2113/gsjfr.6.4.295.

Hecht, A.D., Be, A.W.H., and Lott, L., 1976, Ecologic and Paleoclimatic Implications of Morphologic Variation of Orbulina universa in the Indian Ocean: Science, v. 194(4263), p. 422–424, DOI:10.1126/science.194.4263.422.

Howe, J. N. W., Piotrowski, A. M., Noble, T. L., Mulitza, S., Chiessi, C. M., and Baton, G. (2016a). North atlantic deep water production during the last glacial maximum. Nat. Commun. 7, 11765. doi: 10.1038/ncomms11765

Howe, J. N. W., Piotrowski, A. M., Oppo, D. W., Huang, K. F., Mulitza, S., Chiessi, C., et al. (2016b). Antarctic intermediate water circulation in the South Atlantic over the past 25,000 years. Paleoceanography 31, 1302–1314. doi: 10.1002/2016PA002975

651 Huber, B. T., Petrizzo, M. R., Young, J. R., Falzoni, F., Gilardoni, S. E., Bown, P. R., and Wade,
652 B. Pfroams@microtax: A new online taxonomic database for planktonic foraminifera:
653 Micropaleontology, v. 62, p. 429–438. DOI: 10.47894/mpal.62.6.02.
654 Hutson, W.H., 1980. The Agulhas Current During the Late Pleistocene : Analysis of Modern
655 Faunal Analogs: Science, v. 207, p. 64–66.
656 Iwasaki, S., Kimoto, K, Sasaki, O, Kano, H, Honda, M. C., and Okazaki, Y., 2015, Observation
657 of the dissolution process of *Globigerina bulloides* tests (planktic foraminifera) by X-ray
658 microcomputed tomography: Paleoceanography, v.30, p. 317–331 DOI:
659 10.1002/2014PA002639.
660 Iwasaki, S., Kimoto, K., Okazaki, Y., and Ikehara, M., 2019, Micro-CT scanning of tests of three
661 planktic foraminiferal species to clarify dissolution: Process and Progress Geochemistry,
662 Geophysics, Geosystems v. 20(12), p. 6051-6065, DOI:10.1029/2019GC008456.
663 Kaiho, K., Takeda, K., Petrizzo, M. R., Zachos, J. C., 2006, Anomalous shifts in tropical Pacific
664 planktonic and benthic foraminiferal test size during the Paleocene-Eocene thermal
665 maximum: Palaeogeography, Palaeoclimatology, Palaeoecology, v.237, p. 456–464,
666 DOI:10.1016/j.palaeo.2005.12.017.
667 Kemle-von Mücke, S., and Hemleben, C., 1999, Foraminifera, in: Boltovskoy, D. (Ed.), South
668 Atlantic Zooplankton. Backhuys Publishers, pp. 43–73.
669 Knappertsbusch, S., 2016, Evolutionary prospection in the Neogene planktic foraminifer
670 Globorotalia menardii and related forms from ODP Hole 925B (Ceara Rise, western
671 tropical Atlantic): evidence for gradual evolution superimposed by long distance dispersal:
672 Swiss Journal of Palaeontology, v.135, p. 205-248, DOI:10.1007/s13358-016-0113-6.

673 Kucera, M., and Malmgren, B. A., 1998, Terminal Cretaceous warming event in the mid-latitude
674 South Atlantic Ocean: Evidence from poleward migration of *Contusotruncana contusa*
675 (planktonic foraminifera) morphotypes: Palaeogeography,.Palaeoclimatology,
676 Palaeoecology, v. 138, p. 1–15, DOI: 10.1016/S0031-0182(97)00124-7.
677 Kucera, M., 2007, Planktonic Foraminifera as tracers of past oceanic environments, in: Hillaire–
678 Marcel, C.A. de V. (Ed.), Proxies in Late Cenozoic Paleoceanography. Elsevier,
679 Amsterdam, p. 213–254.
680 Lessa, D. de O. V., Portilho-Ramos, R., Barbosa, C. F., Silva, A. R. da, Belem, A., Turcq, B.,
681 and Albuquerque, A. L., 2014, Planktonic foraminifera in the sediment of a western
682 boundary upwelling system off Cabo Frio, Brazil. Marine Micropaleontology, v. 106, p.
683 55–68, DOI: 10.1016/j.marmicro.2013.12.003.
684 Locarnini, R. A., Mishonov, A. V., Antonov, J. I., Boyer, T. P., Garcia, H. E., Baranova, O. K.,
685 Zweng, M. M., Paver, C. R., Reagan, J. R., Johnson, D. R., Hamilton, M., and Seidov, D.,
686 2013. Volume 1: Temperature, in: Levitus, S., Mishonov, A. (Eds.), World Ocean Atlas
687 2013. NOAA Atlas NESDIS 73, p. 40.
688 Lombard, F., Labeyrie, L., Michel, E., Spero, H. J., and Lea, D. W., 2009, Modelling the
689 temperature dependent growth rates of planktic foraminifera: Marine Micropaleontology, v.
690 70, p. 1–7. DOI:10.1016/j.marmicro.2008.09.004.
691 Malmgren, B. A., Kucera, M., Nyberg, J., and Waelbroeck, C., 2001, Comparison of statistical
692 and artificial neural network techniques for estimating past sea surface temperatures from
693 planktonic foraminifer census data: Paleoceanography, v. 16, p. 520–530. DOI:
694 10.1029/2000PA000562.

695 Marshall, B. J., Thunell, R. C., Spero, H. J., Henehan, M. J., Lorenzoni, L., and Astor, Y., 2015,
696 Morphometric and stable isotopic differentiation of Orbulina universa morphotypes from
697 the Cariaco Basin, Venezuela: Marine Micropaleontology 120, p. 46–64. DOI:
698 10.1016/j.marmicro.2015.08.001.
699 Mojtahid, M., Manceau, R., Schiebel, R., Hennekam, R., and de Lange, G. J., 2015, Thirteen
700 thousand years of southeastern Mediterranean climate variability inferred from an
701 integrative planktic foraminiferal-based approach: Paleoceanography and
702 Paleoclimatology, v. 30(4), p. 402-422, DOI:10.1002/2014PA002705.
703 Möller, O. O., Piola, A. R., Freitas, A. C., and Campos, E. J. D., 2008, The effects of river
704 discharge and seasonal winds on the shelf off southeastern South America: Continental
705 Shelf Research, v. 28, p. 1607–1624, DOI:10.1016/j.csr.2008.03.012.
706 Moller, T., Schulz, H., and Kucera, M., 2013, The effect of sea surface properties on shell
707 morphology and size of the planktonic foraminifer *Neogloboquadrina pachyderma* in the
708 North Atlantic: Palaeogeography, Palaeoclimatology, Palaeoecology, v. 391, p. 34–48.
709 DOI: 10.1016/j.palaeo.2011.08.014.
710 Morard, R., Escarguel, G., Weiner, A. K. M., André, A. Douady, A., C.J., Wade, C.M., Darling,
711 K.F., Ujiié, Y., Seears, H.A., Quillévéré, F., Garidel-Thoron, T., de Vargas, C., and Kucera,
712 M., 2016, Nomenclature for the nameless: a proposal for an integrative molecular
713 taxonomy of cryptic diversity exemplified by Planktonic Foraminifera: Systematic
714 Biology , v. 65(5), p. 925–940, DOI:10.1093/sysbio/syw031.
715 Morard, R., Füllberg, A., Brummer, G. J. A., Greco, M., Jonkers, L., Wizemann, A., Weiner, A.
716 K. M., Darling, K., Siccha, M., Ledevin, R., Kitazato, H., de Garidel-Thoron, T., De
717 Vargas, C., and Kucera, M., 2019, Genetic and morphological divergence in the warm-

718 water planktonic foraminifera genus Globigerinoides: PLOS One, v.14, p. 1–30,
719 DOI:10.1371/journal.pone.0225246.
720 Moy, A. D., Howard, W. R., Bray, S. G., and Trull, T. W., 2009, Reduced calcification in
721 modern Southern Ocean planktonic foraminifera: Letters Nature Geoscience, v. 2, p. 276-
722 280. DOI: 10.1038/NGEO460.
723 Naidu, P.D., and Malmgren, B.A., 1995. Monsoon upwelling effects on test size of some
724 planktonic foraminiferal species from the Oman Margin, Arabian Sea: Paleoceanography,
725 v. 10, p. 117–122, DOI:10.1029/94PA02682.
726 Oppo, D. W., Lu, W., Huang, K.-F., Umling, N. E., Guo, W., Yu, J., Curry, W. B., Marchitto, T.
727 M., and Wang, S., 2023, Deglacial Temperature and Carbonate Saturation State Variability
728 in the Tropical Atlantic at Antarctic Intermediate Water Depths, Paleoceanography and
729 Paleoclimatology 38 (9), e2023PA004674. https://doi.org/10.1029/2023PA004674
730 Ortiz, J. D., Mix, A. C., and Collier, R. W., 1995, Environmental control of living symbiotic and
731 asymbiotic foraminifera of the California Current: Paleoceanography, v. 10, p. 987–1009,
732 DOI:10.1029/95PA02088.
733 Palma, E. D., and Matano, R. P., 2009, Disentangling the upwelling mechanisms of the South
734 Brazil Bight: Continental Shelf Research, v. 29, p. 1525–1534,
735 DOI:10.1016/j.csr.2009.04.002.
736 Patterson, R. T., and Fishbein, A., 1989, Re-examination of the statistical methods used to
737 determine the number of point counts needed for micropaleontological quantitative
738 research: Paleontological Society, v. 63, p. 245–248, DOI: 10.1017/S0022336000019272.

739 Pereira, L. S., Arz, H. W., Pätzold, J., and Portilho-Ramos, R.C., 2018, Productivity evolution in
740 the South Brazilian bight during the last 40,000 Years: Paleoceanography and
741 Paleoclimatology, v. 33, p. 1339–1356, DOI:10.1029/2018PA003406.
742 Peterson, R.G., and Stramma, L., 1991, Upper-level circulation in the South Atlantic Ocean:
743 Progress Oceanography, v. 26, p. 1–73, DOI:10.1016/0079-6611(91)90006-8.
744 Petró, S. M., Pivel, M. A. G., and Coimbra, J.C., 2018, Foraminiferal solubility rankings: a
745 contribution to the search for consensus: Journal of Foraminiferal Research, v. 48, p. 301–
746 313., DOI:10.2113/gsjfr.48.4.301.
747 Petró, S. M., Pivel, M. A. G., and Coimbra, J. C., 2021, Evidence of supra-lysoclinal dissolution
748 of pelagic calcium carbonate in the late Quaternary in the western South Atlantic: Marine
749 Micropaleontology, v. 166, p. 102013, DOI:10.1016/j.marmicro.2021.102013.
750 Pimenta, F. M., Campos, E. J. D., Miller, J. L., and Piola, A. R., 2005, A numerical study of the
751 Plata River plume along the southeastern South American continental shelf: Brazilian
752 Journal Oceanography, v. 53, p. 129–146, DOI:10.1590/s1679-87592005000200004.
753 Piola, A. R., Matano, R. P., Palma, E. D., Möller, O. O., and Campos, E. J. D., 2005, The
754 influence of the Plata River discharge on the western South Atlantic shelf: Geophysical
755 Research Letter, v. 32, p. 1–4, DOI:10.1029/2004GL021638.
756 Piola, A. R., and Matano, R. P., 2009, Brazil and Falklands (Malvinas) Currents, in: Steele, John
757 H.; Thorpe, Steve A.; Turekian, K.K. (Ed.), Ocean Currents. Elsevier Ltd, London, p. 627.
758 Portilho-Ramos, R. C., Pinho, T., Chiessi, C., Band arbosa, C., 2019, Understanding the
759 mechanisms behind high glacial productivity in the southern Brazilian margin: Climate of
760 the Past., v.15, p. 943–955, DOI:10.5194/cp-2018-98.

761 Principato, M. S., Crudeli, D., Ziveri, P., Slomp, C. P., Corselli, C., Erba, E., and de Lange, G. J.,
762 2006, Phyto and zooplankton paleofluxes during the deposition of sapropel S1 (eastern
763 Mediterranean): biogenic carbonate preservation and paleoecological implications,
764 Palaeogeography, Palaeoclimatology,. Palaeoecology, v. 235, p. 8–27, DOI:
765 10.1016/j.palaeo.2005.09.021.
766 R Core Team, 2020, R: a language and environment for statistical computing (Vienna, Austria: R
767 Foundation for Statistical Computing). Available at: http://www.R-project.org/.
768 Renaud, S., and Schmidt, D. N., 2003, Habitat tracking as a response of the planktic foraminifer
769 Globorotalia truncatulinoides to environmental fluctuations during the last 140 kyr: Marine
770 Micropaleontology, v. 49, p. 97–122, DOI:10.1016/S0377-8398(03)00031-8
771 Rillo, M. C., Mauro T. C., Sugawara, C. B., Jonkers, L., Baranowski, U., Kucera, M., Ezard, T.
772 H. G., 2019, On the mismatch in the strength of competition among fossil and modern
773 species of planktonic Foraminifera: Global Ecology and Biogeography, v. 28(12), p. 1866-
774 1878, DOI:10.1111/geb.13000
775 Rillo, M. C., Miller, C. G., Kucera, M., and Ezard, T. H. G., 2020, Intraspecific size variation in
776 planktonic foraminifera cannot be consistently predicted by the environment: Ecology and
777 Evolution, v.10(20), p. 11579–11590, DOI:10.1002/ece3.6792
778 Rodrigues, R. R., Lorenzzetti, J. A., 2001, A numerical study of the effects of bottom topography
779 and coastline geometry on the Southeast Brazilian coastal upwelling: Continental Shelf
780 Research., v. 21, p. 371–394, DOI:10.1016/S0278-4343(00)00094-7.Rodrigues, A. R.,
781 Pivel, M. A. G., Schmitt, P., de Almeida, F. K., and Bonetti, C., 2018, Infaunal and
782 epifaunal benthic foraminifera species as proxies of organic matter paleofluxes in the

Pelotas Basin, south-western Atlantic Ocean: Marine Micropaleontology, v. 144, p. 38–49, DOI:10.1016/j.marmicro.2018.05.007.

Santana, B. F. B. B., Freitas, T. F., Leonel, J.,and Bonetti, C., 2021, Biometric and biomass analysis of Quaternary Uvigerinidae (Foraminifera) from the Southern Brazilian continental slope: Marine Micropaleontology, v. 169, p. 102041, DOI:10.1016/j.marmicro.2021.102041.

Schiebel, R., Waniek, J., Bork, M., and Hemleben, C., 2001, Planktic foraminiferal production stimulated by chlorophyll redistribution and entrainment of nutrients: Deep Research: Part I Oceanographic Research Paper, v. 48, p. 721–740: DOI:10.1016/S0967-0637(00)00065-0.

Schiebel, R., and Hemleben, C., 2017, Planktic Foraminifers in the Modern Ocean. Sringer-Verlag, Berlin Heidelberg, DOI:10.1007/978-3-662-50297-6.

Schlitzer, R., 2021, Ocean Data View. Available at: https://odv.awi.de.

Schmidt, G.A., and Mulitza, S., 2002, Global calibration of ecological models for planktic foraminifera from core-top carbonate oxygen-18: Marine Micropaleontology, v. 44, p. 125–140, DOI:10.1016/S0377-8398(01)00041-X.

Schmidt, D.N., Renaud, S., and Bollmann, J., 2003, Response of planktic foraminiferal size to late Quaternary climate change: Paleoceanography, v. 18(2), p. 1039, DOI:10.1029/2002PA000831.

Schmidt, D.N., Thierstein, H.R., and Bollmann, J., 2004a, The evolutionary history of size variation of planktic foraminiferal assemblages in the Cenozoic: Palaeogeography, Palaeoclimatology, Palaeoecology., v. 212, p. 159–180, DOI:10.1016/j.palaeo.2004.06.002.

Schmidt, D.N., Renaud, S., Bollmann, J., Schiebel, R., and Thierstein, H.R., 2004b, Size distribution of Holocene planktic foraminifer assemblages: biogeography, ecology and

adaptation: Marine Micropaleontology, v. 50, p. 319–338, DOI:10.1016/S0377-8398(03)00098-7.

Schmidt, D.N., Elliott T., and Kasemann, S. A., 2008, The influences of growth rates on planktic foraminfiers as proxies for palaeostudies – a review: Geological Society London, Special Publications, v. 303, p. 73-85, DOI:10.1144/SP303.6.

Schmidt, D. N., Caromel, A. G. M., Seki, O., Rae, J. W. B., Renaud, S., 2016, Morphological response of planktic foraminifers to habitat modifications associated with the emergence of the Isthmus of Panama: Marine Micropaleontology, v. 128, p. 28–38, DOI:10.1016/j.marmicro.2016.08.003.

Schulte, S., and Bard, E., 2003. Past changes in biologically mediated dissolution of calcite above the chemical lysocline recorded in Indian Ocean sediments, Quaternary Science Reviews, 22(15-17), 1757–1770. https://doi.org/10.1016/S0277-3791(03)00172-0

Secteur Sciences et Technologies – AMU (2018). *Globigerinoides ruber*. CC BY 4.0 DEED Attribution 4.0 International. Available at: https://sketchfab.com/3d-models/globigerinoides-ruber-c626771f89ae4ae782228ee41e325954

Shakun, J. D., Lea, D. W., Lisiecki, L. E., and Raymo, M. E., 2015, An 800-kyr record of global surface ocean $\delta^{18}O$ and implications for ice volume-temperature coupling: Earth Planet Science Letter, v. 426, p. 58–68, DOI:10.1016/j.epsl.2015.05.042.

Siccha, M., and Kucera, M., 2017, Data Descriptor: ForCenS, a curated database of planktonic foraminifera census counts in marine surface sediment samples: Science Data, v. 4, p. 1–12. DOI:10.1038/sdata.2017.109.

827 Silveira, I. C. A., de Schmidt, A. C. K., Campos, E. J. D., de Godoi, S. S., and Ikeda, Y., 2000, A
828 corrente do Brasil ao largo da costa leste brasileira: Brazilian Journal of Oceanography., v.
829 48, p. 171–183, DOI:10.1590/s1679-87592000000200008.
830 Sousa, S. H. M., de Godoi, S. S., Amaral, P. G. C., Vicente, T. M., Martins, M. V. A., Sorano,
831 M. R. G. S., Gaeta, S. A., Passos, R. F., and Mahiques, M. M., 2014, Distribution of living
832 planktonic foraminifera in relation to oceanic processes on the southeastern continental
833 Brazilian margin (23°S-25°S and 40°W-44°W): Continental Shelf Research., v. 89, p. 76–
834 87, DOI:10.1016/j.csr.2013.11.027.
835 Souto, D. D., Lessa, D. V. O., Albuquerque, A. L. S., Sifeddine, A., Turcq, B. J., and Barbosa, C.
836 F., 2011, Marine sediments from southeastern Brazilian continental shelf: A 1200 year
837 record of upwelling productivity: Palaeogeography, Palaeoclimatology, Palaeoecology, v.
838 299, p. 49–55, DOI:10.1016/j.palaeo.2010.10.032.
839 Suárez-Ibarra, J. Y., Petró, S. M., Frozza, C. F., Freire, T. M., Pivel, M. A. G., 2020, Planktonic
840 Foraminifera assemblages from sediment core SAT-048A: PANGAEA,
841 DOI:10.1594/PANGAEA.924469
842 Suárez-Ibarra, J. Y., Frozza, C. F., Petró, S. M., and Pivel, M. A. G., 2021, Fragment or broken?
843 Improving the planktonic foraminifera fragmentation assessment: Palaios, v.36, p. 165–
844 172, DOI: 10.2110/palo.2020.062.
845 Suárez-Ibarra, J. Y., Frozza, C. F., Palhano, P. L., Petró, S. M., Weinkauf, M. F. G., and Pivel,
846 M. A. G., 2022, Calcium carbonate dissolution triggered by high productivity during the
847 last glacial-interglacial interval in the deep western South Atlantic: Frontiers in Earth Scice,
848 v.10, DOI: 10.3389/feart.2022.830984.

Suárez-Ibarra, J. Y., Freire, T. M., Frozza, C. F., Pinho, T. M. L., Petró, S. M., Dias, B. B., Chalk, T. B., Chaabane, S., Srivastava, M., Costa, K. B., Toledo, F. A. L., de Garidel-Thoron, T., Coimbra, J. C., and Pivel, M. A. G., 2023, Surface fertilisation and organic matter delivery enhanced carbonate dissolution in the western South Atlantic: Frontiers in Ecology and Evolution, v. 11, p. 1238334, DOI: 10.3389/fevo.2023.1238334.

Thunell, R.C., and Honjo, S., 1981, Calcite dissolution and the modification of planktonic foraminiferal assemblages: Marine Micropaleontology, v. 6, p. 169–182, DOI:10.1016/0377-8398(81)90004-9.

Todd, C. L., Schmidt, D. N., Robinson, M. M., and de Schepper, S., 2020, Planktic Foraminiferal test size and weight response to the late Pliocene environment: Paleoceanography and. Paleoclimatology, v. 35, p. 1–15. DOI:10.1029/2019PA003738.

Ujiié, Y., de Garidel-Thoron, T., Watanabe, S., Wiebe, P., de Vargas, C., 2010, Coiling dimorphism within a genetic type of the planktonic foraminifer *Globorotalia truncatulinoides*: Marine Micropaleontology, v. 77, p. 145–153, DOI:10.1016/j.marmicro.2010.09.001.

Ujiié, Y., Lipps, J. H., 2009, Cryptic diversity in planktic foraminifera in the Northwest Pacific Ocean: Journal of Foraminiferal Research, v. 39 (3), p. 145–154, DOI:10.2113/gsjfr.39.3.145.

Wade, B. S., and Olsson, R. K., 2009, Investigation of pre-extinction dwarfing in Cenozoic planktonic foraminifera. Palaeogeography, Palaeoclimatology, Palaeoecolology, v. 284, p. 39–46, DOI:10.1016/j.palaeo.2009.08.026.

Wade, B. S., Poole, C. R., and Boyd, J.L., 2016, Giantism in Oligocene planktonic foraminifera *Paragloborotalia opima*: Morphometric constraints from the equatorial Pacific Ocean: Newsletters Stratigraphy., v. 49, p. 421–444, DOI:10.1127/nos/2016/0270.

Wang, L., Pflaumann, U., and Sarnthein, M., 1995, Paleo-sea surface salinities in low latitude Atlantic: the $\delta^{18}O$ record of *Globigerinoides ruber* (white): Paleoceanography, 10 (4), p. 749–761, DOI:10.1029/95PA00577.

Weiner, A. K. M., Weinkauf, M. F. G., Kurasawa, A., Darling, K. F., and Kucera, M., 2015, Genetic and morphometric evidence for parallel evolution of the *Globigerinella calida* morphotype: Marine Micropaleontology, v. 114, p. 19–35. DOI:10.1016/j.marmicro.2014.10.003.

Weinkauf, M. F. G., Moller, T., Koch, M. C., and Kucera, M., 2013, Calcification intensity in planktonic Foraminifera reflects ambient conditions irrespective of environmental stress: Biogeosciences, v. 10, p. 6639–6655, DOI:10.5194/bg-10-6639-2013.

Weinkauf, M. F. G., Bonitz, F. G. W., Martini, R., and Kucera, M., 2019, An extinction event in planktonic Foraminifera preceded by stabilizing selection: PLOS ONE, v. 14, p. 1–21, DOI:10.1371/journal.pone.0223490.

West-Eberhard, M.J., 1989, Phenotypic plasticity and the origins of diversity: Annual Review of Ecology and Systematics, v. 20, p. 249-278, DOI:10.1146/annurev.es.20.110189.001341.

Woodhouse, A., Swain, A., Fagan, W. F. et al., 2023, Late Cenozoic cooling restructured global marine plankton communities: Nature, v. 614, p. 713–718, DOI:10.1038/s41586-023-05694-5.

Yasuhara, M., Wei, C. L., Kucera, M., Costello, M. K., Tittensor, D. P., Kiessling, W., Bonebrake, T. C., Tabor, C. R., Feng, R., Baselga, A., Kretschmer, K., Kusumoto, B., and

Kubota, Y., 2020, Past and future decline of tropical pelagic biodiversity: PNAS, v. 117 (23), p. 12891-12896, DOI:10.1073/pnas.1916923117.

Zarkogiannis, S., Kontakiotis, G., and Antonarakou, A., 2020, Recent planktonic foraminifera population and size response to Eastern Mediterranean hydrography: Revue de Micropaléontologie, v. 69, p. 100450, DOI:10.1016/j.revmic.2020.100450.

APPENDICES

TABLES CAPTIONS

Table 1. Number of individuals utilised to analyse the test size variation from core SAT-048A, per species per sample. Samples with less than 20 specimens are bold and denoted by *.

Table 2. Estimate results of the multiple linear correlations performed on the test size variation (as described by the mean and 95th percentile of the squared root of the cross-sectional area) against MAT-temperature (at 25 and 75 m depth), productivity ($PC1_P$), salinity at 25 m depth (S_{25m}) and dissolution ($PC1_D$). *p*-values are denoted as: ° <0.1, * <0.05, ** <0.01, *** <0.001, and significant (p <0.05) numbers are indicated in bold. Perc stands for percentile.

Table 3. Results of the Pearson correlations performed on the test size variation (as described by the mean and 95th percentile of the squared root of the cross-sectional area) against the relative abundance (%) of each taxon. *p*-values are denoted as: ° <0.1, * <0.05, and significant (p <0.05) numbers are indicated in bold.

Table 4. Area loss with the removal of the last chamber, relative to the whole test, from the open-source 3D models. After the removal of the last chamber, the table shows how much the size of the test can be decreased.

FIGURE CAPTIONS

Figure 1. Modern oceanographic conditions at the western South Atlantic illustrated by the mean annual sea surface temperature (°C). Data are from the World Ocean Atlas 2013 (Locarnini et al.,

2013). A simplified schematic representation of the Brazil and Malvinas currents is based on Peterson and Stramma (1991) and Möller et al. (2008). The white dot indicates the location of core SAT-048A analysed in this study. Plotted with Ocean Data View (Schlitzer, 2021).

Figure 2. Test sizes (as 95th percentile, upper panel, and mean, lower panel, of squared root of cross-sectional area) records of species-specific (*Globigerinoides ruber albus, Globigerinita glutinata* and *Globigerina bulloides*) and the partial assemblage (*Globigerinoides ruber ruber, Globorotalia inflata, Globigerinella calida* and *Neogloboquadrina incompta*) for core SAT-048A. Marine Isotope Stages (MIS) are indicated by vertical white (MIS 3 and MIS 1) and blue (MIS 2) background. The white rectangle within MIS 2 indicates the Last Glacial Maximum (LGM).

Figure 3. Comparison of **(A)** relative abundances and reconstructed environmental parameters for core SAT-048A. In **B)** reconstructed sea surface temperature for 25 and 75 m obtained using the Modern Analogue Technique (MAT), **C)** $\delta^{18}O_{G.ruber\ ruber}$ (‰ VPDB) **D)** salinity at 25 m depth based on $\delta^{18}O_{sw}$ (‰ SMOW), and synthesized records of **E)** productivity ($PC1_P$) and **F)** dissolution ($PC1_D$) (from Suárez-Ibarra et al., 2022). Marine Isotope Stages (MIS) are indicated by vertical white (MIS 3 and MIS 1) and blue (MIS 2) backgrounds. The white rectangle within MIS 2 indicates the Last Glacial Maximum (LGM).

Figure 4. Pearson correlation between the square-root of cross-sectional area and maximum diameters based on 422 random specimens, belonging to different species and varied sizes, obtained from core SAT-048A.

Figure 5. Comparison of stereomicroscope views and corresponding scanning electron microscope images of *Globigerinoides ruber albus* tests taken from core SAT-048 displaying

943 scars where the final chamber(s) was(were) attached to. From **A** to **E**, broken shells become less
944 evident. Scale-bar: 100 μm.

945 **Figure 6**. Open-source 3D models of *Globigerinoides ruber* "any" (see **Table 6**). On the left side
946 whole specimens and on the right side the same specimens after the artificial removal of the last
947 chamber showing resemblance with a complete test.

Age (ka BP)	*Globigerinoides ruber albus*	*Globigerinita glutinata*	*Globigerina bulloides*	Partial assemblage
5.8	163	40	**17***	300
7.1	145	30	**15***	249
8.5	133	44	**15***	281
9.4	129	45	**18***	266
10.4	189	72	33	424
11.9	198	101	68	518
13.9	129	60	46	331
15.5	126	71	63	366
16.2	109	60	34	282
16.8	116	63	56	352
17.4	84	61	31	233
17.7	93	77	51	297
17.9	87	55	34	264
18.3	127	55	42	312
18.9	101	68	54	312
19.3	72	34	54	231
20.1	90	68	26	259
21.4	93	64	55	291
21.8	107	47	88	348
22.7	93	51	60	321
23.3	72	50	90	325
23.6	98	80	57	407
24.0	113	78	66	451
24.5	66	49	95	320
25.1	107	110	56	446
25.4	103	57	59	423
25.8	76	45	39	312
26.3	52	31	54	229
27.8	69	49	59	273
28.6	79	37	67	284
29.1	98	47	61	304
29.7	114	66	79	400
30.7	142	72	83	480
31.5	95	79	68	342
32.0	109	71	53	346
32.6	73	54	38	272
33.5	93	55	52	349
34.3	79	40	50	262
34.9	75	42	71	289

35.2	82	54	74	308
35.6	113	85	81	422
36.5	94	89	75	345
37.4	142	110	91	432
37.9	71	77	79	286
38.2	68	80	104	306
38.9	61	48	77	238
40.0	79	64	142	339
41.1	63	67	66	261
42.3	117	56	65	339

		Partial assemblage		*G. ruber albus*		*G. glutinata*		*G. bulloides*	
Regression	T	Mean	95th Perc	Mean	95th Perc	Mean	95th Perc	Mean	95th Perc
Temperature	25 m	1.16	4.22°	0.28	0.41	0.19	-0.86	**2.58****	2.79
	75 m	-1.40	-0.43	**-3.62****	4.98°	-0.78	-0.46	**-1.93***	**-6.03****
$PC1_P$	25 m	**-5.22*****	**-8.80****	**-3.62***	-3.88	-0.3	-0.39	-0.01	-1.70
	75 m	**-6.57*****	**-11.09*****	**-5.77*****	-6.85°	-0.83	-0.23	**-2.34***	**-6.41****
S_{25m}	25 m	1.45	-1.53	1.84	4.65	-0.85	0.42	-2.14	-1.24
	75 m	4.32°	5.87	4.63	8.53	-0.01	-0.73	3.45	7.31
$PC1_D$	25 m	-1.00	-2.41	-2.73°	**-8.57****	**-1.82***	-2.12	0.42	1.55
	75 m	-1.64°	-3.95	**-3.44****	**-9.54****	**-2.02***	-1.90	-0.79	-0.41
Adjusted R^2	25 m	**0.67*****	**0.59*****	**0.45*****	**0.39*****	**0.22****	-0.03	**0.25****	0.03
	75 m	**0.68*****	**0.55*****	**0.55*****	**0.43*****	**0.24****	-0.03	**0.16***	**0.21****

		Mean	95th Percentile
G. ruber albus (%)	R	0.19	0.24
	p	0.19	0.09°
G. glutinata (%)	R	-0.28	-0.18
	p	**0.05***	0.21
G. bulloides (%)	R	-0.17	-0.04
	p	0.25	0.80

Name of the file	Area loss without the final chamber (%)	Reference
Globigerinoides ruber (albus modern; plankton tow SW Pacific)	28.4	Secteur Sciences et Technologies – AMU (2018)
Globigerinoides ruber Miocene Age	41.8	Foraminarium (2022)
Globigerinoides ruber (fossil)	22.0	Foraminarium (2021a)
Globigerinoides elongatus	22.8	Foraminarium (2021b)
Globigerinoides ruber (modern; plankton tow)	12.0	Foraminarium (2021c)

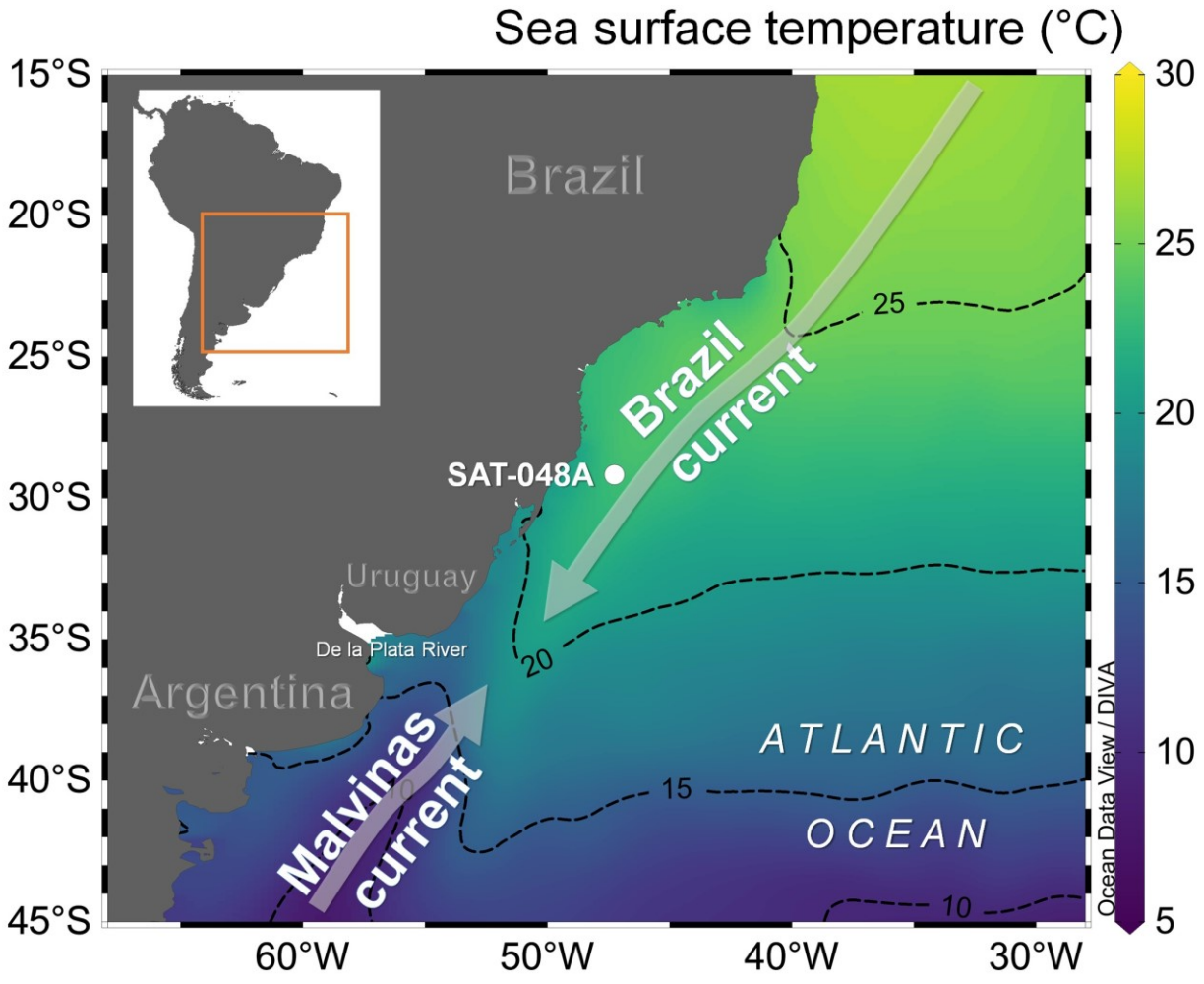
Sea surface temperature (°C)
15°S
20°S
25°S
30°S
35°S
40°S
45°S
60°W
50°W
40°W
30°W
Brazil
Uruguay
Argentina
De la Plata River
SAT-048A
Brazil current
Malvinas current
ATLANTIC
OCEAN
25
20
15
10
30
25
20
15
10
5
Ocean Data View / DIVA

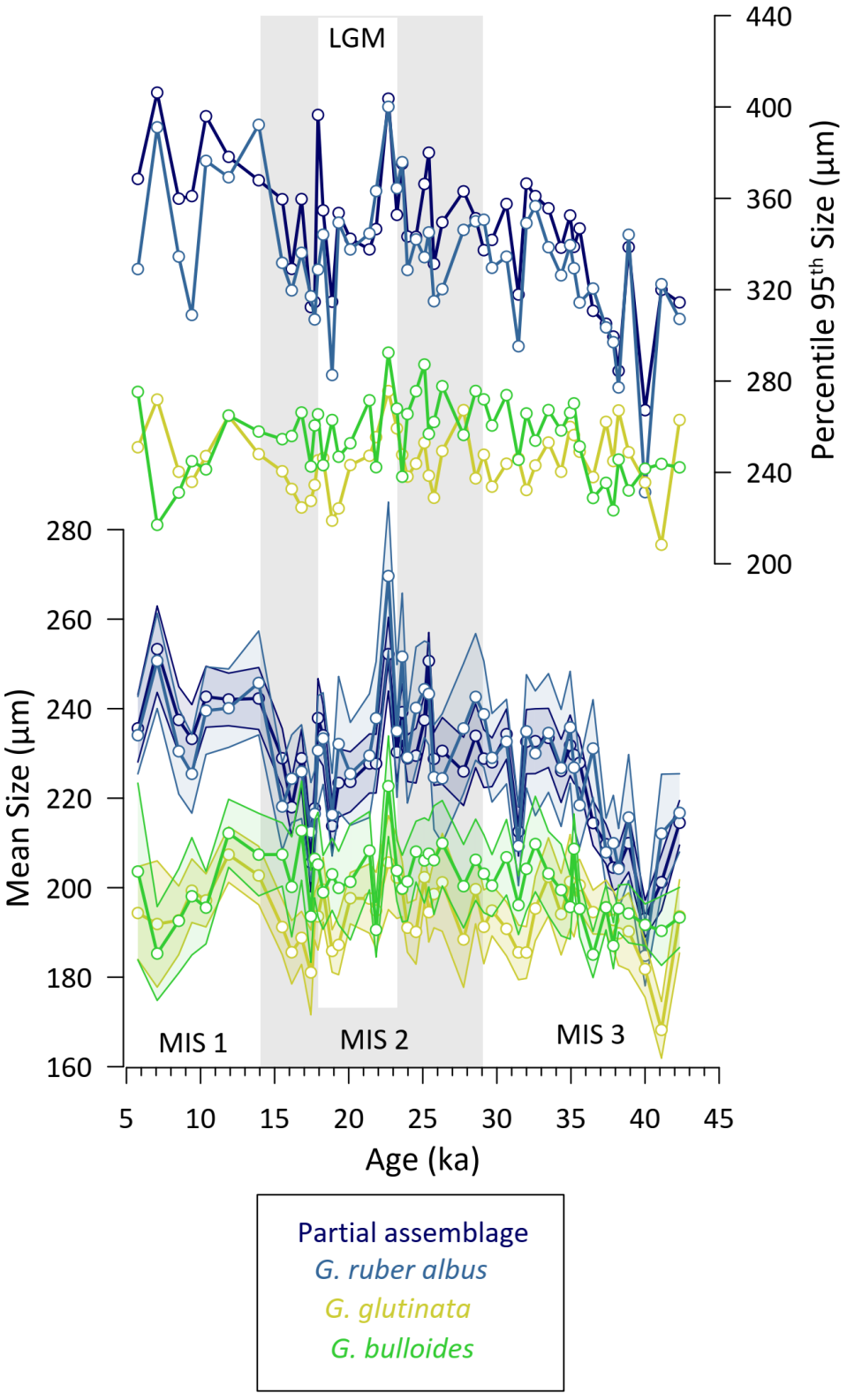
LGM
MIS 1
MIS 2
MIS 3
Mean Size (µm)
Percentile 95th Size (µm)
Age (ka)
160
180
200
220
240
260
280
200
240
280
320
360
400
440
5
10
15
20
25
30
35
40
45
Partial assemblage
G. ruber albus
G. glutinata
G. bulloides

961

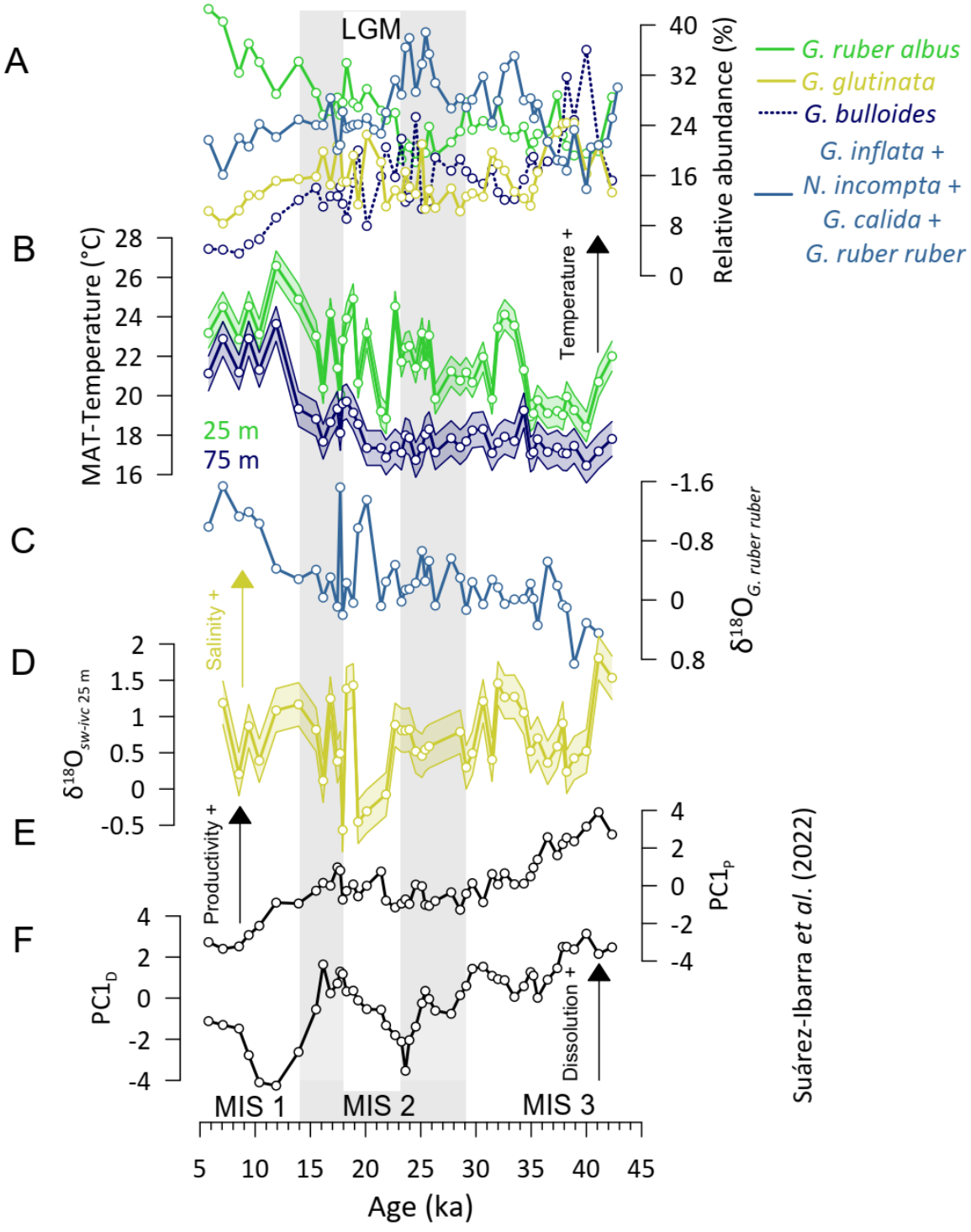
A
B
C
D
E
F
LGM
G. ruber albus
G. glutinata
G. bulloides
G. inflata +
N. incompta +
G. calida +
G. ruber ruber
Relative abundance (%)
40
32
24
16
8
0
MAT-Temperature (°C)
28
26
24
22
20
18
16
25 m
75 m
Temperature +
-1.6
-0.8
0
0.8
δ18OG. ruber ruber
Salinity +
δ18Osw-ivc 25 m
2
1.5
1
0.5
0
-0.5
Productivity +
PC1P
4
2
0
-2
-4
PC1D
Dissolution +
MIS 1
MIS 2
MIS 3
5
10
15
20
25
30
35
40
45
Age (ka)
Suárez-Ibarra et al. (2022)

963

964 SUÁREZ-IBARRA, FIGURE 4

965

966

967

968

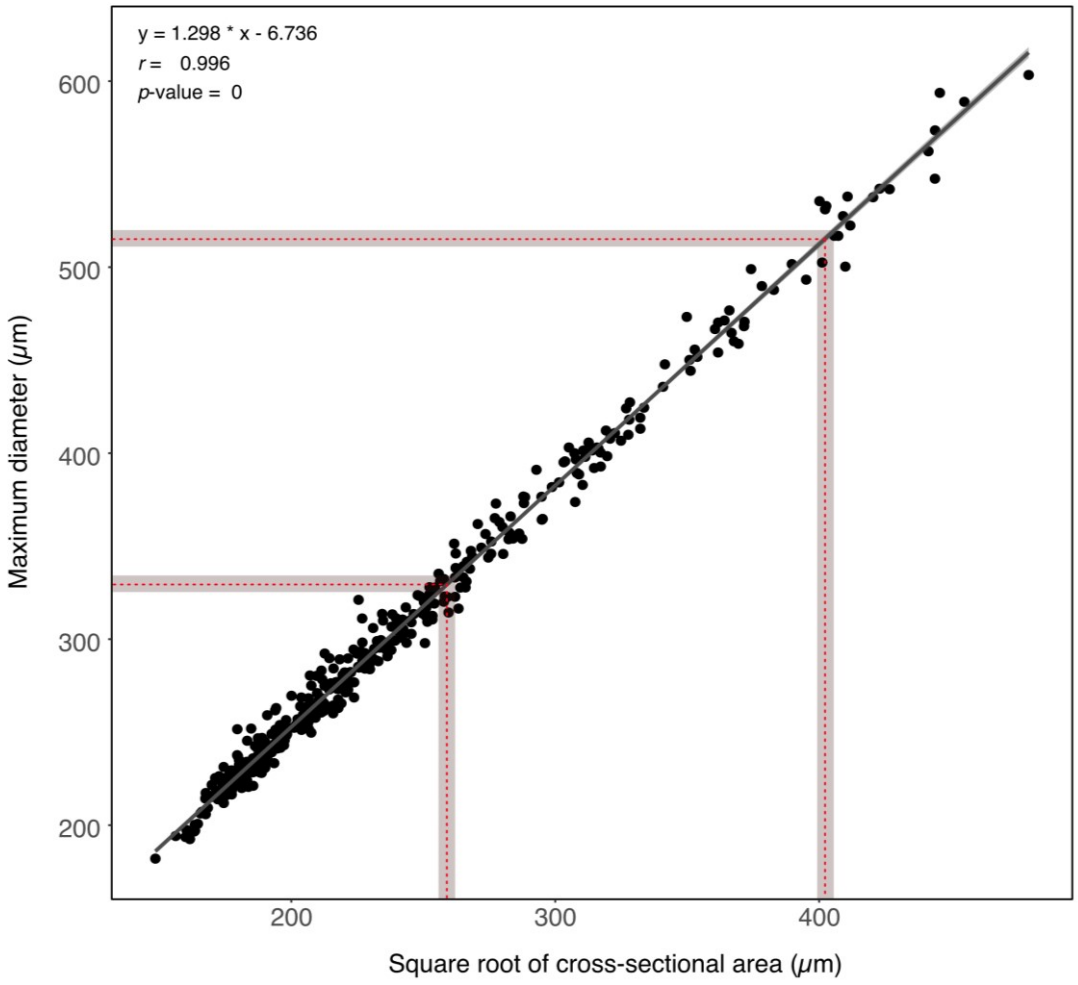

969

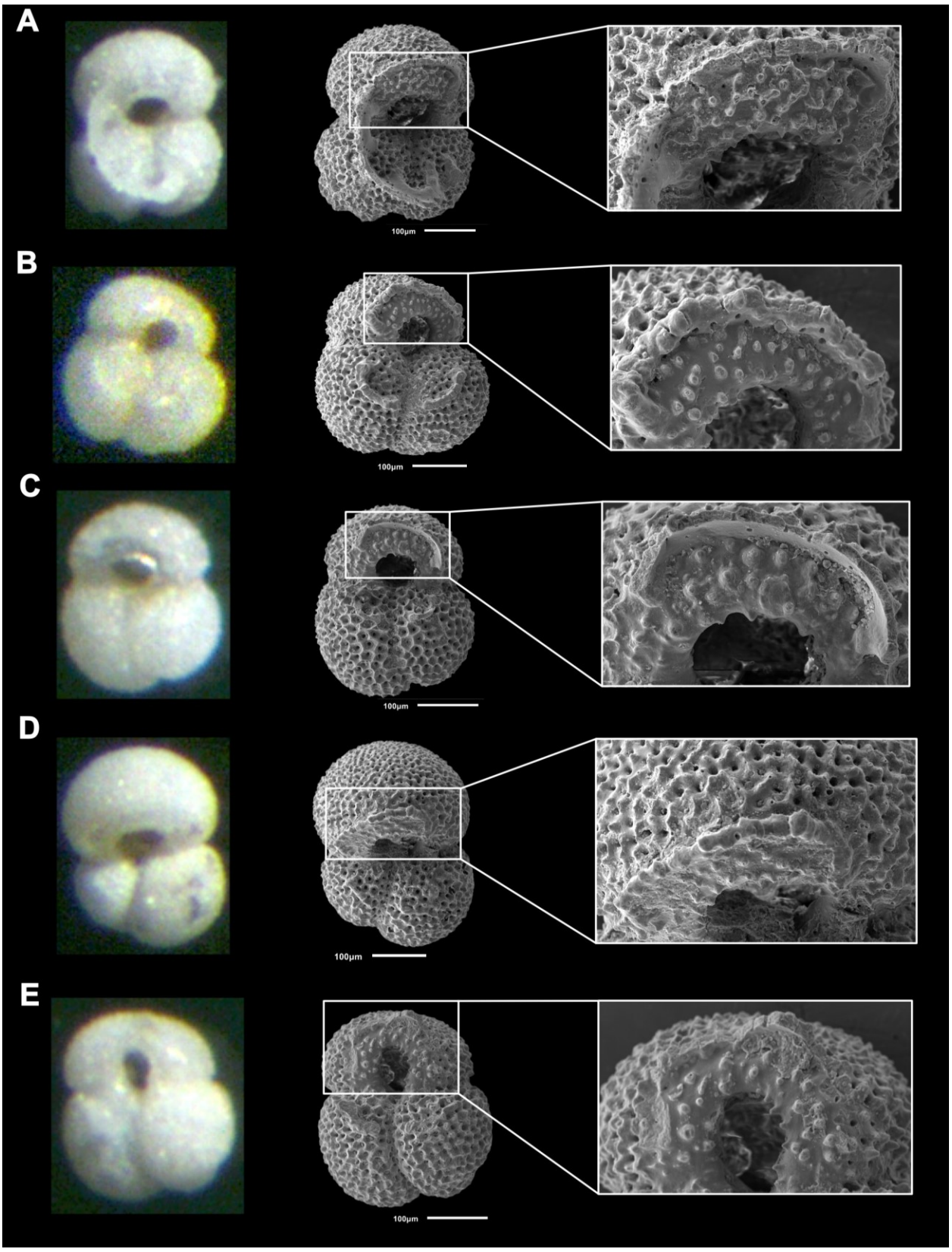

971

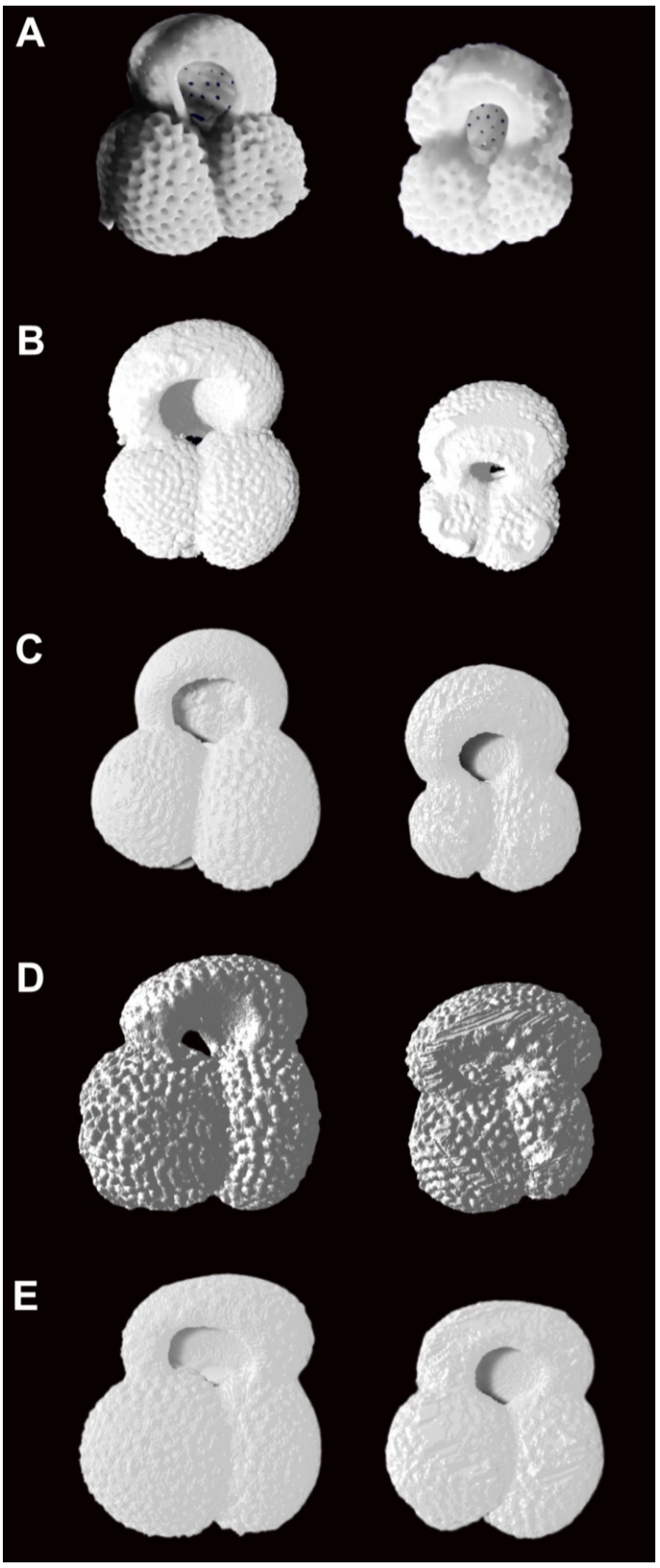

973

Supplementary material for

PLANKTONIC FORAMINIFERA TEST SIZE DICTATED BY CONDITIONS IN LIFE AND POST-MORTEM

JAIME Y. SUÁREZ-IBARRA[1*], INGRID VIEIRA[2], CRISTIANE F. FROZZA[2], SONIA CHAABANE[3,4,5], PÂMELA L. PALHANO[2], VOJTĚCH KOVÁŘ[1], THOMAS B. CHALK[3], GEISE S. ANJOS-ZERFASS[6], THIBAULT DE GARIDEL-THORON[3], KATARÍNA HOLCOVÁ[1], MARÍA A.G. PIVEL[7]

*Corresponding author, jysuarezibarra@gmail.com, suarezij@natur.cuni.cz

[1] Institute of Geology and Palaeontology, Faculty of Science, Charles University, Prague, Czech Republic

[2] Programa de Pós-Graduação em Geociências, Instituto de Geociências, Universidade Federal do Rio Grande do Sul, Porto Alegre, Brazil

[3] Aix-Marseille Université, CNRS, IRD, INRAE, CEREGE, Europôle Méditerranéen de l'Arbois, Aix-en-Provence, France

[4] Department of Climate Geochemistry, Max Planck Institute for Chemistry, Mainz, Germany,

[5] Fondation pour la recherche sur la biodiversité (FRB-CESAB), Montpellier, France

[6] Petrobras, Leopoldo Américo Miguez de Mello Research, Development and Innovation Center, Rio de Janeiro, Brazil

[7] Centro de Estudos de Geologia Costeira e Oceanica (CECO), Instituto de Geociências, Universidade Federal do Rio Grande do Sul, Porto Alegre, Brazil.

Contents of this file

Introduction

This file presents data related to the age model construction (tables S1 and S2), the reconstruction of sea subsurface temperatures (Figure S1), statistical analysis (Spearman's rank correlation, Table S3 and Figure S2) and a list of 25 planktonic foraminifera specimens showing signs of broken/removed terminal chambers (Table S3).

Age model

The age model for core SAT-048A used in this paper is presented in Suárez-Ibarra et al. (2022). This age model uses 10 monospecific planktonic foraminifera Accelerator Mass Spectrometry ^{14}C, carried out at the *Laboratório de Radiocarbono* at *Universidade Federal Fluminense,* and firstly presented by Frozza et al. (2020) (Table S1). The reservoir correction (deltaR= -85 +/-40) is based on ages from Nadal de Masi (1999), Angulo et al. (2005), and Alves et al. (2015), quantified using the online tool http://calib.org/ "Marine Reservoir Correction". The age model was run on the r*bacon* package (Blaauw & Christen, 2011; version 2.4.2), for open-source R software (R Core Team, 2020), using the calibration curve Marine20 (Heaton et al., 2020) (Table S2).

Table S1. Accelerator Mass Spectrometry ^{14}C dates used to construct the age model for core SAT-048A (Frozza et al., 2020).

Sample depth (cm)	LAC-UFF sample code	Species	Age ^{14}C (ka BP)	Error (kyr)
23	170059	*G. cultrata*	5.226	0.028
23	170209	*G. ruber*	5.471	0.032
54	180167	*G. ruber*	10.594	0.117
65	190321	*G. ruber*	13.548	0.038
85	180168	*G. ruber*	16.599	0.212
113	180169	*G. ruber*	15.531	0.185
149	190704	*G. ruber*	19.536	0.104
183.5	190323	*G. ruber*	31.174	0.271
217	180170	*G. ruber*	22.997	0.451
295	190540	*G. ruber*	38.997	0.260

Table S2. SAT-048A data points for the construction of the age model on *rbacon* package (Suárez-Ibarra et al., 2022).

LabID	Age (years)	Error (years)	Depth (cm)	Calibration curve	delta.R	delta.STD
LACUFF170059	5226	28	23	2	-85	40
LACUFF170209	5471	32	23	2	-85	40

LACUFF180167	10594	117	54	2	-85	40
LACUFF190321	13548	38	65.5	2	-85	40
LACUFF180168	16599	212	85	2	-85	40
LACUFF180169	15531	185	113	2	-85	40
LACUFF190704	19536	104	149	2	-85	40
LACUFF190323	31174	271	183.5	2	-85	40
LACUFF180170	22997	451	217	2	-85	40
LACUFF190540	38997	260	295	2	-85	40
Laschamp	41000	0	352	0	0	0

Sea Surface Temperatures

Sea subsurface temperature estimates for 25 and 75 m depths (T_{75m} and T_{75m}, °C, Figure S1) used the relative abundances of whole planktonic foraminifera assemblages from Suárez-Ibarra et al. (2020) and the Modern Analog Technique (MAT, Hutson, 1980) tool within the statistical software PAST (version 3.2; Hammer et al., 2001). The calibration was performed using 1,538 core tops from the Atlantic Ocean (421 samples from the South Atlantic), recovered from the ForCenS database (Siccha and Kucera, 2017) and García-Chapori & Laprida (2020) for the Brazil-Malvinas Confluence. Mean annual temperatures for 25 and 75 m depth were extracted from the World Ocean Atlas 2013 (WOA13, Locarnini et al., 2013, at a resolution of 0.25°), using the Ocean Data View software (Schlitzer, 2021). On A and B), the coefficient of determination values (R^2) between reconstructed T_{75m} and T_{75m} (°C) and measured WOA13 T_{75m} and T_{75m} (°C, (Locarnini et al., 2013) are 0.992 and 0.987, respectively. On C and D) the residuals from the performances are shown. Horizontal lines encompass 95% of the residuals.

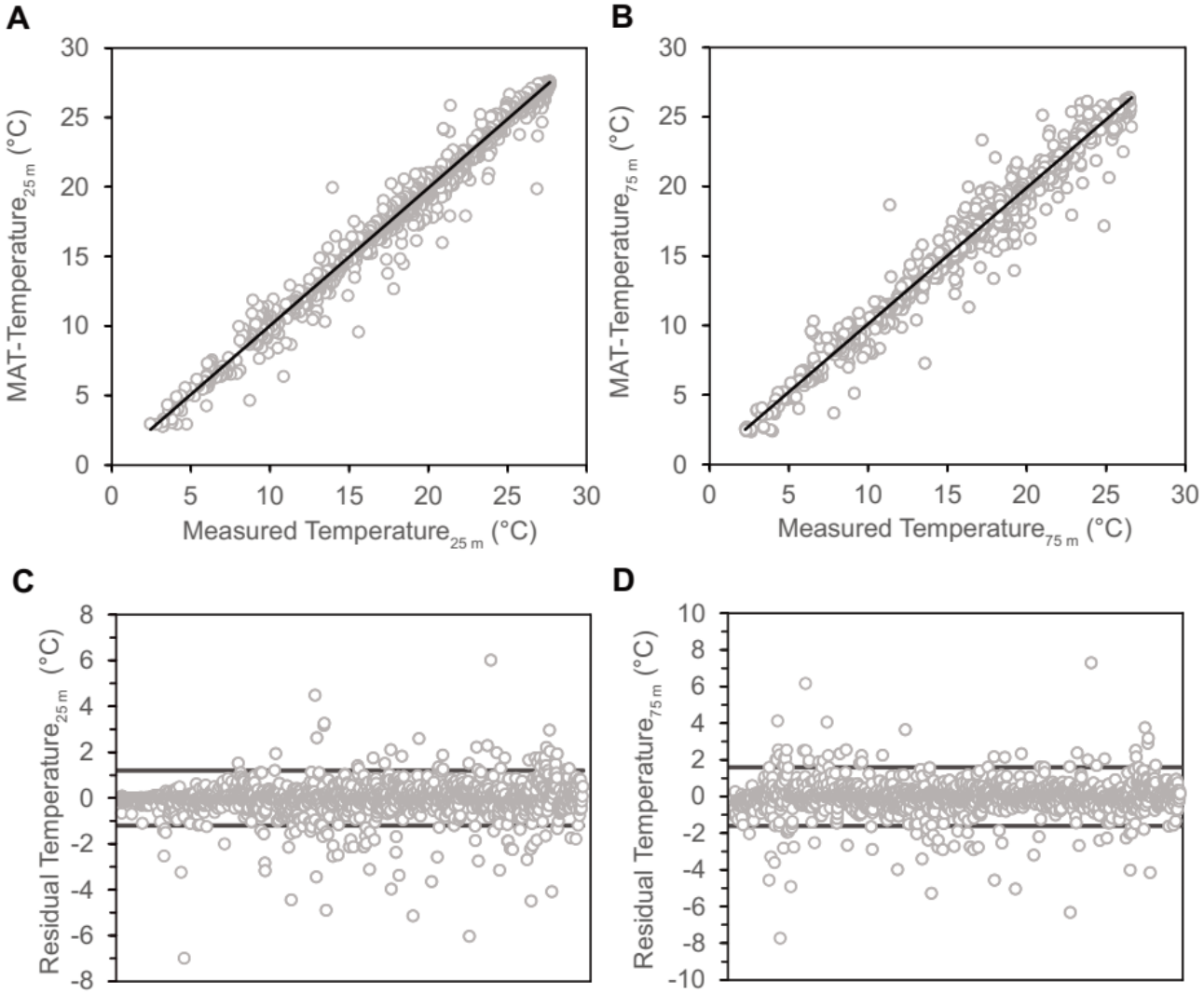

Figure S1. Modern Analog Technique (MAT) performance for core SAT-048A of sea subsurface mean annual temperature estimates for 25 and 75 m depths at the study site. On A and B), the coefficient of determination (R^2) values are 0.992 and 0.987, respectively. On C) and D), the residuals of the performance are shown, horizontal lines encompass 95% of the residuals.

Statistical analysis

To further test the ecological optimum hypothesis, we run Pearson and Spearman's rank correlation analyses between the sizes (mean and 95th percentile) and the respective relative abundances of each analysed species. Results from the Pearson correlations are shown in Table 3 in the main text and Figure S2. Results from the Spearman's rank correlations are shown in Table S3.

Table S3. Results of the Spearman's rank correlations performed on the test size (as described by the mean and 95th percentile of the squared root of the cross-sectional area) against the relative abundance (%) of each species. None of the *p*-values are significant (p <0.05).

		Mean	Perc 95th
G. ruber albus (%)	R^2	0.00	0.02
	p	0.62	0.39
G. glutinata (%)	R^2	0.05	0.02
	p	0.11	0.34
G. bulloides (%)	R^2	0.03	0.00
	p	0.27	0.99

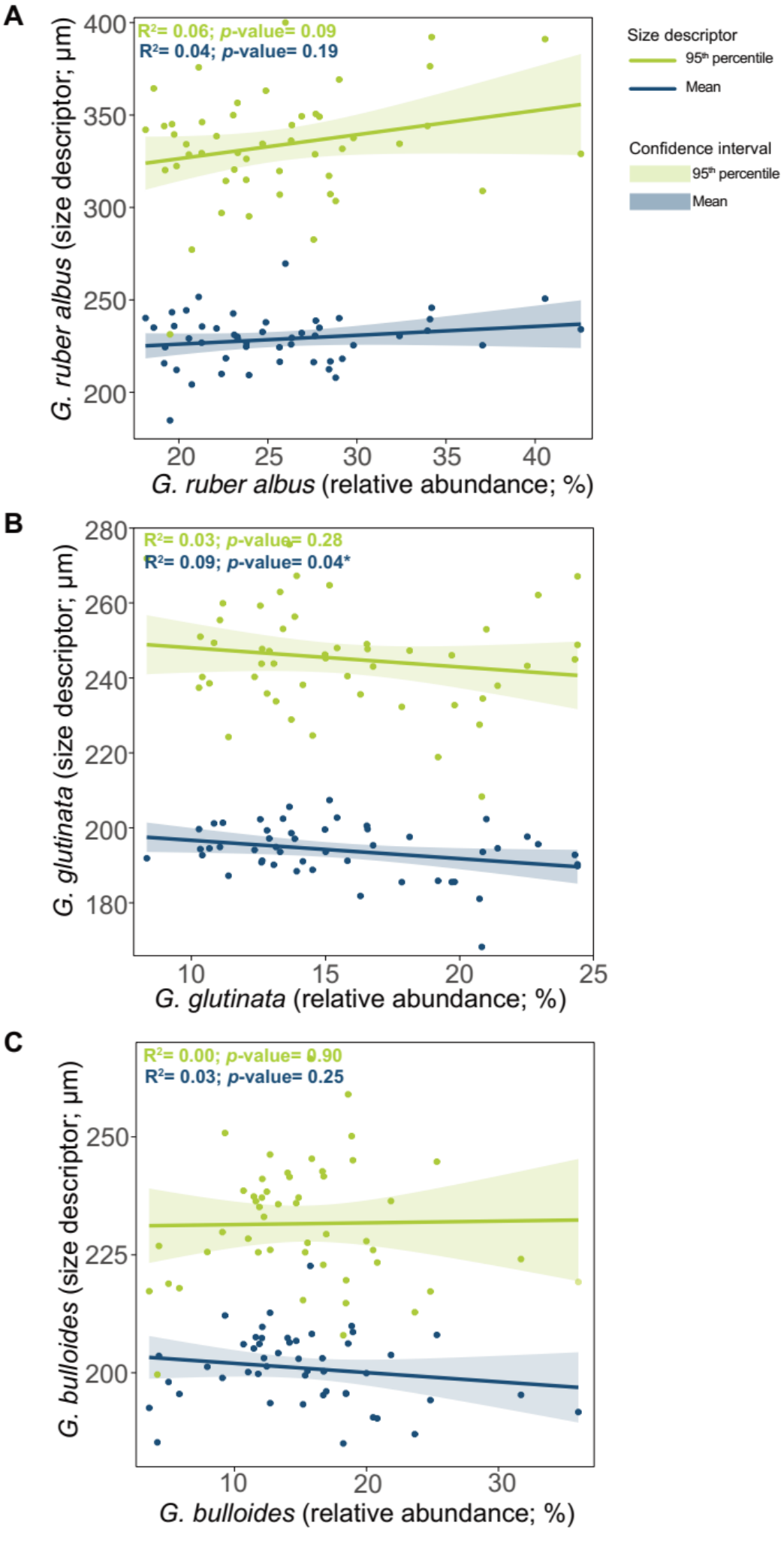
A
R²= 0.06; p-value= 0.09
R²= 0.04; p-value= 0.19
G. ruber albus (size descriptor; µm)
G. ruber albus (relative abundance; %)
Size descriptor
95th percentile
Mean
Confidence interval
95th percentile
Mean
B
R²= 0.03; p-value= 0.28
R²= 0.09; p-value= 0.04*
G. glutinata (size descriptor; µm)
G. glutinata (relative abundance; %)
C
R²= 0.00; p-value= 0.90
R²= 0.03; p-value= 0.25
G. bulloides (size descriptor; µm)
G. bulloides (relative abundance; %)

Figure S2. Graphical results of the Pearson correlations performed between the test sizes (as 95th percentile and mean values of squared root of cross-sectional area) and the relative abundances of *Globigerinoides ruber albus, Globigerinita glutinata* and *Globigerina bulloides* for core SAT-048A. Note that just *G. glutinata* (size, mean value) is significantly correlated with is own relative abundance, however, with low values.

Broken shells through the geological record

Here we list 25 individuals showing signs of a broken/removed terminal chamber. Scars are evident with scatter electron microscopy.

Table S3. List of species showing signs of final broken or removed chambers.

Species	Age	Link
Planoheterohelix globulosa	Cenomanian-Maastrichtian	pforams@mikrotax - Planoheterohelix globulosa
Braunella punctulata	Campanian-Maastrichtian	pforams@mikrotax - Braunella punctulata
Helvetoglobotruncana helvetica	Turonian	https://www.mikrotax.org/pforams/index.php?taxon=Helvetoglobotruncana%20helvetica&module=pf_mesozoic
Helvetoglobotruncana praehelvetica	Turonian-Cenomanian	pforams@mikrotax - Helvetoglobotruncana praehelvetica
Contusotruncana contusa	Maastrichtian-Maastrichtian	pforams@mikrotax - Contusotruncana contusa
Globotruncana orientalis	Santonian-Maastrichtian	pforams@mikrotax - Globotruncana orientalis
Chiloguembelina adriatica	Eocene-Oligocene	pforams@mikrotax - Chiloguembelina adriatica

Chiloguembelina cubensis	Eocene-Oligocene	pforams@mikrotax - Chiloguembelina cubensis
Jenkinsina columbiana	Paleocene-Miocene	pforams@mikrotax - Jenkinsina columbiana
Parvularugoglobigerina alabamensis	Paleocene	pforams@mikrotax - Parvularugoglobigerina alabamensis
Globigerina archaeobulloides	Oligocene	pforams@mikrotax - Globigerina archaeobulloides
Ciperoella anguliofficinalis	Eocene-Miocene	pforams@mikrotax - Ciperoella anguliofficinalis
Globigerinoides eoconglobatus	Miocene-Recent	pforams@mikrotax - Globigerinoides eoconglobatus
Dentoglobigerina juxtabinaiensis	Miocene	pforams@mikrotax - Dentoglobigerina juxtabinaiensis
Dentoglobigerina altispira	Miocene-Pliocene	pforams@mikrotax - Dentoglobigerina altispira
Dentoglobigerina globosa	Oligocene-Pliocene	pforams@mikrotax - Dentoglobigerina globosa
Globorotaloides testarugosus	Oligocene-Miocene	pforams@mikrotax - Globorotaloides testarugosus
Subbotina gortanii	Eocene-Oligocene	pforams@mikrotax - Subbotina gortanii
Globoconella miotumida	Miocene	pforams@mikrotax - Globoconella miotumida
Globorotalia praemenardii	Miocene	pforams@mikrotax - Globorotalia praemenardii
Neogloboquadrina atlantica	Miocene-Quaternary	pforams@mikrotax - Neogloboquadrina atlantica
Alicantina lozanoi	Eocene	pforams@mikrotax - Alicantina lozanoi

Acarinina soldadoensis	Paleocene-Eocene	pforams@mikrotax - Acarinina soldadoensis
Turborotalia ampliapertura	Eocene-Oligocene	pforams@mikrotax - Turborotalia ampliapertura
Globuligerina altissapertura	Middle Jurassic	JM - Middle Jurassic (Bajocian) planktonic foraminifera from the northwest Australian margin (copernicus.org)

References

Alves, E., Macario, K., Souza, R., Pimenta, A., Douka, K., Oliveira, F., Chanca, I., and Ângulo, E., 2015. Radiocarbon reservoir corrections on the Brazilian coast from pre-bomb marine shells. Quaternary Geochronology, 29, 30–35. https://doi.org/10.1016/j.quageo.2015.05.006

Angulo, R. J., de Souza, M. C., Reimer, P. J., and Sasaoka, S. K., 2005. Reservoir effect of the southern and southeastern Brazilian coast. Radiocarbon, 47, 67–73. https://doi.org/10.1017/S0033822200052206

Blaauw, M., and Christen, J. A., 2011. Flexible Paleoclimate Age-Depth Models using autoregressive gamma process. Bayesian Analysis 6 (3), 457–474. https://doi.org/10.1214/11-BA618

Frozza, C. F., Pivel, M. A. G., Suárez-Ibarra, J. Y., Ritter, M. N., and Coimbra, J. C., 2020. Bioerosion on late Quaternary planktonic Foraminifera related to paleoproductivity in the western South Atlantic. Paleoceanography and Paleoclimatology, 35, e2020PA003865. https://doi.org/10.1029/2020PA003865

García-Chapori, N., and Laprida, C., 2021, Planktonic foraminifera assemblages from the Brazil–Malvinas Confluence: palaeoceanographic implications of sub-surface temperature reconstructions in the western South Atlantic: Lethaia, v. 54(4), p. 477–494, DOI: 10.1111/let.12416.

Heaton, T., Köhler, P., Butzin, M., Bard, E., Reimer, R., Austin, W., et al., 2020. Marine20—The Marine Radiocarbon Age Calibration Curve (0–55,000 cal BP). Radiocarbon 62 (4), 779-820. doi:10.1017/RDC.2020.68

Lisiecki, L. E., and Stern, J. V., 2016. Regional and global benthic $\delta^{18}O$ stacks for the last glacial cycle. Paleoceanography 31 (10), 1368–1394. https://doi.org/10.1002/2016PA003002

Locarnini, R. A., Mishonov, A. V., Antonov, J. I., Boyer, T. P., Garcia, H. E., Baranova, O. K., Zweng, M. M., Paver, C. R., Reagan, J. R., Johnson, D. R., Hamilton, M., and Seidov, D., 2013. Volume 1: Temperature, in: Levitus, S., Mishonov, A. (Eds.), World Ocean Atlas 2013. NOAA Atlas NESDIS 73, p. 40.

Nadal De Masi, M. A., 1999. Prehistoric hunter-gatherer mobility on the southern Brazilian coast: Santa Catarina Island. Ph.D. Thesis, Stanford University, Palo Alto, CA (unplublished).

R Core Team, 2020. R: a language and environment for statistical computing. Vienna, Austria: R Foundation for Statistical Computing. http://www.R-project.org/

Suárez-Ibarra, J. Y., Frozza, C. F., Palhano, P. L., Petró, S. M., Weinkauf, M. F. G., and Pivel, M. A. G. (2022). Calcium carbonate dissolution triggered by high productivity during the last glacial-interglacial interval in the deep western south atlantic. Front. Earth Sci. 10. doi: 10.3389/feart.2022.830984